

Characterization of the invasion of hematopoietic myeloid cells into the CNS during EAE

Dissertation

for the award of the degree

“Doctor rerum naturalium (Dr.rer.nat.)

of the Georg-August-Universität Göttingen

within the PhD programme Biology

of the Georg-August University School of Science (GAUSS)

submitted by

Michael Haberl

From Munich

Göttingen, 2021

Thesis committee

Prof. Dr. Jürgen Wienands, Dept. of Cellular and Molecular Immunology, University Medical Center, Göttingen

Prof. Dr. Dr. Hannelore Ehrenreich, Clinical Neurosciences, Max Planck Institute of Experimental Medicine, Göttingen

Prof. Dr. Alexander Flügel, Dept. of Neuroimmunology, University Medical Center, Göttingen

Members of the examination board

Reviewer: Prof. Dr. Alexander Flügel, Dept. of Neuroimmunology, University Medical Center, Göttingen

Second Reviewer: Prof. Dr. Dr. Hannelore Ehrenreich, Clinical Neurosciences, Max Planck Institute of Experimental Medicine, Göttingen

Further members of the examination board:

Prof. Dr. Jürgen Wienands, Dept. of Cellular and Molecular Immunology, University Medical Center, Göttingen

Prof. Dr. Christine Stadelmann, Institute of Neuropathology, University Medical Center, Göttingen

Prof. Dr. Susann Boretius, Functional Imaging Laboratory, German Primate Center, Göttingen

Prof. Dr. Stefan Pöhlmann, Infection Biology Unit, German Primate Center, Göttingen

Date of the oral examination: 20.12.2021

Table of Contents

List of Figures	V
List of abbreviations	VII
Abstract.....	1
1. Introduction	2
1.1 Multiple Sclerosis	2
1.2 Monocyte subsets	4
1.3 EAE as an experimental model for MS	5
1.4 Monocytes in EAE.....	6
1.5 Overcoming the blood-brain-barrier during CNS autoimmunity.....	7
1.6 Leukocyte adhesion cascade	7
1.7 Monocyte migration in EAE	9
1.8 Intravital two-photon imaging to study leukocyte trafficking in the CNS	10
1.9 Quantitative analysis of immune cell migration	11
1.10 Aims of the work.....	13
2. Material and Methods	15
2.1 Materials	15
2.1.1 Proteins	15
2.1.2 Antibodies.....	15
2.1.3 Buffers and Media.....	15
2.1.4 Procedure kits	16
2.1.5 Chemicals/Sera/Solvents.....	17
2.1.6 RT-qPCR Primer and probes.....	18
2.2 Methods.....	19
2.2.1 Animals	19
2.2.2 Generation of transgenic T cell cultures	19
2.2.3 Adoptive transfer EAE.....	21
2.2.4 Intravital live imaging with the two-photon laser scanning microscope	21
2.2.5 Processing of raw data from IVM.....	22
2.2.6 Analysis of leukocyte motility	22
2.2.7 Hierarchical clustering analysis of leukocyte cell motility	23
2.2.8 Labelling of myeloid cells for IVM.....	24
2.2.9 Animal preparation and organ processing	24

2.2.10	Isolation of PBMCs from blood	24
2.2.11	Isolation of leukocytes from spleen	25
2.2.12	Isolation of leukocytes from spinal cord and spinal cord meninges	25
2.2.13	Isolation of endothelial cells from spinal cord meninges and parenchyma ...	25
2.2.14	Flow cytometry	26
2.2.15	Cell sorting	26
2.2.16	RNA isolation, cDNA synthesis and RT-qPCR	26
2.2.17	RNA-sequencing and library preparation	26
2.2.18	RNA-sequencing analysis	27
2.2.19	Interference with integrin signalling	27
2.2.20	Interference with chemokine signalling	28
2.2.21	Hybridoma culture and monoclonal antibody production.....	28
3.	Results	29
3.1	Monocytes closely follow infiltrating T _{MBP} cells into the CNS during atEAE.....	29
3.2	Visualization of monocytes in the leptomeninges of the spinal cord	31
3.2.1	Labelling of monocytes by intravenous injection of fluorescent liposomes.....	31
3.2.2	Characterization of liposome up-taking cells	32
3.3	Migratory behaviour of monocytes in spinal cord leptomeninges during atEAE	33
3.4	Computational analysis of cell migration patterns	38
3.5	Automated migratory pattern classification of DiI ⁺ monocytes during atEAE	41
3.6	Identifying molecular cues shaping migratory patterns of immune cells during atEAE 43	
3.6.1	Interfering with VLA-4 signalling changes migratory pattern signature in DiI ⁺ monocytes but not T _{MBP} cells.....	43
3.6.2	Interfering with LFA-1-signaling does not interfere with intraluminal migration of DiI ⁺ monocytes	46
3.6.3	Global G α i inhibition interferes with initial steps of intravascular migration of DiI ⁺ monocytes	48
3.7	Cell-extrinsic factors shaping immune cell migratory patterns	51
3.7.1	Vessel diameter correlates with leukocyte migratory phenotypes.....	51
3.7.2	Vessel junctions do not affect migratory patterns	53
3.8	Molecular cues shaping migratory phenotypes	56
3.8.1	DiI ⁺ monocytes do not change their expression profile during the course of atEAE.....	56
3.9	Impact of endothelial cell expression pattern on DiI ⁺ motility patterns	61
3.9.1	Spinal cord leptomeningeal endothelial cells change their expression profile during preclinical EAE.....	61
3.10	Comparison of expression profiles between blood monocytes and encephalitogenic T cells.....	63

4.	Discussion.....	66
4.1	Establishing the system.....	66
4.2	Migratory behaviour of monocytes in spinal cord leptomeninges during adoptive transfer EAE.....	67
4.3	Automated characterization and classification of cell motility reveals heterogeneity in immune cell populations	69
4.4	Molecular cues shaping motility patterns	71
4.5	Change of monocyte motility patterns is due to transcriptional changes of leptomeningeal blood vessel endothelial cells	74
4.6	Cell extrinsic factor shaping motility patterns	75
4.7	Monocytes display different motility pattern profiles than encephalitogenic T cell	77
5.	Summary.....	78
	Bibliography	79
	Lebenslauf.....	90

List of Figures

FIGURE 1 COMMONLY USED MIGRATORY PARAMETERS TO QUANTIFY CELL MIGRATION DERIVED FROM INTRAVITAL TIME LAPSE IMAGING	13
FIGURE 2 HIERARCHICAL CLUSTERING USES A “BOTTOM UP” APPROACH TO ACHIEVE CLUSTERING.	24
FIGURE 3 RAT MONOCYTE SUBPOPULATIONS CAN BE DISCRIMINATED BY THEIR EXPRESSION OF CD43.....	30
FIGURE 4 INFILTRATION KINETIC OF T _{MBP-LA} CELLS AND MONOCYTES DURING ATEAE.	30
FIGURE 5 PHAGOCYTIC CELLS IN THE BLOOD CIRCULATION CAN BE VISUALIZED IN THE LEPTOMENINGES IN VIVO BY INTRAVENOUS INJECTION OF DIA STAINED LIPOSOMES.	31
FIGURE 6 CD172A+ CD43 ^{HIGH} MONOCYTES MAINLY TAKE UP FLUORESCENT LIPOSOMES IN THE CIRCULATION.	33
FIGURE 7 CHEMOKINE RECEPTOR EXPRESSION IN DII POSITIVE AND NEGATIVE MONOCYTES.	33
FIGURE 8 DII ⁺ MONOCYTES ACCUMULATE AT THE SPINAL CORD LEPTOMENINGES DURING EAE.....	35
FIGURE 9 DII ⁺ MONOCYTES CHANGE THEIR MOTILITY PARAMETERS DURING EAE.....	35
FIGURE 10 DII ⁺ MONOCYTES CHANGE THEIR MIGRATION MODE DURING EAE.	36
FIGURE 11 THE MEDIAN ANGLE IN RELATION TO THE BLOOD FLOW AS A NEW PARAMETER TO QUANTIFY INTRALUMINAL CELL MIGRATION.	37
FIGURE 12 T _{MBP} CELLS AND DII ⁺ MONOCYTES EXHIBIT DIFFERENT INTRALUMINAL MIGRATORY PHENOTYPES.	38
FIGURE 13 CLUSTERING-BASED CLASSIFICATION OF MIGRATORY PATTERNS OF CELLS.....	40
FIGURE 14 AUTOMATED MIGRATORY PATTERN CLASSIFICATION OF DII ⁺ MONOCYTES AND T _{MBP} CELLS.	42
FIGURE 15 LEUKOCYTE ADHESION CASCADE.	43
FIGURE 16 BLOCKING VLA-4 INTERFERES PARTIALLY WITH INTRALUMINAL DII ⁺ MONOCYTE MIGRATION DURING PRECLINICAL EAE.	45
FIGURE 17 BLOCKING LFA-1 INTERFERES PARTIALLY WITH INTRALUMINAL DII ⁺ MONOCYTE DURING PRECLINICAL EAE.	47
FIGURE 18 GLOBAL BLOCKING OF GAI-SIGNALING INTERFERES PARTIALLY WITH INTRALUMINAL DII ⁺ MONOCYTE DURING PRECLINICAL EAE.....	50
FIGURE 19 COMPARISON OF AUTOMATED VS MANUAL VESSEL DIAMETER MEASUREMENT.....	52
FIGURE 20 BLOOD VESSEL DIAMETER CORRELATES WITH MONOCYTE MIGRATORY PATTERNS.	53
FIGURE 21 INTRAVASCULAR MIGRATING IMMUNE CELLS ARE NOT PREFERENTIALLY OBSERVED AT VESSEL BRANCH JUNCTIONS.	55
FIGURE 22 ANALYSIS OF MONOCYTE AND T _{MBP} MOTILITY PATTERN DISTRIBUTION AT VESSEL BRANCH JUNCTIONS.	56
FIGURE 23 DI ⁺ AND DI ⁻ MONOCYTES DO NOT CHANGE THEIR EXPRESSION OF CHEMOKINE RECEPTORS AND INTEGRINS.	58
FIGURE 24 DI ⁺ AND DI ⁻ MONOCYTES DO NOT CHANGE THEIR SURFACE EXPRESSION OF INTEGRINS.	59
FIGURE 25 DII ⁺ AND DI ⁻ MONOCYTES SHOW DISTINCT TRANSCRIPTOMES BUT IN EACH MONOCYTE SUBPOPULATION, TRANSCRIPTIONAL PROFILES DO NOT CHANGE DRASTICALLY DURING THE COURSE OF EAE.....	60

VI

FIGURE 26 LEPTOMENINGEAL ENDOTHELIAL CELLS CHANGE THEIR GENE EXPRESSION PROFILES DURING PRECLINICAL EAE AND UPREGULATE ADHESION MOLECULES AND CHEMOKINES.....	62
FIGURE 27 TRANSCRIPTOME ANALYSIS OF MONOCYTES AND T _{MBP} CELLS.....	64
FIGURE 28 MIGRATORY PARAMETERS OF HOMEOSTATIC MONOCYTES AND T _{MBP} CELLS BEFORE AND AFTER ANTI-VLA-4 TREATMENT.	71

List of abbreviations

Abbreviation	Full description
ACK	ammonium chloride potassium
ALCAM	activated leukocyte cell adhesion molecule
APC	antigen-presenting cell
atEAE	adoptive transfer experimental autoimmune encephalomyelitis
BBB	blood-brain barrier
BBB-EC	blood-brain barrier endothelial cell
BCSFB	blood-cerebrospinal fluid barrier
BSA	bovine serum albumin
CCL2	C-C motif chemokine ligand 2
CCL20	C-C motif chemokine ligand 20
CCR2	C-C motif chemokine receptor type 2
CCR5	C-C motif chemokine receptor type 5
CCR6	C-C motif chemokine receptor type 6
cDNA	complementary DNA
CNS	central nervous system
CSF	cerebrospinal fluid
CX3CR1	CX3C chemokine receptor 1
CXCR3	C-X-C motif chemokine receptor type 3
CXCR4	C-X-C motif chemokine receptor type 4
DiA	4-Di-16-ASP (4-(4-(Dihexadecylamino)styryl)-N-Methylpyridinium Iodide)
DiI	1,1'-Dioctadecyl-3,3,3',3'-Tetramethylindocarbocyanine Perchlorate
DMEM	Dulbecco's modified Eagle's medium
DMSO	dimethyl sulfoxide
DNA	deoxyribonucleic acid
EAE	experimental autoimmune encephalomyelitis
EDTA	dthylenediaminetetraacetic acid
EH	Eagle's HEPES
FACS	fluorescence-activated cell sorting
FCS	fetal calf serum
FITC	fluorescein isothiocyanate

VIII

GFP	green fluorescent protein
GM-CSF	granulocyte-macrophage colony-stimulating factor
GPCR	G protein-coupled receptor
GWAS	genome-wide association study
HBEC	human brain endothelial cell
HLA	human leukocyte antigen
ICAM1	intercellular adhesion molecule 1
ICAM2	intercellular adhesion molecule 2
IL-17	interleukin 17
INF γ	interferon gamma
IVM	intravital microscopy
LFA-1	lymphocyte function-associated antigen 1
MBP	myelin basic protein
MHC	major histocompatibility complex
MO	monocytes
MOG	myelin oligodendrocyte glycoprotein
mRNA	messenger ribonucleic acid
MS	Multiple sclerosis
OVA	chicken egg ovalbumin
OX40	tumor necrosis factor receptor superfamily member 4
p.t.	post transfer
PBMC	peripheral blood mononuclear cells
PBS	phosphate-buffered saline
PCA	principal component analysis
PCR	polymerase chain reaction
PLP	proteolipid protein
PSGL-1	P-selectin glycoprotein ligand
PTX	pertussis toxin
RNA	ribonucleic acid
RRMS	relapse-remitting multiple sclerosis
RT-qPCR	quantitative reverse transcription polymerase chain reaction
SAS	subarachnoid space
SEM	standard error of the mean
SNP	single-nucleotide polymorphism
SP-MS	secondary progressive multiple sclerosis
TCGF	T cell growth factor

IX

TCGM	T cell growth medium
TCM	T cell medium
Th17	T-helper 17
TMBP	myelin basic protein-specific T cells
TMBP-LA	LifeAct-mTurquoise2+ myelin basic protein-specific T cells
TPLSM	two-photon laser scanning microscopy
VCAM1	vascular cell adhesion protein 1
VLA-4	very late antigen 4

Abstract

Experimental autoimmune encephalomyelitis (EAE), the classical animal model of multiple sclerosis, is caused by T cells directed against myelin antigens. Upon intravenous transfer, these cells appear in the vessels of the blood-brain-barrier (BBB) where they crawl extensively before entering the CNS. Once in the target tissue these cells are locally reactivated and start an inflammatory process leading to further recruitment of other inflammatory cells such as myeloid cells. Myeloid cells are known to play an important role in the effector phase of the disease, however, how they move in the vessels of the BBB, and which are the molecular cues that determine their motility is still not fully understood.

Using intravital two-photon microscopy in Lewis rat EAE, we analyzed simultaneously the migratory behavior of encephalitogenic T cells and monocytes at the BBB. We show that these immune cell populations exhibit complex motility behavior that could not be depicted by standard motility analysis. Using a newly developed analysis based on unsupervised machine-learning, we found that monocytes and autoaggressive T cells employed heterogeneous motility patterns and these migratory patterns were distinct between the two immune cell populations.

To identify the molecular cues shaping these motility patterns, we functionally interfered with integrins and chemokines. We found that not only the observed motility phenotypes responded differently to the interfering strategies but also this response was distinct between monocytes and T cells.

Using our newly developed analysis system, we investigated how mechanical cues of the vasculature shape immune cell motility patterns and found that hemodynamic properties have a negligible effect on the motility of immune cells.

In summary, our advanced motility analysis revealed that immune cell motility behavior at the BBB is guided by different rules. More importantly, immune cell subsets seem to be heterogeneous in themselves, reflected by their motility phenotype profiles, and in their usage of molecular cues. In-depth molecular characterization of these immune cell subsets is crucial for designing better therapeutic strategies in MS.

1.Introduction

1.1 Multiple Sclerosis

Multiple sclerosis (MS) is the most common autoimmune disease of the central nervous system (CNS) affecting approximately more than 2 million people worldwide. It mostly affects young people between 30 and 40 years of age with females having a higher predisposition than males. Demyelinating lesions which form the name-giving sclerotic plaques are the hallmark of multiple sclerosis and represent the end stage of a process involving inflammation, demyelination, remyelination, and axon degeneration (Compston and Coles, 2008). Multiple sclerosis manifests in three distinct patterns; in about 85% of MS patients, the disease starts as relapse-remitting MS (RRMS). The patients display abrupt and recurrent neurological dysfunction (relapse) about 1-2 times per year which are followed by gradual improvement (remission). Approximately 50% of patients convert to the secondary progressive type of MS (SP-MS) within 10 years of disease onset, which is characterized by progression of disability. In contrast, patients with primary progressive MS (PP-MS, 10% of all MS patients) disability progresses constantly from the onset of disease (Hauser and Oksenberg, 2006). The cause for multiple sclerosis remains still elusive but it is widely believed that the disease is initiated by autoreactive T cells specific for myelin antigens that get activated in the periphery – potentially through molecular mimicry (Harkiolaki et al., 2009; Münz et al., 2009; Olson et al., 2001) or bystander activation – traffic to the CNS cross the BBB and start autoimmune inflammation directed against myelin antigens leading to demyelination and axonal damage. Several lines of evidence support this hypothesis (reviewed in Hemmer et al., 2015); epidemiological studies have shown that there is an important effect of genetic risk factors on disease susceptibility, although, MS is not caused by a single mutated gene but the effect of several genes contributing to disease susceptibility. The HLA-DRB2 gene is the strongest genetic factor associated with MS predisposition (Sawcer et al., 2011). The human leukocyte antigen class II and class I molecules are the human version of the major histocompatibility complex (MHC) and are essential for antigen presentation in the context of T cell receptor activation to CD4⁺ and CD8⁺ T cells, respectively. Further evidence for the importance of genetic risk factors was presented by genome-wide association studies (GWAS), which identified more than 100 genetic variants (single nucleotide polymorphism SNPs) that are associated with multiple sclerosis. Most of these gene loci are linked to the immune system (Beecham et al., 2013; Farh et al., 2014; Raj et al., 2014; Sawcer et al., 2011). While no comorbidities with other autoimmune diseases are reported for MS, there is a substantial number of genetic variants associated with MS (~ 22%)

that are also associated with other autoimmune diseases, such as rheumatoid arthritis, psoriasis, and autoimmune thyroid disease (Beecham et al., 2013). Albeit the important role of genetic factors in MS, the concordance rate in monozygotic twins is only about 15-25%, suggesting that also non-genetic factors can affect disease susceptibility (Ramagopalan et al., 2008). Several studies have shown that environmental factors greatly contribute to MS development; several of these lead to persistent activation of the immune system, like smoking, or infection with Epstein-Barr virus (Levin et al., 2010). Recently, low serum Vitamin D levels were also associated with an increased multiple sclerosis risk, which are thought to modulate T cell differentiation (Allen et al., 2012; Ascherio et al., 2010). These findings can be combined to a unifying hypothesis, that the risk of developing multiple sclerosis is mainly due to genes that affect the adaptive immune system and environmental factors that modulate the peripheral adaptive immune response (Hemmer et al., 2015).

Apart from the adaptive arm of the immune system, also innate immunity plays an important role in multiple sclerosis. Mononuclear phagocytes, such as macrophages and microglia, are the dominant immune cells in MS lesions. They can interact with cells of the adaptive immune system but can also directly cause tissue damage. Myeloid phagocytes are the main perpetrators of myelin damage and removal, forming demyelinating lesions, the hallmark of MS (Henderson et al., 2009; Lassmann et al., 1998), but also axonal damage (Trapp et al., 1998). Furthermore, activated macrophages and microglia are a major source of oxidative stress in active multiple sclerosis lesions, therefore probably contributing to white and grey matter damage (Fischer et al., 2012; Haider et al., 2011). Studies using animal models of CNS injury suggested that phagocytes can also contribute to tissue repair mechanisms during lesion resolution (Shechter et al., 2009, 2013). Whether phagocytes exert destructive or reparative function during progression of multiple sclerosis is, at least in part, related to the distinct origin and phenotypes of the phagocytes: phagocytes that differentiate from peripheral monocytes and show an activated phenotype with increased expression of pro-inflammatory cytokines, matrix metalloproteinases, and costimulatory molecules enter the CNS during lesion formation and are likely to cause tissue damage (Bar-Or et al., 2003; Kouwenhoven et al., 2001), however CNS-resident phagocytic cells, i.e. activated microglia, meningeal and perivascular macrophages, are often almost indistinguishable from blood-borne phagocytes in tissue section. Therefore, it is difficult to decipher whether these two phagocyte populations have similar or opposing functions in active MS lesions.

1.2 Monocyte subsets

Monocytes are a population of mononuclear leukocytes derived from hematopoietic precursor cells in the bone marrow and are released into the blood circulation as non-dividing cells. Geissmann and colleagues described that monocytes consists of two principal subsets based on their expression levels of the fractalkine chemokine receptor CX₃CR1 (Geissmann et al., 2003). Using mice expressing GFP in one allele of the CX₃CR1 gene locus, two monocyte populations were identified which differed in their GFP intensity and CX₃CR1 surface expression levels. CX₃CR1^{lo} monocytes are characterized by their expression of CD62L (L-selectin), Ly6C/G, VLA-4, LFA-1, and CCR2 whereas CX₃CR1^{hi} monocytes express only VLA-4, LFA-1, and low levels of Ly6C. Using adoptive transfer of monocytes from CX₃CR1^{GFP/+} mice, they could show that in steady-state the monocytes have different homing behaviour. Only CX₃CR1^{lo} monocytes responded to inflammation, are recruited to sites of inflammation, and are able to differentiate into inflammatory peripheral mononuclear phagocytes (Geissmann et al., 2003; Palframan et al., 2001). They are therefore termed “classical inflammatory monocytes”. Pioneering intravital microscopy (IVM) studies have established that CX₃CR1^{hi} monocytes crawl on the luminal side of blood vessel endothelium in steady-state conditions (Auffray et al., 2007), extensively scanning the microvasculature and were named “patrolling monocytes”. This crawling behaviour was independent of the blood flow and mainly mediated via the β_2 -integrin LFA-1. Deletion of CX₃CR1 resulted in a reduction of crawling CX₃CR1^{hi} monocytes by two-third, indicating that this crawling was also dependent on the fractalkine chemokine receptor. Their function is not yet fully understood but it was shown that they are involved in maintaining vessel endothelium integrity. They coordinate intraluminal stress responses via Toll-like receptor 7 in response to local danger signals and induce the recruitment of neutrophils which trigger focal necrosis of endothelial cells (EC). Subsequently patrolling monocytes clear the resultant debris (Carlin et al., 2013).

In the rat also two monocyte subpopulations were identified by different expression levels of CD43 (Ahuja et al., 1995). Characterization of these subsets showed that CD43^{hi} monocytes expressed high amounts of CX₃CR1 and low levels of CCR2 whereas CD43^{lo} monocytes expressed high levels of CCR2 and low levels of CX₃CR1. CD43^{lo} monocytes had a higher surface expression of CD62L (Yrliid et al., 2006). Functional studies using adoptive transfer experiments showed that only CD43^{lo} monocytes were recruited to sites of inflammation when transferred into animals with peritonitis (Yrliid et al., 2006). On the basis of the chemokine receptor expression and functional properties CD43^{hi} monocytes resemble the CX₃CR1^{hi}

patrolling monocyte population in the mouse and the CD43^{lo} monocytes are equivalent to the CX₃CR1^{lo} inflammatory mouse monocytes.

1.3 EAE as an experimental model for MS

A lot of the present knowledge about the inflammatory response in multiple sclerosis stems from findings in animal models of the disease, such as experimental autoimmune encephalomyelitis (Korn et al., 2009). One of the first descriptions of this model dates back to 1925 when Koritschoner and Schweinburg described that rabbits that were immunized with human spinal cord homogenates displayed inflammation in the spinal cord. The protocol used activated, preferentially CD4⁺, T cells and later it was shown in rats that transfer of CD4⁺ T cells sensitized to myelin antigens induce experimental autoimmune encephalomyelitis (Ben-Nun et al., 1981; Paterson, 1960). The identification of CD4⁺ T cells as major effector cells in EAE provides an explanation for the strong correlation of MS susceptibility with human MHC class II alleles (HLA-DRB2). Until now several rodent EAE models have been established. The disease can be induced actively by immunizing susceptible mouse or rat strains with myelin antigens (myelin basic protein [MBP], myelin proteolipid protein [PLP], myelin oligodendrocyte glycoprotein [MOG]) in adjuvant (Simmons et al., 2013) or passively by transfer of activated, myelin-specific CD4⁺ T cells (Ben-Nun et al., 1981; Miller and Karpus, 2007).

To study the migratory steps of myeloid cells at the blood-brain barrier during EAE, a passive transfer model of EAE in Lewis rats has been used in the present work. In this model activated CD4⁺ cells reactive against myelin basic protein are transferred intravenously leading to strong inflammation in the CNS. The incidence in this model is nearly 100%. The transfer of MBP-specific T cells is followed by a characteristic prodromal phase of about 2-3 days after which the animals develop a monophasic disease with rapid progressive ascending paresis. The course of events during the prodromal phase has been studied comprehensively (Flügel et al., 2001; Odoardi et al., 2012). Freshly activated T cell blasts are incapable of directly migrating to the CNS and overcoming the blood-brain barrier after transfer instead, they rapidly disappear from the blood circulation and accumulate in peripheral tissues, mainly within the lung and the spleen. At these sites, they undergo extensive transcriptional changes, thereby acquiring a “migratory phenotype” (Odoardi et al., 2012), which permits these cells to re-enter the blood circulation from where they infiltrate the leptomeninges of the dorsal spinal cord about 2-3 days post transfer (Bartholomäus et al., 2009; Flügel et al., 2001; Odoardi et al., 2012). The transcriptional alterations the T cells undergo during their “reprogramming” in the periphery, comprise downregulation of activation markers (CD25, OX40, INF- γ , IL-17) and upregulation

of migration associated molecules such as chemokine receptors (CXCR3, CXCR4, CCR5) and adhesion molecules (e.g. Nintegrin-1) (Flügel et al., 2001; Odoardi et al., 2012). However, the reprogramming and acquisition of this migratory phenotype are not restricted to CNS-reactive T cells. It was shown that also CNS-ignorant, ovalbumin-specific T cells (T_{OVA} cells) undergo similar transcriptional and phenotypical changes. In consequence, CNS-ignorant T_{OVA} cells were also able to enter the CNS meninges, although in substantially lower numbers, but with similar kinetics compared to their CNS-reactive counterparts (Odoardi et al., 2012). Using two-photon intravital microscopy it was shown that once migratory MBP-specific T cells arrive at the spinal cord leptomeninges, they get arrested on the endothelium of leptomeningeal blood vessels and immediately start to scan the luminal surface before they extravasate (Bartholomäus et al., 2009).

1.4 Monocytes in EAE

Apart from lymphocytes, also myeloid cells play an important role during autoimmune CNS inflammation. Depletion of peripheral macrophages/monocytes by intravenous (i.v.) injection of Clodronate-containing liposomes abrogated EAE in Lewis rats and in an adoptive transfer EAE model in SJL/L mice (Huitinga et al., 1990, 1995; Tran et al., 1998). Further evidence that monocytes are important for EAE pathogenesis is given by the observations that CCL2 (MCP-1), a potent chemoattractant for monocytes, is upregulated during EAE as well as the main CCL2 receptor CCR2 (Glabinski et al., 2003; Huang et al., 2001). CCL2 expression also correlates with disease severity. Mice lacking CCL2 show a delayed onset of EAE and are also resistant to adoptive transfer EAE (Huang et al., 2001). CCR2^{-/-} mice are relatively resistant to actively induced EAE and also failed to develop EAE after passive transfer of primed T cells from wild-type animals (Fife et al., 2000; Izikson et al., 2000; Saederup et al., 2010). Using bone marrow chimeras, Mildner et al. showed that CCR2 deficiency in the radio sensitive compartment leads to delayed onset EAE. Expression of CCR2 in myeloid cells was essential for disease induction, whereas lack of the receptor on T cells did not affect EAE development. Depletion of Ly6C^{hi} inflammatory monocytes by α -CCR2 antibody showed that these cells are pathogenic during the effector phase of EAE. Antibody treatment during the priming phase did not alter the EAE course, showing that Ly6C^{hi} CCR2⁺ are crucial for the effector phase of EAE (Mildner et al., 2009). In line with these findings, it was shown that Ly6C^{hi} precursor cells are mobilized into the circulation during the preclinical phase of EAE and start to accumulate in CNS before onset of disease at which time point the cells showed a CD11c⁻ MHC class II^{lo/hi} phenotype. During the symptomatic phase, CNS Ly6C^{hi} cells were CD11c⁺ MHC class II^{lo/hi} indicating that immature monocytes are recruited to the CNS in the preclinical stage and

differentiate *in situ* to a more mature phenotype during the effector phase (King et al., 2009). Recently it was established that autoaggressive T cells communicate with myeloid cells via the cytokine GM-CSF (Codarri et al., 2011). Expression of the GM-CSF receptor *Csfrb2* in CCR2⁺Ly6C^{hi} monocytes is critical for EAE development whereas *Csfrb2*-deficiency on conventional dendritic cells (cDC), neutrophils, and resident microglia cells did not affect EAE development. Resistance to EAE was not due to impaired recruitment of CCR2⁺ Ly6C^{hi} monocytes to the CNS nor to compromised differentiation of inflammatory monocytes to monocyte-derived Ly6C^{hi} CD11c⁺ MHC class II^{lo/hi} DCs (moDC). Moreover, GM-CSF was not required for the development of moDCs but it was fundamental for their capacity to coordinate tissue inflammation and upregulate phagocytic and proinflammatory functions (Croxford et al., 2015).

1.5 Overcoming the blood-brain-barrier during CNS autoimmunity

Using intravital microscopy imaging, several studies have addressed the question of early migratory steps of T cells into the CNS in EAE models and have proposed three possible routes of entry for encephalitogenic T cells in the CNS (reviewed in Engelhardt and Ransohoff, 2012).

1. Encephalitogenic CD4⁺ Th17⁺ CCR6⁺ cells have been shown to enter the CNS by crossing the blood-CSF barrier (BCSFB) in the choroid plexus. This transmigration is facilitated by the chemokine receptor CCR6 binding to its cognate ligand CCL20, which is produced by the epithelial cells of the choroid plexus, but not microvascular endothelial cells of the BBB (Reboldi et al., 2009).
2. Entry of immune cells through the endothelial BBB of brain and spinal cord parenchymal blood vessels could constitute a second route (Engelhardt and Ransohoff, 2005).
3. Encephalitogenic T cells have been shown to extravasate directly in leptomeningeal micro vessels to enter into the subarachnoid space (Bartholomäus et al., 2009; Schläger et al., 2016).

1.6 Leukocyte adhesion cascade

Independently of the entry route into the CNS, to be recruited into any given tissue, circulating leukocytes have to undergo a multistep process in which a sequential interaction between adhesion/signalling molecules present on leukocytes and endothelial cells takes place. This multistep leukocyte adhesion cascade is started by initial transient contacts between circulating immune cells and the blood vessel endothelium mediated by adhesion molecules of the selectin family (L-, E-, or P-selectin) present on endothelial cells and their respective

glycosylated ligands, e.g., P-selectin glycoprotein ligand (PSGL-1) on leukocytes (Ley et al., 2007). Once captured by this selectin-mediated adhesion, the cells roll along the vascular endothelium, which greatly reduces their velocity. It has been shown that expression of P- and E-selectin is not required for EAE development. Active immunization of E- or P-selectin deficient C57BL/6 or SJL/L mice resulted in an EAE course not distinguishable from wild-type animals (Doring et al., 2007). In line with these findings L-selectin deficient C57BL/6 or SJL/L mice are not resistant to EAE. In these animals, CNS infiltrate-composition was not different to wild-type animals (Ubaldi et al., 2008). Treatment with L-selectin-specific monoclonal antibody did not prevent EAE development in adoptive transfer models in C57BL/6 and SJL/L mice (Brocke et al., 1999).

Alternatively, leukocyte capture and/or rolling can also be mediated by the $\alpha 4$ -integrins $\alpha 4\beta 1$ (VLA-4) and $\alpha 4\beta 7$ (LPAM-1) by binding to their cognate ligands vascular cell adhesion molecule (VCAM) and mucosal addressin cell- adhesion molecule 1 (MadCAM1) on endothelial cells (Berlin et al., 1995; Ley et al., 2007). VLA-4-dependent rolling is mostly seen in monocytes, monocyte-like cell lines (Chan et al., 2001), T cell lines, and T cells (Berlin et al., 1995; Singbartl et al., 2001). In the next step, rolling leukocytes can bind to chemotactic factors of the chemokine family presented on the endothelial surface. Chemokine binding to G-protein-coupled receptors (GPCR) on the surface of immune cells triggers inside-out signalling to $\alpha 4$ - and $\beta 1$ -integrins, therefore increasing integrin affinity and avidity to their respective ligands on the vascular endothelium (VCAM, ICAM) by inducing conformational changes to active integrin forms and clustering of integrins. This sequence of events leads to adhesion strengthening, polarization, and subsequently firm attachment of leukocytes to the vascular wall followed by immune cell crawling on the endothelium (Ley et al., 2007). Immune cell crawling is predominantly mediated by $\beta 2$ -integrins (LFA-1, Mac1) binding to their cognate endothelial ligands ICAM1 and ICAM2 (Phillipson et al., 2006; Schenkel et al., 2004) and required to find permissive sites for transmigration of leukocytes. *In vitro* and *in vivo* studies have shown that T cell crawling and transmigration through CNS endothelial cells is mediated by LFA-1 and ICAM1 in steady-state conditions (Laschinger et al., 2002; Steiner et al., 2010). The role of the LFA-1-ICAM1-axis during CNS autoimmune processes is not fully understood. Conflicting studies report that treatment with LFA-1-blocking antibodies in murine EAE models resulted in amelioration or exacerbation of the disease (Kobayashi et al., 1995; Welsh et al., 1993). Using intravital two-photon imaging in a rat transfer EAE model, it was shown that myelin-specific T cells get arrested to leptomeningeal vessel endothelium and instantaneously started scanning the luminal surface. This crawling behaviour was preferentially against the blood flow

and mediated by the $\alpha 4$ -integrin VLA-4. Functional interference with VLA-4 by blocking antibody abrogated intraluminal T cell crawling and resulted in delayed clinical disease onset (Bartholomäus et al., 2009).

1.7 Monocyte migration in EAE

Whereas the role of distinct adhesion molecules involved in multistep leukocyte adhesion cascade during CNS autoimmune has been carefully dissected, the molecular cues involved in myeloid cell recruitment have so far not been investigated in detail. ICAM1 and VCAM1 are well-described adhesion molecules expressed by BBB endothelial cells during CNS inflammation and are crucial for the adhesion and transmigration of lymphocytes and monocytes (Bullard et al., 2007; Carman and Springer, 2004). Furthermore, the activated leukocyte cell adhesion molecule (ALCAM) was identified as an adhesion molecule present on BBB endothelium which is upregulated in active multiple sclerosis and EAE lesions (Cayrol et al., 2008). Antibody-mediated blocking of ALCAM inhibited transmigration of CD4⁺ lymphocytes and monocytes across BBB endothelial cells *in vitro* and reduced the interaction of human CD14⁺ monocytes with human brain endothelial cells (HBECs) in *in vitro* flow chamber assays, resulting in increased monocyte velocity. Specifically, the rolling and firm arrest stages during the multistep adhesion cascade were blocked (Cayrol et al., 2008; Lyck et al., 2016). Another molecule that is upregulated in MS lesions is nerve injury-induced protein (Ninjurin-1). It was also shown to be induced in human BBB-EC cultures under inflammatory conditions as well as expressed by human CD14⁺ monocytes. Blocking of Ninjurin by antibodies or blocking peptides reduced transmigration of human monocytes across BBB-ECs and inhibited adhesion of human monocytes to BBB-ECs in shear stress flow assays. Functional interference with Ninjurin *in vivo* resulted in amelioration of clinical EAE in mice which was accompanied by decreased recruitment of CD45^{high} CD11b⁺ Ly6C^{hi} myeloid cells (Ifergan et al., 2011). One caveat to be considered in several of these studies is that lymphocytes and myeloid share a great part of all these adhesion molecules involved in the leukocyte adhesion cascade. As multiple sclerosis, as well as its animal model EAE, is considered to be initiated by T lymphocytes, it is, therefore, difficult to discriminate what role adhesion molecules in lymphocytes and myeloid cells during different phases of neuroinflammation play; non-conditional genetic ablation or antibody-mediated interfering strategies always affect both leukocyte populations (Kobayashi et al., 1995; Laschinger et al., 2002; Steiner et al., 2010; Welsh et al., 1993). A possible way to investigate the molecular cues during CNS autoimmune inflammation, regulating adhesion and recruitment of lymphocytes and myeloid cells separately, is to use intravital microscopy. This allows observing leukocyte adhesion in the

target tissue, i.e., leptomeninges of the spinal cord or brain, during the different phases of CNS autoimmunity and by acute blocking of molecular cues immediately observe the outcome. Additionally, it enables the discrimination of several leukocyte populations by using respective fluorescent markers (Auffray et al., 2007; Bartholomäus et al., 2009; Carlin et al., 2013).

1.8 Intravital two-photon imaging to study leukocyte trafficking in the CNS

Intravital microscopy is a powerful tool to advance our knowledge of biological processes occurring *in vivo* by gaining mechanistic insights into the dynamics of these processes. The field of intravital microscopy has seen the advent of many innovations in the past 3 decades and constant development of new technologies, driven by the imaging community, has immensely improved our ability to visualize and study cell behaviour *in vivo* (reviewed in Helmchen and Denk, 2005).

One of the biggest advances in IVM was brought by two-photon laser scanning microscopy (TPLSM), a technology which was pioneered by Denk and colleagues in the lab of Watt W. Webb at Cornell University in 1990 (Denk et al., 1990). In conventional single-photon microscopy, fluorochromes are excited by the absorption of single photons emitted by excitation light sources, such as lasers, mercury, or halogen lamps (Denk and Svoboda, 1997). In consequence, the electrons of the fluorochromes are elevated to an activated, higher energy state (Helmchen and Denk, 2005). When excited molecules relax to the lower energy ground state, fluorescence can occur through the emission of a single photon (Denk et al., 1990). The emitted light is of a longer wavelength than the corresponding excitation light and can be detected (Zipfel et al., 2003). Whereas wavelengths for single-photon excitation are typically within the visible spectrum (380 – 700 nm), TPMLSM relies on short pulses of near-infrared light (680–1300 nm) to excite fluorophores. Single photons with wavelengths in the near-infrared to infrared spectrum do not have enough energy to excite fluorophores, therefore the near-simultaneous absorption of two photons is necessary for fluorochrome excitation. This can only be achieved by focusing pulsed laser light on a small point within the sample. Compared to conventional single-photon microscopy, TPLSM has several advantages for *in vivo* imaging (reviewed in Potter, 1996): firstly, due to the non-linear nature of multiphoton excitation, a high density of photons is needed in time and space at the sample. This can only be achieved by focusing the high-energy pulsed laser beam to a diffraction-limited spot in the specimen. Therefore, only tissue in the perifocal plane is excited while avoiding the excitation of adjacent tissue outside the focal plane (Potter, 1996). Furthermore, as a result of the aforementioned process, the photons combine their energy, which allows low-energy infrared or near-infrared

photons to excite fluorophores, and therefore phototoxic damage within the specimen is reduced to a minimum more (Kawakami and Flügel, 2010). Additionally, near-infrared light penetrates tissue more deeply because long-wavelength light is less affected by scattering in biological tissues than conventional fluorescence microscopy excitation light sources (Rubart, 2004). Finally, another nonlinear optical process called second-harmonic generation can be leveraged by TPLSM. When multiple photons of the same wavelength interact with nonlinear materials, the photons are combined and generate a new photon with double the energy and therefore half the original wavelength (Zipfel et al., 2003). This process makes it possible to visualize non-centrosymmetric structures, like collagen, which is a main component of the extracellular matrix (Zipfel et al., 2003).

This advanced imaging technique was used in the past to study early migratory steps of T cells into the CNS in EAE models, especially adoptive transfer EAE models as they have proven to be advantageous due to their susceptibility to manipulation. With this model, it is possible to label defined effector T cell populations prior to transfer by genetic transduction, i.e. CNS-reactive T cells (encephalitogenic MBP-specific T cells) without interfering with their cellular functions (Flügel et al., 1999). As a result, the coding sequence of fluorescent reporter proteins, like GFP or RFP, is retrovirally introduced into the genome of encephalitogenic T cells, allowing stable expression of the reporter that is not prone to diluting out through mitotic events (Flügel et al., 1999). Using this model, it is possible to follow adoptively transferred fluorescently tagged encephalitogenic T cells *in vivo* by intravital two-photon microscopy. Furthermore, these cells can be isolated by fluorescent activated cell sorting (FACS) and characterized further *ex vivo* (Bartholomäus et al., 2009; Flügel et al., 1999; Kawakami et al., 2004, 2005).

1.9 Quantitative analysis of immune cell migration

Since its advent, intravital time-lapse imaging has opened the possibility to visualize the dynamic behaviour of immune cells and to study the *in vivo* behaviour of various types of immune cells as well as the interaction between them. In order to draw conclusions from the observed cell behaviour and cell motility, a comprehensive quantitative analysis of the position and movement of cells is required (reviewed in Beltman et al., 2009). Such analysis starts with the tracking of cells in the acquired image data so that the position in space of each cell at each time point of the time-lapse data is estimated. From the positional data and time of observation of each cell, several motility parameters can be calculated, which are used to quantitate cell motility behaviour. To get a first qualitative impression of the migratory behaviour of immune

cells, the first step is to plot their trajectories over time in two- or three-dimensional space. Visualizing the trajectories on top of the acquired images helps to relate cell movement to other structural features of the imaged tissue. Using this approach, it could be shown that mutations in the signalling lymphocyte activation molecule-associated protein (SAP, SH2D1A) cause follicular T helper cells to be mostly excluded from germinal centres and instead reside mainly in the follicular mantle of the B cells regions (Qi et al., 2008). Another methodology is to translate the origin of each cell's trajectory to the same point in space while maintaining their orientation, allowing to estimate, whether the cells have a preferred migration direction (Figure 1 A). A random distribution of all possible directions of migration in this translation plot can indicate that cell migration is more or less random on the timescale of the duration of the plotted tracks. However, plotting of cell trajectories gives only a first qualitative indication of cell movement but from the positional data actual migratory parameters can be calculated to quantitate migration behaviour of immune cells. The most commonly used analysed parameters are:

Speed. Pioneering studies using intravital TPLSM in lymph nodes have shown, that T cells are activated in several phases *in vivo* that differ in their motility parameters, such as their migration speed (Memel et al., 2004; Miller et al., 2004). These studies have shown clearly that there is a direct connection between motility parameters of migrating immune cells and their function or status in immunological contexts. Two parameters of velocity can be found in literature: 1) the instantaneous velocity is the mean speed over the time interval between the acquisition of two imaging volumes. It can be approximated by dividing the distance the cell migrated by the time period between the acquisitions. 2) The mean speed is the average instantaneous velocity over an extended imaging period.

Displacement. The term displacement is used ambiguously in cell motility analysis. In general, displacement is the shortest distance between the positions of a cell at two time points. It is distinct from the total length of the entire path a cell has moved (Figure 1 B). The mean displacement is often used to determine the locomotion behaviour of the visualized cell populations by analysing how the mean displacement depends on the square root of the time period. If this relationship is linear, it indicates that the migration of cells happens in a random walk. A faster than linear increase is indicative of directed movement, whereas a lower than linear increase is reminiscent of confined migration (Beltman et al., 2009). However, in the present work, the term displacement (also displacement length) is used to describe the shortest distance between the starting- and end positions of a cell's trajectory (Figure 1 B).

Straightness. This motility parameter, which is also known as confinement ratio or meandering index, is a measure for the straightness of cell tracks. It is calculated by dividing the length of the direct displacement distance of a cell by the total length of the path that a cell has moved during the observation time. As the path length is at least equal to the distance of the direct displacement, the straightness can vary between 0 (the cell returns to the exact position from where it started) and 1 (a perfectly straight trajectory). The combination of straightness and velocity was used to investigate the role of CD44, a receptor for extracellular matrix proteins and glycosaminoglycans, in the migration of tumour-invading CD8 cytotoxic T lymphocytes, quantifying various migration behaviours among these lymphocytes (Mrass et al., 2008).

Together with the above-described motility parameters, in the present work also the track duration, which is the time period a cell track is observed in the acquired image data, is used to describe immune cell motility behaviour.

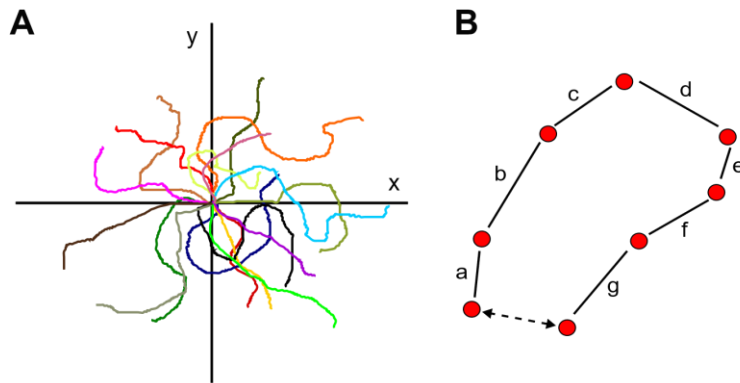


Figure 1 Commonly used motility parameters to quantify cell motility derived from intravital time-lapse imaging **A** Plotting of cell trajectories shifted with their starting point to the same location in space gives qualitative information of cell movement. **B** Straightness is calculated by dividing the displacement of the cell (dashed line) by its total path length (solid lines). Each of these two parameters can additionally be used as migratory parameters.

1.10 Aims of the work

The aim of this thesis was to provide a detailed characterization of intravascular migration of immune cells at the blood-brain barrier, including molecular cues and environmental factors that shape immune cell locomotion in the context of CNS autoimmune inflammation. To this end, intravital two-photon microscopy (TPLSM) was employed to record the intravascular migration behaviour of adoptively transferred encephalitogenic T cells and endogenous homeostatic monocytes during the preclinical phase of EAE *in vivo*. Further, we developed an advanced computational migration analysis to describe motility patterns of the recorded intravascular immune cell locomotion and to investigate how physical parameters of the CNS vascular bed influence immune cell motility patterns. Finally, to investigate the molecular cues

shaping motility patterns, we interfered with integrin- and chemokine signalling during intravital TPLSM and used RNA-sequencing for transcription profiling of immune cells and endothelial cells of the CNS vascular bed.

2. Material and Methods

2.1 Materials

2.1.1 Proteins

Myelin basic protein (MBP)	House-made from guinea pig (Eylar et al., 1974)
----------------------------	---

2.1.2 Antibodies

Primary Antibodies

Mouse anti-rat CD3 (clone)	Biolegend
Mouse anti-rat CD43 (clone W3/13)	Biolegend
Mouse anti-rat CD31 (clone TLD-3A12)	Bio-Rad
Mouse anti-rat CD172a (clone ED9)	Bio-Rad
Mouse anti-rat CD45 (clone OX-1)	Biolegend
Mouse anti-rat CD45RA (clone OX-33)	Biolegend
Mouse anti-rat granulocytes (clone RP-1)	BD Biosciences

Secondary Antibodies

Goat anti-mouse IgG (H+L) (allophycocyanin (APC) – Jackson ImmunoResearch conjugated)

2.1.3 Buffers and Media

ACK red blood cell lysis buffer	<ul style="list-style-type: none"> - 0.15 mol/L NH₄Cl (Carl Roth) - 1 mmol/L KHCO₃ (Carl Roth) - 0.1 mmol/L Na₂×EDTA (Carl Roth) - adjusted to pH 7.2 – 7.4 with HCl (Carl Roth)
Dulbecco's Modified Eagle's medium (DMEM)	<ul style="list-style-type: none"> - Gibco DMEM Powder (Invitrogen) - 1.2 g/l NaHC₃ (Carl Roth)
Digestion buffer	<ul style="list-style-type: none"> - EH (in-house production) - 0.4 U/ml Liberase TM (Roche) - 120 U/ml DNase I (Roche)
EH medium	<ul style="list-style-type: none"> - DMEM - 25 mM Gibco Hepes (Invitrogen)
Flow cytometry staining buffer	<ul style="list-style-type: none"> - 1×PBS (in-house production) - 0.5 % BSA (Carl Roth GmbH) - 2 mM EDTA (Carl Roth GmbH)

Freezing medium day 2	<ul style="list-style-type: none"> - 80 % heat-inactivated horse serum (Biochrom AG) - 10 % TCM (in-house production) - 10 % DMSO (Carl Roth)
Isotonic Percoll	<ul style="list-style-type: none"> - 9 vol Percoll (GE Healthcare) - 1 vol. 10×PBS (in-house production)
Lymphocyte separation medium LSM 1077	PAA
Phosphor buffered salt solution (PBS, 10)	<ul style="list-style-type: none"> - 8.10 mM Na₂HPO₄ (Carl Roth) - 1.47 mM NaH₂PO₄ (Carl Roth) - 137 mM NaCl (Carl Roth) - 2.68 mM KCl (Carl Roth) - adjusted to pH 7.2
Re-stimulation medium (RM)	<ul style="list-style-type: none"> - TCM (in-house production) - 1 % rat serum (in-house production)
T cell growth medium (TCGM)	<ul style="list-style-type: none"> - TCM (in-house production) - 10 % heat-inactivated horse serum (Biochrom AG) - 10 % conditioned medium from splenocytes treated with the mitogen Concanavalin A (ConA supernatant) (in-house production)
T cell medium (TCM)	<ul style="list-style-type: none"> - 10 ml sodium pyruvate (Invitrogen) - 10 ml L-glutamine (PAN Biotech GmbH) - 10 ml L-asparagine monohydrate (Sigma Aldrich) - 4 µl 2-β-mercaptoethanol (13.6 mol/L) (Invitrogen) per litre
Thawing medium	<ul style="list-style-type: none"> - 90 % EH medium (in-house production) - 10 % heat-inactivated fetal bovine serum (Biochrom AG)

2.1.4 Procedure kits

qPCR Master Mix	Eurogentec
RevertAid™ First Strand cDNA synthesis kit	Thermo Scientific
RNeasy® Micro Kit	Qiagen
RNeasy® Mini Kit	Qiagen
RNase-Free DNase Set	Qiagen

2.1.5 Chemicals/Sera/Solvents

Agarose Low Melt	Carl Roth
Beads (BD CaliBRITETM)	BD Bioscience
β -mercaptoethanol	Carl Roth
Chloroform	Carl Roth
Liposomes	Clodronate.org
Concanavalin A	Carl Roth
Concanavalin A supernatant	In-house production
Dextran tetramethylrhodamine (2.000.000 MW)	Invitrogen
Dextran Texas Red® (3.000 MW, 70.000 MW)	Invitrogen
Diethyl ether	Carl Roth
Dimethyl sulfoxide (DMSO)	Carl Roth
Distilled water DNase/RNase-free	Invitrogen
DMEM powder	Invitrogen
Ethanol	Carl Roth
DiA	Invitrogen
FAST DiITM oil	Invitrogen
Fetal bovine serum	Biochrom AG
Glycogen	Sigma
G418-Sulphate	Invitrogen
HEPES	Invitrogen
Horse serum	Biochrom AG
Hydrochloric acid (HCl)	Carl Roth
Incomplete Freund's Adjuvant	Difco Laboratories
Isoflurane	Abbott
Isotone sodium chloride solution (NaCl 0.9 %)	B Braun
Ketamine (10 %)	Medistar Arzneimittelvertrieb GmbH
M. Tuberculosis H37Ra	Difco Laboratories
Puromycin	Carl Roth
QIAzol® Lysis Reagent	Qiagen
Sodium chloride	Gibco
Trypan blue solution (0.4 %)	Sigma Aldrich
Trypsin EDTA (10-fold)	PAA
Xylarium	Ecuphar
2-propanol	Carl Roth
4',6-diamidino-2-phenylindole	Sigma Aldrich

2.1.6 RT-qPCR Primer and probes

β-actin Fwd	GTA CAA CCT TGC AGC TCC T
β actin Rev	TTG TCG ACG AGC GC
β actin Probe	CGC CAC CAG TTC GCC ATG GAT
rat VLA-4 Fwd	GAA GGA AGA GTG TTC GTG TAC ATC A
Tie-2: Few	AGGTACATAGGAGGAAACCTGTTCA
Tie-2 Rev	GGGTCCCCACTTCTGAGCTT
Tie-2 Probe	CTCGGCCTTCACCAGGCTGATTGT
Occludin Fwd	CCTAATGTGGAAGAGTGGGTAAATA
Occludin Rev	GTCGACTCTTTCCGCATAGTCA
Occludin Probe	CACACAAGACATGCCTCCACCCCC
Claudin-5 Fwd	CGGGCGTCCAGAGTTCAGT
Claudin-5 Rev	TAGACGTAGTTCTTCTTGTCGTAATCG
Claudin-5 Probe	CCAGTCAAGTACTCAGCACCAAGGCGA
CXCL 10 Fwd	CGT GCT GAG TCT GAG T
CXCL 10 Rev	GTC TCA GCG GCT GTT CAT
CXCL 10 Probe	CTC AAG GGA TCC CTC TCG CAA GAA C
CXCL11 Fwd	GGT TCC AGG CTT CGT TAT GTT C
CXCL11 Rev	AAC TTC CTT GAT TGC CAT T
CXCL11 Probe	CTG TCT TTG CAT CGA CCG CGG AGT
CXCL12 Fwd	GTC AAA CAT CTG AAA ATC CTC AAC AC
CXCL12 Rev	GGT CAA TGC ACA CTT GTC TGT
CXCL12 Probe	ACT GTC CCC TTC AGA TTG CAA GGC T

2.2 Methods

2.2.1 Animals

All experimental animals were Lewis rats on a LEW/CrI background (*Rattus norvegicus*). The animals were bred and kept at the animal facility of the University Medical Centre Göttingen (UMG). The animals were kept under standardized conditions with a 12/12 h light-dark cycle and were provided with food *ad libitum*. All experiments were performed according to local regulations of animal welfare of Lower Saxony.

2.2.2 Generation of transgenic T cell cultures

2.2.2.1 Immunization

To elicit generation of MBP- or OVA-specific CD4⁺ T cells, 6-8-week-old female Lewis rats were subcutaneously immunized (into the base of the tail and into the hind limb popliteal cavity) with 150 µl guinea pig MBP (Eylar et al., 1974) or OVA protein (each 1 mg/ml) emulsified in an equal volume of complete Freund's adjuvant containing *Mycobacterium tuberculosis* (2 mg/ml). The emulsion was prepared with the help of tuberculin glass syringes and a custom-made homogenizer. Animals were sacrificed for primary T cell culture 10 days after immunization.

2.2.2.2 Culture of packaging cells

Retroviral transduction of T cells was facilitated by co-culture with GP+E86 packaging cells, which produce a replication-deficient LifeAct-mTurquoise2- or eGFP-coding retrovirus. The retroviral vector pMSCV was used for the gene transfer of a puromycin resistance cassette in combination with the LifeAct-mTurquoise or eGFP sequence. GP+E86 packaging cells were cultured in selection medium (T cell medium (TCM) containing 10 % of fetal calf serum (FCS) and puromycin (2 µg/ml) in 10 cm cell culture dishes in an incubator set at 5 % CO₂ humidified atmosphere and 37°C. During cell culture, the adherent packaging cells form monolayers. The packaging cell line cultures were split upon reaching a confluence of 70- 80 % by washing once with 1×PBS, followed by 1-2 min incubation with the endopeptidase trypsin (10× stock solution diluted 1:10 with PBS). Once packaging cells started detaching from cell culture dishes, digestion was stopped by adding EH medium containing 10% FCS. Cells were centrifuged for 5 min with 1200 rpm at 4°C to remove trypsin-containing medium. The supernatant was discarded, and the pellet was resuspended in TCM containing 10 % of FCS and 2 µg/ml puromycin and replated.

2.2.2.3 Primary rat T cell culture

Retroviral engineering of T cells reactive against MBP or OVA to express fluorescent proteins was conducted as reported (Flügel et al., 1999). The cells were kept in a humidified atmosphere containing 10 % CO₂ at 37°C. To establish antigen-specific CD4⁺ T cell lines, draining lymph nodes (popliteal, inguinal, and paraaortal LNs) of immunized animals (see chapter 2.2.2.1) were isolated 10 days after immunization. The isolated LNs were mechanically dissociated through a metal mesh. Single-cell suspension then was pelleted (1200 rpm, 8 min, 4°C), supernatant discarded, and the cell pellet was resuspended and washed once with Eagles HEPES (EH) medium. Subsequently, 2 x 10⁵ lymph node cells per well were plated in a total volume of 100 µl re-stimulation medium containing 10 µg/ml of MBP (RM) in U-bottom 96-well plates, seeded with 1.5 x 10⁴ GP+E86 packaging cells. After 2 days of co-culture, T cell growth medium (TCGF) was added (50 µl per well). TCGF contains the supernatant of Concanavalin A stimulated murine splenocytes (ConA supernatant). ConA supernatant contains the cytokine IL-2, which induces the proliferation of T cells. On day 3 or 4 of primary cell culture, 50 µl of medium per well were removed and T cells were carefully aspirated and transferred into flat-bottom 96-well plates. After transfer 100 µl fresh TCGF containing puromycin (1 µg/ml) was added per well. Antibiotic selection with puromycin was maintained for 10 days. The first re-stimulation of T cells was performed 6 days after the start of the culture. Firstly, 100 µl medium per well were removed with a multi-channel pipette and subsequently 1.4 x 10⁶ irradiated thymocytes (irradiation dose 30 Gray [Gy]), that served as antigen-presenting cells (APCs), in 100 µl RM containing MBP protein (10 µg/ml) were added per well. Two days after re-stimulation 50 µl TCGF were added per well to induce T cell proliferation. Three to four days after re-stimulation, the wells with the best viral T cell transduction rate (measured by mTurquoise2 or eGFP fluorescence intensity and highest T cell density) were picked and pooled into 60 mm dishes.

2.2.2.4 Re-stimulation of T cells

Established primary T cell lines were further propagated with re-stimulation cycles every 6 days in 60 mm dishes. 3.5 x 10⁶ resting T cells were co-cultured with 70 x 10⁶ irradiated thymocytes (30 Gy) in RM containing the appropriate concentration of antigen (10 µg/ml MBP). Two days after re-stimulation, TCGF was added to the T cell culture to promote further proliferation. T cells were transferred into 10 cm culture dishes and split further when necessary to maintain optimal density.

2.2.3 Adoptive transfer EAE

Adoptive transfer EAE (atEAE) was induced by intravenous injection of 5×10^6 activated, encephalitogenic T cell blasts (day 2 after re-stimulation) in 1 ml of EH medium into the tail vein of naïve Lewis rats (between 6-8 weeks of age). Animals were anaesthetized in diethyl ether for tail vein injection. The body weight of the animals and clinical symptoms were followed and recorded over the whole experimental period. Clinical signs of EAE were assessed according to the following score system: 0, no sign of disease; 0.5, loss of tail tonus; 1, tail paralysis; 2, gait disturbance; 3, hind limb paralysis; 4, tetraparesis and 5, moribund. Animals were sacrificed when reaching a score of 3.5.

2.2.4 Intravital live imaging with the two-photon laser scanning microscope

In vivo imaging of T_{MBP}-GFP OR T_{MBP}-LifeAct-mTurquoise2 (TMBP-LA) cell motility and behaviour was conducted with two-photon laser scanning microscopy (TPLSM) within the CNS meningeal compartments in living animals. In order to access the dorsal spinal cord meninges, the well-established “open spine window” procedure was performed as previously described (Bartholomäus et al., 2009).

2.2.4.1 Surgical procedure for intravital TPLSM

Animals were anaesthetized by intra-muscular injection of 10mg kg⁻¹ xylazine combined with 50mg kg⁻¹ ketamine. Thereafter, animals were intubated via a small tracheotomy and immediately ventilated with 1.5–2% isoflurane using a custom-built ventilation system. This system was driven by an Inspire Advanced single animal pressure-controlled ventilation machine. The ventilator was fed by medical oxygen mix with pressurized air before the gas mixture was routed through an isoflurane vaporizer. During imaging, animals were stabilized in a custom-made microscope stage and their body temperature was maintained through a heating pad connected to a custom-built thermo controller at 37°C. Sterile saline (0.9 % NaCl) was supplied via a tail vein catheter during intravital imaging using a Perfuse FM device to prevent dehydration. For intravital TPLSM recordings of the leptomeninges, a spinal cord window was prepared as described previously at level Th12/L1 (Bartholomäus et al., 2009). Briefly, the skin was incised 2–3cm on the back of the animals, followed by subsequent detachment of the paravertebral musculature from the spine. Next, a laminectomy was performed on one of the three exposed vertebral bodies. Exposed meningeal tissue was immediately covered with physiological 0.9% NaCl solution to prevent dehydration.

2.2.4.2 Two-photon laser scanning microscopy

TPLSM was performed using a LSM710/Axio Examiner. Z1 confocal microscope combined with a >2.5Watts Ti:Sapphire Chameleon Vision II Laser device. The excitation laser wavelength was tuned to 880nm or 1100nm and routed through a 20x waterNA1.0 immersion objective W Plan Apochromat. Scanning areas were 424.27 μm x 424.27 μm in height and width (512 x 512px) with 50–100 μm z-stacks acquired. Images were acquired with bidirectional scanning and 2-times line averaging at a rate of approximately 1.3s per z-plane. For reproducible motility analyses, the time interval between z-volume acquisitions was kept exactly to 32sec by varying the numbers of z-sections (usually between 18 and 25) or distances between 2 z-planes (step-size, typically between 2 and 6 μm). Emitted fluorescence was detected using non-descanned detectors equipped with 442/46nm (second harmonic signal), 525/50nm (GFP, mTurquoise2), 550/49nm (FITC-dextran), and 624/40nm (DiI or DiA labelling) band-pass filters.

2.2.5 Processing of raw data from IVM

TPLSM time-lapse recordings were acquired and processed by Zen 2009 Software obtaining 2D movies/images by generating maximum intensity projections out of 3D-and 4D stacks. For representation, time-lapse videos and images were exported as .avi or .tif files, respectively, without any compression algorithm. 2D data were further processed using ImageJ 1.46i software. Brightness and contrast as well as colour balance adjustments of single channels were performed with implemented plugins. Annotations were made using ImageJ and Inkscape (version 0.92.3).

2.2.6 Analysis of leukocyte motility

Imaris 8.0.1 software was used for 4D analysis of acquired raw time-lapse data. Immune cells were tracked with the automated Imaris Track module with subsequent manual revision. Motility parameters including leukocyte mean speed, displacement length, total track length, crawling duration, and straightness were calculated from the obtained x, y, z-coordinates using the Imaris statistics function. Rolling T cells appeared as several round-shaped dots in the direction of the blood flow as described (Bartholomäus et al., 2009). Cells that were visible for less than 2 frames (~1min) were excluded from the analysis. The straightness was defined as the ratio between direct displacement length between start- and endpoint of leukocyte movement and the sum of all single displacement steps during a 30min time interval. Statistical evaluations were performed with the statistical software R 3.5.0.

2.2.7 Hierarchical clustering analysis of leukocyte cell motility

To develop this new tool, we employed unsupervised machine learning, i.e., hierarchical clustering. This approach is often used for the classification of problems where features of unknown (unlabelled) data are used to detect “hidden” (common) structures in the data. Hierarchical clustering employs a “bottom-up” strategy where each observation starts in its own cluster and pairs of clusters are merged as the algorithm moves up in hierarchy until only one cluster is left. The results of hierarchical clustering are usually presented as a dendrogram. (Figure 2). As input for the clustering algorithm, we used several motility parameters of the tracked cells. The rationale behind this was the assumption that the migratory pattern is encoded by the combined migratory parameters of the cells. The combined input parameters were the following: velocity (speed), track length, track duration, track displacement length, straightness, and median angle to blood flow. All the parameters were derived from software-based 4D (x-y-z-t) cell tracking of the acquired intravital TPLSM imaging data, from a total of 4739 cells. This pool included 979 T_{MBP} cells and 3760 DiI^+ monocytes. Corresponding cell numbers and clinical phase at intravital TPLSM recording are summarized in Table 1. For the unsupervised classification of migratory patterns, we arbitrarily chose to stop clustering at six clusters. This results in a number of motility classes that is higher than what we used in the manual classification analysis, therefore taking into consideration the higher complexity of migratory patterns exhibited by DiI^+ monocytes but leading to a still interpretable number of classes. The pre-processed motility parameter data was clustered using the trackdescriptor package for the statistical programming language R. As a readout, if the unsupervised classification was successful and lead to interpretable classes, the representative cell track for each of the six clusters was visualized for inspection and validation purposes. The representative member of a cluster is the object which has the least distance (dissimilarity) to all the other members of that cluster and can be seen as the mean, also called a medoid. The representative members of each of the six clusters derived from hierarchical clustering are depicted alongside the unique “fingerprint”, which are the normalized motility parameters values used for clustering of the respective cluster representative, in Figure 13.

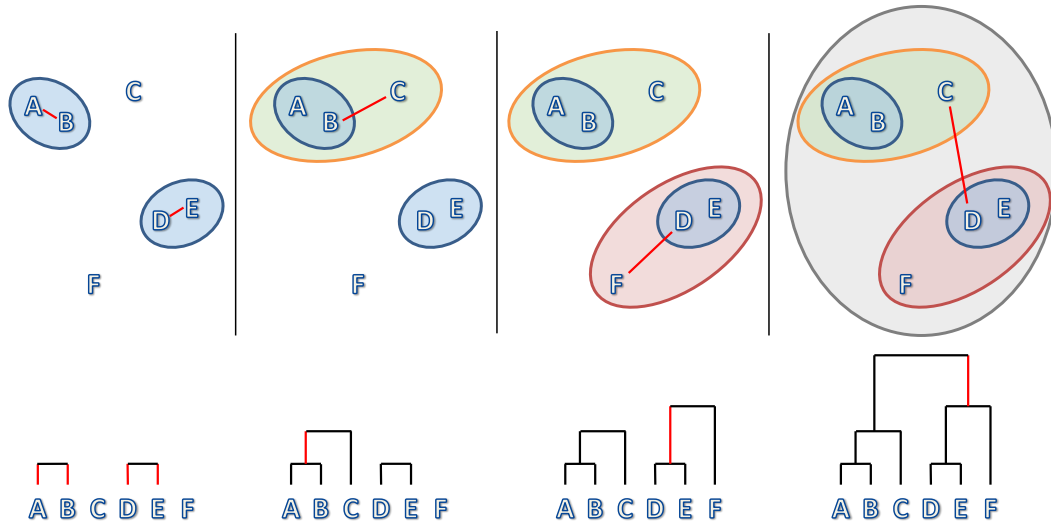


Figure 2 Hierarchical clustering uses a “bottom-up” approach to achieve clustering. Diagram graphically depicting hierarchical clustering from the individual elements by progressively merging clusters based on pairwise distance measurement. Letters represent objects in the data on which hierarchical clustering is applied. In each iteration, the objects with the least dissimilarity are merged.

2.2.8 Labelling of myeloid cells for IVM

To visualize monocytes along with fluorescent T cells during intravital TPLSM, phagocytic activity of monocytes in the blood circulation was exploited. Briefly, 18 h before intravital imaging fluorescently stained liposomes were intravenously injected into the tail vein of the animals. Furthermore, a monoclonal antibody against CD11b (Hybridoma clone OX-42) labelled with the fluorescence dye SeTau647 was injected directly before TPLSM to label all blood-borne myeloid cells.

2.2.9 Animal preparation and organ processing

Rats were sacrificed by CO₂ inhalation at indicated time points after induction of adoptive transfer EAE and immediately transcardially perfused with 50 ml ice-cold PBS. All dissected tissues were kept in EH medium on ice. Tissues were weighed before further processing to be able to normalize numbers of infiltrated cells to tissue weight. Organs were then processed as described below.

2.2.10 Isolation of PBMCs from blood

To isolate peripheral blood monocytic cells, blood was taken by cardiac puncture into 5 ml syringes containing 300 µl 80 mM EDTA solution. Blood samples were mixed with an equal volume of 1×PBS and layered over 0.5 volumes lymphocyte separation medium (LSM 1077). Sample gradients were centrifuged at 2000 rpm, 22°C for 30 min with minimal acceleration

and brakes turned off. PBMCs were taken from the interphase between plasma and separation medium, transferred into a new Falcon tube and washed with cold 1×PBS, and resuspended in 1 ml EH medium.

2.2.11 Isolation of leukocytes from spleen

Dissected spleens were mechanically dissociated through a metal grid in EH medium to prepare single-cell suspensions. After centrifugation at 1200 rpm for 8 minutes at 4°C, the cell pellet was resuspended in 4 ml ACK buffer for erythrocyte lysis and incubated for 4 minutes on ice. Subsequently, Falcon tubes were filled up with cold 1×PBS, and cells were washed and resuspended in 15 ml EH medium.

2.2.12 Isolation of leukocytes from spinal cord and spinal cord meninges

Spinal cords were dissected from spinal column and the meninges were removed from the parenchyma. Tissues were homogenized in EH medium through a metal grid and cells were spun down (8 minutes at 1200 rpm at 4°C). To remove myelin and debris from cell suspension, cells were centrifuged on a two-phase Percoll gradient. For this, cell pellets were resuspended in 25 ml EH medium and mixed with 10 ml isotonic Percoll solution, followed by carefully layering of 10 ml underlay Percoll under the cell suspension. The gradient was centrifuged with 2780 rpm for 30 minutes at room temperature with minimum acceleration and no brakes. The interphase of the sample was collected using Pasteur pipettes, transferred to a new tube, spun down (1200 rpm for 8 minutes at 4°C) and washed with cold 1×PBS. The supernatant was discarded, and cell pellet was resuspended in 1ml EH medium.

2.2.13 Isolation of endothelial cells from spinal cord meninges and parenchyma

Spinal cords were dissected, and the meninges were removed from the parenchyma. Spinal cord parenchyma was homogenized in EH-medium in a Dounce-homogenizer with 5 strokes with pastel A and 20 strokes with pastel B. Spinal cord meninges were cut in fine pieces with scissors in EH medium. Spinal cord meninges and parenchyma homogenates were centrifuged at 1200 rpm for 6 minutes, supernatant was discarded, and the pellets were taken up in 3 and 5 ml of digestion buffer, respectively. Tissues were digested in a water bath at 37°C for 1h with gentle pipetting of the solution every 6 minutes. Tissue solutions were brought to a final volume of 14 ml with cold EH-medium with 2mM EDTA and passed through a 40µm cell strainer. To remove myelin debris, 6ml of isotonic Percoll solution was added to cell suspensions and gradient centrifugation was carried out at 2780 rpm for 30 min without brakes. The supernatant was removed, and cell pellets were washed with 50 ml EH plus 2mM EDTA, spun down for 5 min

at 1200 rpm, and pellets were taken up in 200 µl staining buffer for FACS-staining followed by FACS-sorting.

2.2.14 Flow cytometry

Single-cell solutions were surface-stained on ice at a concentration of $1-5 \times 10^6$ cells per sample in 100 µl FACS buffer with combinations of monoclonal antibodies labelled with fluorochromes for 30 minutes. After staining, the samples were washed and resuspended in 100 µl FACS buffer. Stained cells were analysed on a Beckman Coulter CytoFLEX flow cytometer. Final analysis was performed using CytExpert (Beckman Coulter) and FlowJo (BD Biosciences) software. The transferred T cells could be tracked due to their expression of fluorescent reporter proteins.

2.2.15 Cell sorting

Animals were sacrificed by CO₂ inhalation and immediately transcardially perfused with 50ml ice-cold 1×PBS. Tissues were dissected and prepared as described above. Cell sorting was performed using a BD FACSAria III with minimum flow speed at 4°C. The sorted cells were transferred into Eppendorf tubes and centrifuged with 300×g for 4 minutes at 4°C. The cell pellet was resuspended in 500 µl QIAzol Lysis Reagent and stored at -80°C until further processing.

2.2.16 RNA isolation, cDNA synthesis and RT-qPCR

RNA isolation from QIAzol samples was performed according to the manufacturer's protocol. Subsequently, cDNA synthesis was performed using RevertAid First Strand cDNA Synthesis Kit with random hexamer primers as described in the manufacturer's protocol. Real-time quantitative PCR (RT-qPCR) was performed with the qPCR master mix on a StepOnePlus Real-Time PCR system using target-specific FAM and TAMRA labelled TaqMan probes. Analysis was done using StepOnePlus Software v2.0. The expression was normalized to that of the housekeeping gene beta-actin using the delta-delta Ct method ($2^{-\Delta\Delta C_t}$).

2.2.17 RNA-sequencing and library preparation

RNA for sequencing was isolated from QIAzol samples. Library preparation and sequencing were performed at the Microarray and Deep-Sequencing Core Facility of the University Medical Centre Göttingen.

2.2.18 RNA-sequencing analysis

The raw sequencing files (FASTQ files) were quality-controlled with FastQC and MultiQC software. Reads were aligned to the Ensembl rat transcriptome Rnor_6.0 (Ensembl release 94) and quantified with Salmon software (Patro et al., 2017). Gene-level abundance estimates were generated and imported in R statistical software (3.5.0) with the R package tximport (Soneson et al., 2016). Differential expression analysis of isolated leukocytes was performed with the DESeq2 R package (Love et al., 2014). Specifically, the data were normalized and tested for differentially expressed genes based on a generalized linear model likelihood ratio test assuming negative binomial data distribution. Candidate genes were filtered to a minimum of 2-fold change ($\log_2 1$) and adjusted p-value < 0.05 . The Benjamini-Hochberg false discovery rate procedure was used to correct p values for multiple testing. Heat maps of differentially expressed genes between leukocytes were generated with the R package pheatmap.

For the ligand-receptor analysis, a list of receptor-ligand pairs was assembled from databases and literature (Ramilowski et al., 2015). To extract meaningful receptor-ligand pairs that are associated with cell migration and adhesion and that are located in the extracellular domain, a list of relevant GO terms was generated, and genes annotated with these GO terms were queried from databases in the R/Bioconductor environment using the biomaRt package. The intersection of these two lists was used as the receptor-ligand pair list and used as input for further analysis. Next, using the lists of differentially expressed genes defined above, all receptors were selected that were upregulated in any of the leukocyte subpopulations. This resulted in receptor lists of T cells, inflammatory and homeostatic monocytes. Then ligands present on leptomeningeal blood vessel endothelial cells were extracted by filtering all genes expressed higher than a normalized expression value of 10 and intersecting this list with the list of ligands defined in the first step of the analysis. Last, the number of receptor-ligand interactions of each leukocyte population with endothelial cells were quantified.

2.2.19 Interference with integrin signalling

To block $\alpha 4\beta 1$ integrin signalling, a neutralizing mouse anti-rat monoclonal antibody against VLA-4 (anti-CD49d, clone TA-2; Hojo et al., 1998; Issekutz and Wykretowicz, 1991) was injected i.v. at a concentration of 4mg kg^{-1} during intravital TPLSM recordings. Prof. Thomas Issekutz kindly provided the antibody (Grace Health Center, Dalhousie University, Halifax, Canada). After recording, saturated binding of the antibody was controlled as described (Bartholomäus et al., 2009). To block $\alpha L\beta 2$ integrin signalling, a blocking mouse anti-rat

monoclonal antibody against LFA-1 (anti-CD11a, clone WT.1) was injected i.v. at a concentration of 4mg kg^{-1} during intravital TPLSM recordings.

2.2.20 Interference with chemokine signalling

For intravital studies focusing on intraluminal leukocyte migration, $20\mu\text{g kg}^{-1}$ pertussis toxin A Oligomer was applied during the intravital imaging intravenously via an OPS 50 ml Luer lock infusion set with a total volume of 1 ml.

2.2.21 Hybridoma culture and monoclonal antibody production

In order to produce monoclonal antibodies for *in vivo* applications the hybridoma cell lines OX-42, RP-1, RP-3, and WT.1 were used. Hybridoma were cultured in RPMI medium containing 10% FCS. Cells were subcultured every 2-3 days. For antibody production cells were pelleted with 1200 rpm for 8 min at 4°C and resuspended in serum-free PFHM II medium. Cells were then cultured for 10-14 days without further subculturing until most of the cells were dead. Hybridoma supernatant containing the desired antibodies was harvested by centrifugation of cultures and immediately frozen at -20°C until further processing.

Antibody purification was performed using HiTrap Protein G Purification 1ml columns according to the manufacturer's protocol. Eluates from purifications were buffer exchanged to $1\times\text{PBS}$ using PD-10 desalting columns and subsequently measured for protein concentration by NanoDrop measurement.

3. Results

3.1 Monocytes closely follow infiltrating T_{MBP} cells into the CNS during atEAE

The kinetic of myeloid cell recruitment was investigated during EAE induced by adoptive transfer of 5×10^6 activated T cells reactive against the myelin component myelin basic protein (MBP). To allow tracking of these auto-antigen-specific T cells, e.g. by intravital TPLSM or flow cytometry, they were retrovirally transduced to stably express the fluorescent reporter GFP (T_{MBP}-GFP) (Flügel et al., 1999). The kinetic of recruitment of the transferred T cells and endogenous monocytes in different organs including spleen, blood, spinal cord meninges, and spinal cord parenchyma and at different time points post EAE induction was investigated by flow cytometric quantification. For this purpose, endogenous monocytes were surface stained for CD172a and CD43. Two main subpopulations of monocytes could be discriminated in flow cytometry, CD172a⁺ CD43^{high} (homeostatic monocytes) and CD172a⁺ CD43^{low} (inflammatory monocytes) (Ahuja et al., 1995) (Figure 3). Flow cytometric quantification of monocytes in naïve animals showed that the CD172a⁺ CD43^{high} monocyte subpopulation was more prevalent than the CD172a⁺ CD43^{low} monocyte population in blood and the spleen. Notably, even in naïve animals, a small number of monocytes could be detected in the spinal cord meninges and parenchyma. The appearance of T_{MBP} cells in the circulation was accompanied by increasing numbers of both monocyte subpopulations. However, the number of circulating monocytes dropped on day 3 p.t. when an increase of monocytes in the meninges of the spinal cord could be observed, suggesting recruitment of monocytes from the circulation to spinal cord meninges. The number of recruited monocytes in the meninges peaked one day later (4 d.p.t.). Invasion of monocytes into the spinal cord parenchyma started on day 3 p.t. One day later (4 d.p.t.) parenchymal infiltration of monocytes reached its maximum (Figure 4). The peak of monocyte recruitment to the spinal cord meninges and parenchyma coincided with maximal T_{MBP} cell infiltration in the respective tissues (Figure 4). Of note, in the CNS at all the observed time points the CD172a⁺ CD43^{low} monocytes were more frequent than the CD172a⁺ CD43^{high} monocyte population. This data show that despite both monocyte populations are infiltrating the spinal cord meninges and spinal cord parenchyma during atEAE.

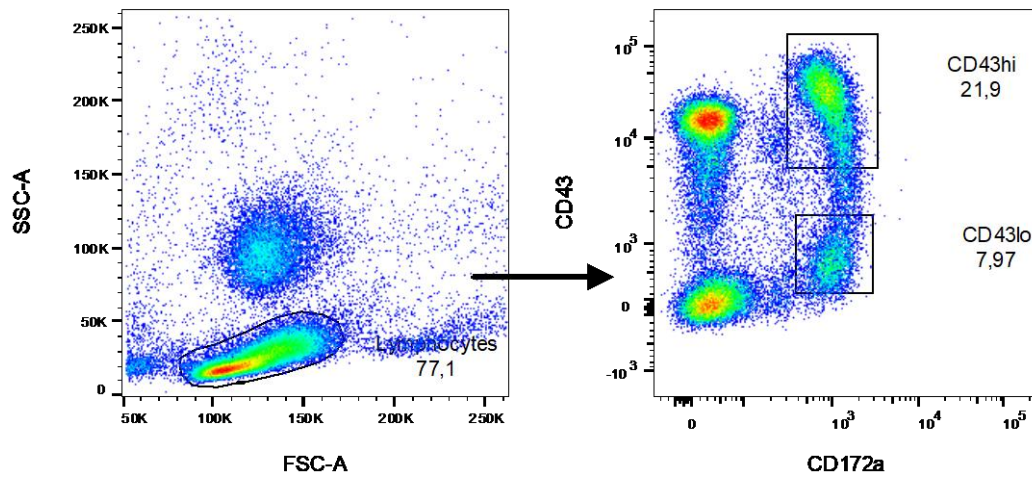


Figure 3 Rat monocyte subpopulations can be discriminated by their expression of CD43. Flow cytometric analysis of peripheral blood monocytic cells (PBMCs). Monocyte subpopulations express CD172a. The majority of monocytes are CD172a⁺ CD43^{high}. Plots from flow cytometry of PBMCs from naïve animals. Cells were surface stained for CD172a and CD43. A representative plot from at least 3 independent experiments is shown.

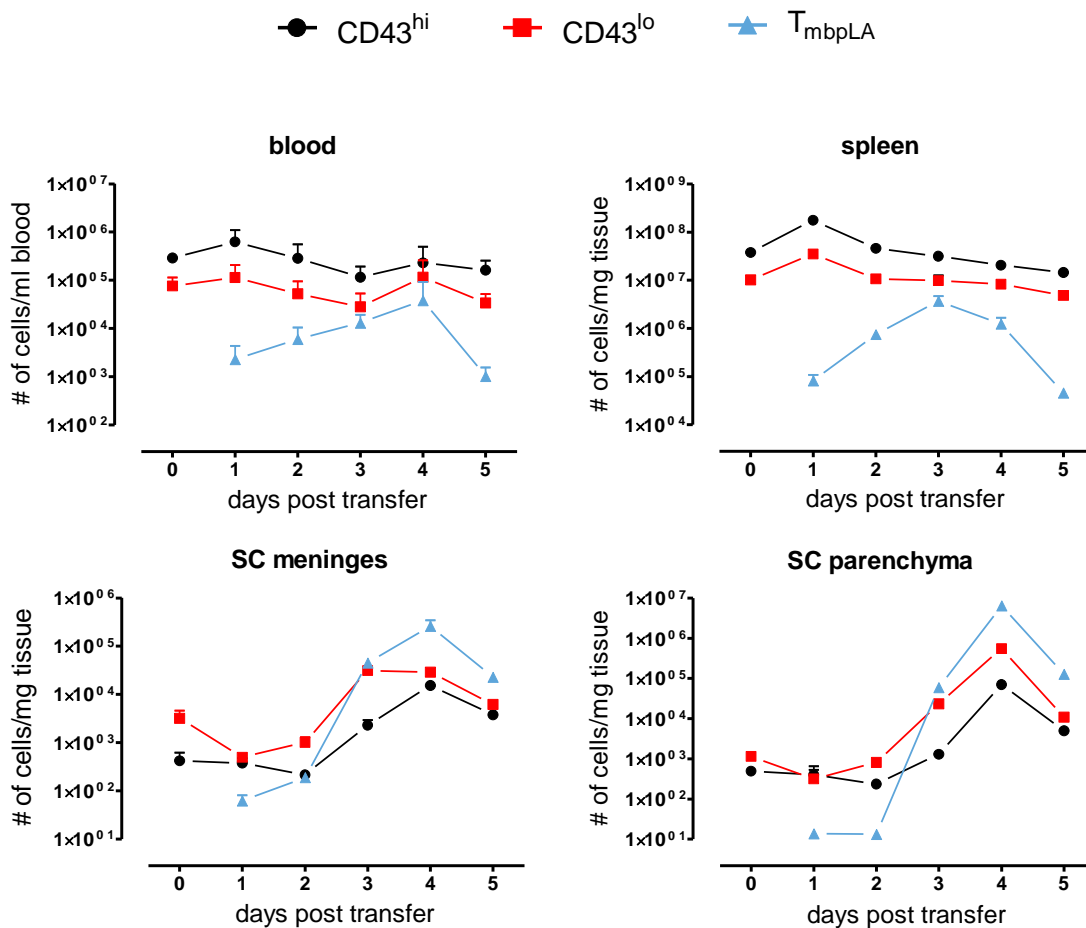


Figure 4 Infiltration kinetic of T_{MBP-LA} cells and monocytes during atEAE. Flow cytometric quantification of T_{MBP-LA} and CD172a⁺ CD43^{high} and CD172a⁺ CD43^{low} monocyte subpopulations during the time course of atEAE

induced by transfer of 5×10^6 T_{MBP-LA} cells on d0. Spleen, blood, spinal cord meninges, and parenchyma were taken daily. Numbers of monocytes and transferred T_{MBP} cells were quantified by flow cytometry.

3.2 Visualization of monocytes in the leptomeninges of the spinal cord

3.2.1 Labelling of monocytes by intravenous injection of fluorescent liposomes

In order to study the migratory behaviour of monocytes in the leptomeninges of the spinal cord by intravital TPLSM, we first established a labelling set-up to visualize these cells. In the mouse, the resident monocyte subpopulation characterized by low surface expression of Ly6C, high expression of the fractalkine chemokine receptor CX_3CR1 , and low expression of the chemokine receptor CCR2, can be marked by intravenous injection of fluorescently labelled liposomes which are taken up by these cells due to their high phagocytic activity (Sunderkötter et al., 2004). This monocyte subpopulation is correspondent to the $CD43^{high}$ monocytes in the rat (Strauss-Ayali et al., 2007).

This approach for labelling the cells was adapted to the rat model. Liposomes were stained with the lipophilic dyes DiI or DiA and injected intravenously into naïve rats. Intravital TPLSM of the leptomeninges of the spinal cord was performed on these animals 24 hours after liposome injection. DiA^+ cells could be detected inside the vessels of spinal cord leptomeninges (Figure 5 A). Some of the cells were associated to the vessel walls, migrating along them. Trajectories derived from cell tracking with IMARIS software are shown in Figure 5 B.

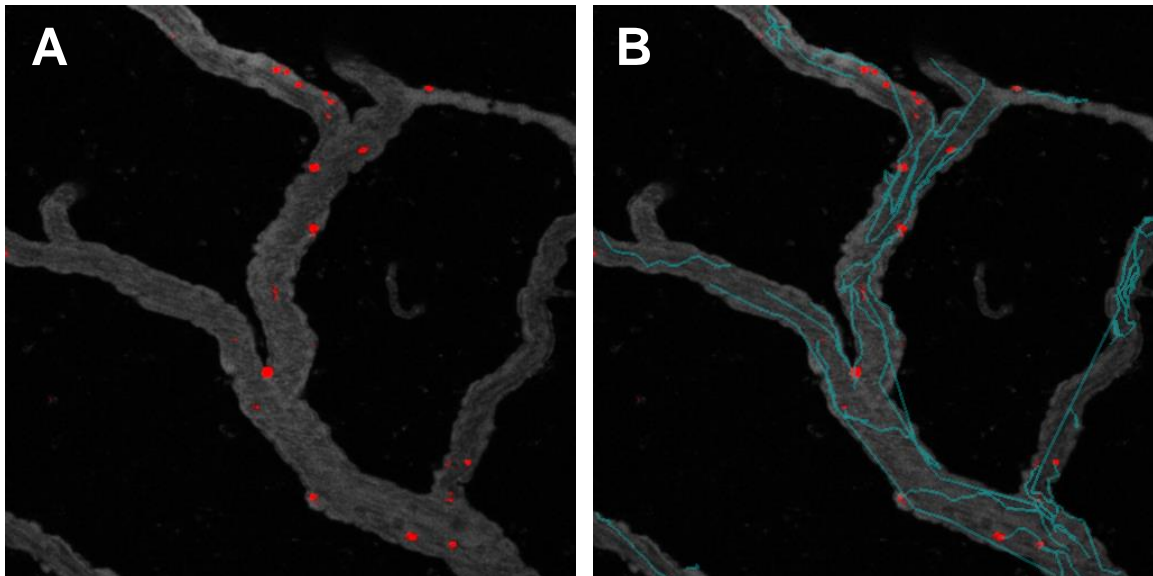


Figure 5 Phagocytic cells in the blood circulation can be visualized in the leptomeninges in vivo by intravenous injection of DiA stained liposomes. Intravital TPLSM recordings of the leptomeninges of the spinal cord. Liposomes were stained with the lipophilic dye DiA and injected i.v. into naïve Lewis rats. TPLSM was performed 24 hours after injection. Leptomeningeal vessels were visualized by i.v. injection of 70kDa FITC labelled Dextran (grey) immediately before image acquisition. A. Original snapshot of DiA^+ cells (red) migrating on the vessel endothelium A and 30 min trajectories (blue, B) are represented.

3.2.2 Characterization of liposome up-taking cells

Although it was possible to label cells by intravenous injection of fluorescent liposomes, the identity of these liposome-up-taking cells was not known. In order to elucidate their identity and characterize them, blood was taken from naïve animals 24 hours after i.v. injection of DiI-stained liposomes. Peripheral blood cells were surface-stained for CD3 and CD45RA, specific markers for T- and B-lymphocytes respectively, CD172a which is specific for monocytes, and for RP1, a marker specific for neutrophils. Flow cytometry analysis revealed that CD3⁺ T-lymphocytes, as well as CD45RA⁺ B-lymphocytes, were negative for DiI (Figure 6A). Among the investigated leukocyte subpopulations only CD172a⁺ monocytes were positive for DiI (Figure 6 A) and thus taking up the DiI-liposomes. When the total monocyte population was investigated further by surface staining of CD43, it became apparent that the majority of the DiI-liposome up-taking cells were of the CD172⁺ CD43^{high} subpopulation (Figure 6 B). The flow cytometry data was confirmed on the mRNA level by RT-qPCR. CD172a⁺ DiI⁺ monocytes isolated from blood by FACS-sorting expressed higher levels of CX₃CR1 compared to the FACS-sorted CD172a⁺ DiI⁻ monocytes (Figure 7 A). The opposite was observed for expression levels of CCR2. Here the DiI⁻ monocytes expressed higher levels of mRNA than the DiI⁺ monocytes (Figure 7 B). Taken together these data show that CD172a⁺ CD43^{high} monocytes can be labelled with DiI-liposomes allowing to study their migration behaviour *in vivo* by TPLSM.

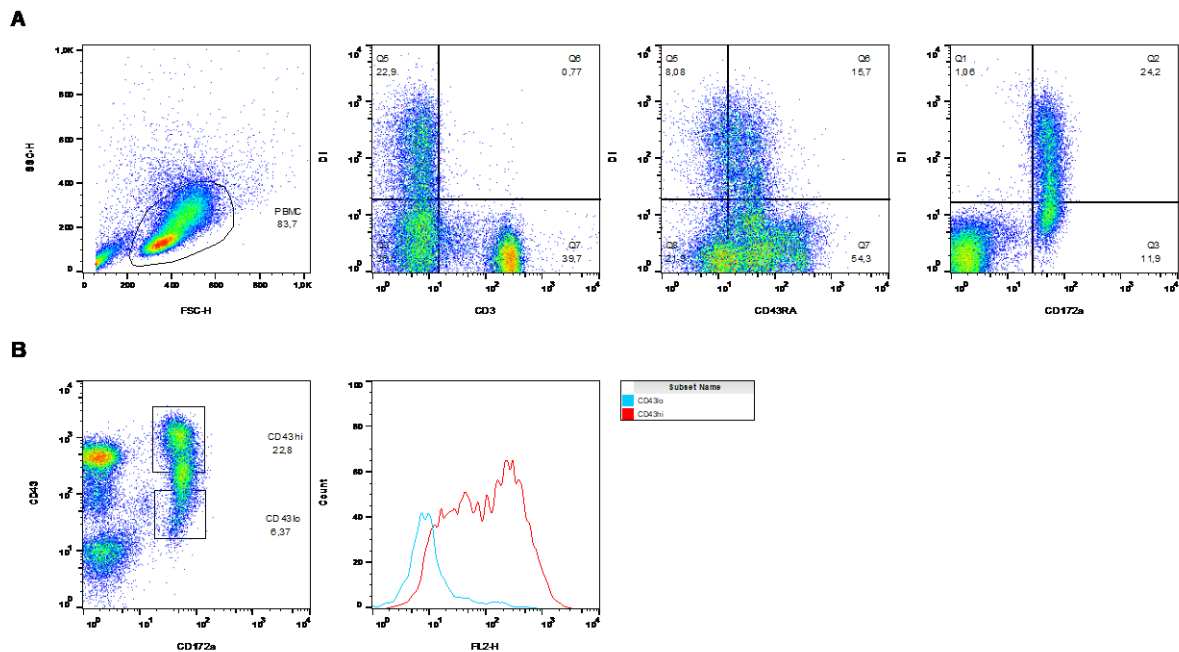


Figure 6 CD172a⁺ CD43^{high} monocytes mainly take up fluorescent liposomes in the circulation. Flow cytometry analysis of blood leukocytes 24 hours after i.v. injection of DiI-labelled liposomes. **A** Uptake of DiI positive liposomes in CD3⁺ T lymphocytes, CD45RA⁺ B lymphocytes, CD172a⁺ monocytes, and RP1⁺ neutrophils. Only monocytes were positive for DiI. **B** Uptake of DiI positive liposome in CD43^{high} and CD43^{low} monocyte subpopulations. CD43^{high} monocytes constituted the majority of the liposome-up-taking monocytes. Representative dot plots from 3 independent experiments.

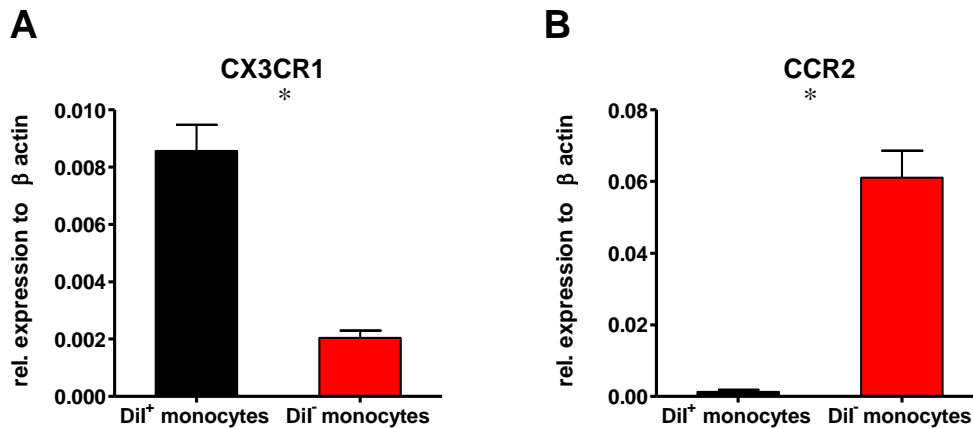


Figure 7 Chemokine receptor expression in DiI positive and negative monocytes. Blood-derived CD172⁺ DiI⁺ and CD172⁺ DiI⁻ monocytes were FACS sorted. Isolated mRNA from both subpopulations was analysed by RT-qPCR. Expression of **A** CX3CR1 and **B** CCR2 for monocyte subpopulation is shown as relative expression to β -actin. Data from 3 independent experiments. Bars represent mean \pm SEM.

3.3 Migratory behaviour of monocytes in spinal cord leptomeninges during atEAE

Having established a method for *in vivo* labelling of monocytes by intravital TPLSM, we next studied their kinetic and migratory behaviour in the leptomeningeal vessels by intravital TPLSM during adoptive transfer EAE. Therefore, EAE was induced in Lewis rats by intravenous transfer of 5×10^6 activated T_{MBP} cell blasts. Intravital TPLSM was performed every day, starting from d0 until d5 after T cell transfer. 24 hours before imaging endogenous monocytes were labelled by DiI-liposome injection. On d0 we observed only few DiI⁺ monocytes migrating along the endothelium of the leptomeningeal blood vessels. On day 1 p.t., even before the first encephalitogenic T cells arrived at the leptomeninges, numbers of intraluminal migrating DiI⁺ monocytes increased (Figure 8). With EAE progression, increasing numbers of DiI⁺ monocytes were recruited to the spinal cord leptomeningeal vessels and their numbers peaked 3 d.p.t. (Figure 8). At this time point, T_{MBP} cells had transgressed the vascular wall, were evenly distributed in the subarachnoid space (SAS) and started to infiltrate the spinal cord parenchyma. Starting from day 4 p.t., the number of DiI⁺ monocytes in the vessels steadily

decreased. The observations from the intravital TPLSM were in line with the FACS quantification of monocytes (Figure 4). The quantitative increase of the intraluminal DiI⁺ monocytes with disease progression was associated with changes in their motility patterns and migratory phenotypes. On day 0 the few DiI⁺ monocytes moved very straight in the direction of the blood flow. Starting from 2 days post transfer, when also T_{MBP} cells arrived at leptomeningeal blood vessels, the DiI⁺ monocytes became more confined in their migration behaviour. This phenomenon was most prominent between 3-4 days p.t., when T_{MBP} cells started to infiltrate the spinal cord parenchyma and animals showed clinical symptoms. Software-based 4D (x-y-z-t) cell tracking of the acquired intravital TPLSM imaging data confirmed that the motility parameters of the monocytes changed with EAE progression. The cells became slower, the time spent migrating on the vessel endothelium increased and the straightness of the cell trajectories decreased (Figure 9 A-C). These changes indicated that starting with the appearance of the first T_{MBP} cells, DiI⁺ monocytes adhered more tightly to vascular endothelial cells and intensified scanning of the vessel lumen.

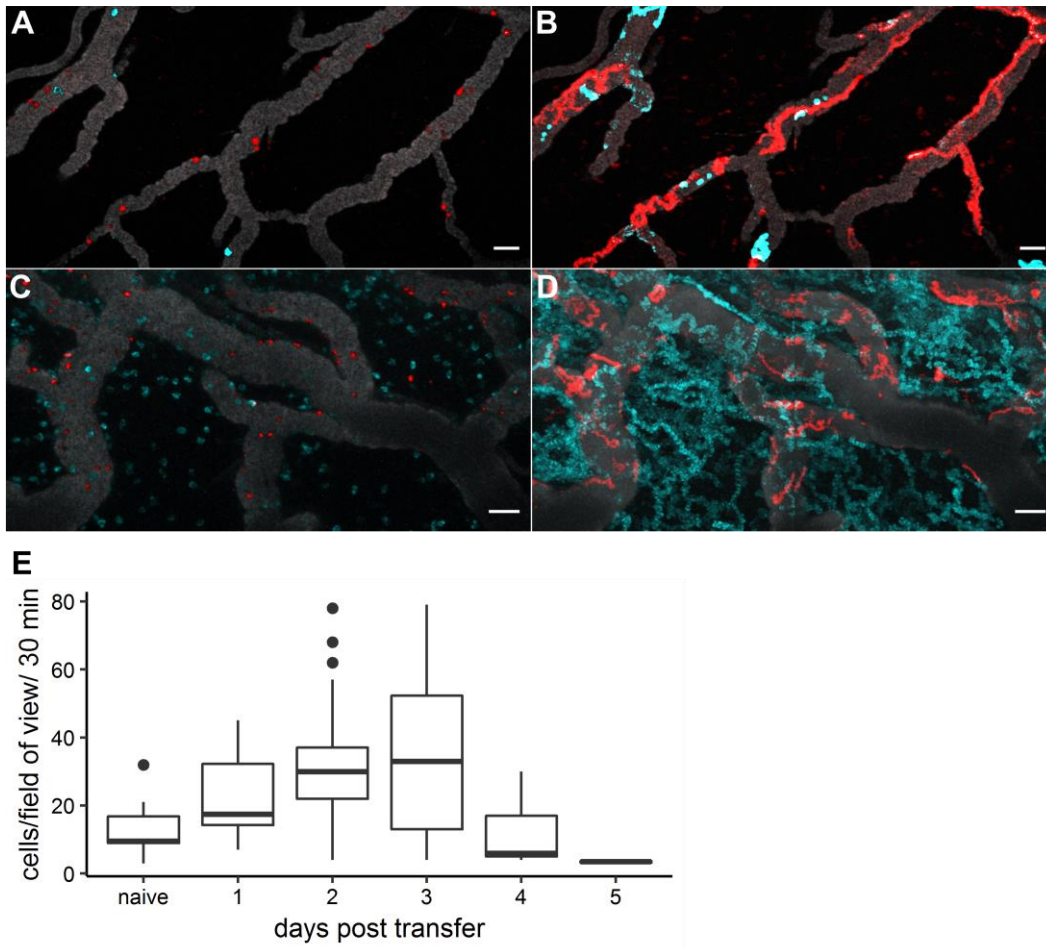


Figure 8 DiI⁺ monocytes accumulate at the spinal cord leptomeninges during EAE. A-D Intravital TPLSM recordings of spinal cord leptomeninges on 2 and 3 days post transfer of T_{MBP} cells. Grey: vessel lumen. Cyan: T_{MBP} cells. Red: DiI⁺ monocytes. Right panels are time projections of left images. Representative recordings from at least 3 independent experiments per time point depicted. E Quantification of DiI⁺ monocytes attached to the vessel/field of view per time point shown. Data from at least 3 independent experiments depicted.

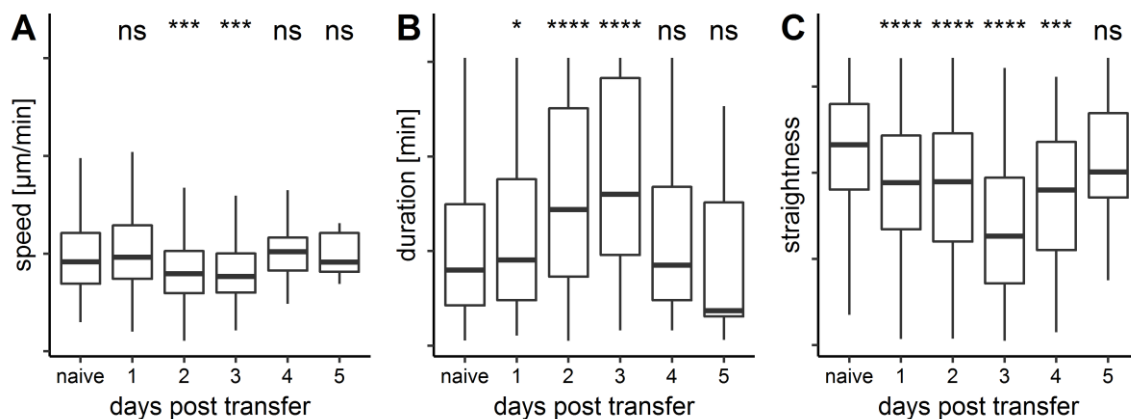


Figure 9 DiI⁺ monocytes change their motility parameters during EAE. Data are based on 30 min intravital TPLSM recordings in the spinal cord leptomeningeal vessels during EAE. A Average velocities, B track duration and C track straightness are depicted at the indicated days post TMBP cell transfer. Boxplots are depicted as 10-90 percentile. Data include 1680 cells from at least 3 independent experiments per time point. *P<0.05, **P<0.01, ***P<0.001, Kruskal-Wallis-Test with naïve as reference sample.

Furthermore, it became apparent during cell tracking that DiI⁺ monocytes exhibited very heterogeneous migration modes compared to the transferred autoreactive T cells (Bartholomäus et al., 2009) and these modes changed during EAE progression. To quantify their prevalence, we classified the migration modes of DiI⁺ monocytes into four classes: 1) cells rolling along vessel endothelium and only transiently adhering to vessel endothelium. 2) Cells migrating very straight in the direction of the blood flow. 3) Cells migrating independently of the direction of the blood flow, looping inside vessel lumen. 4) Cells with a very confined migration (Figure 10 A). Quantification of the migratory phenotypes showed that before the arrival of T_{MBP} cells in the leptomeningeal blood vessels the majority of DiI⁺ monocytes exhibited straight migration in the direction of the blood flow with the next most prevalent migration mode being rolling. Only a minority of cells showed independent or confined migration modes (Figure 10 B). With EAE progression the percentage of straight migration and rolling cells decreased and DiI⁺ monocytes switched to independent crawling and confined migratory phenotypes (Figure 10 B). These results corroborated the previous findings and suggested that with increased inflammation during EAE DiI⁺ monocytes adhered more tightly to the vessel endothelium.

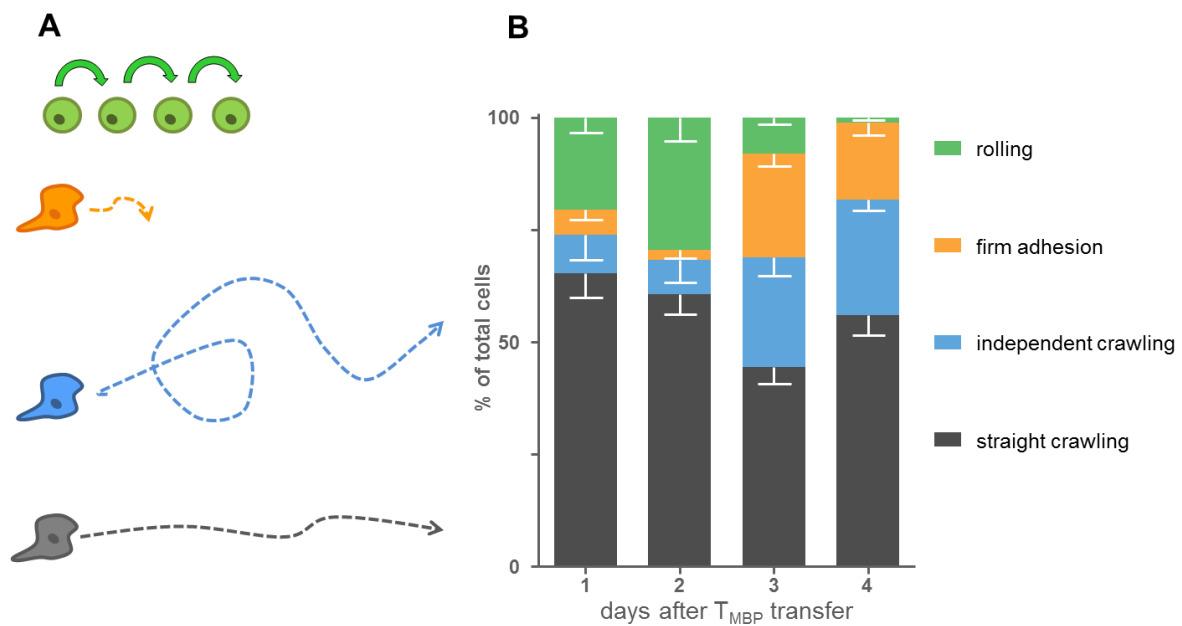


Figure 10 DiI⁺ monocytes change their migration mode during EAE. **A** Different intravascular migration modes exhibited by DiI⁺ monocytes: rolling (green), confined migration (orange), independent crawling (blue), straight migration (grey). **B** Quantification of migration modes of DiI⁺ monocytes during EAE. Percentages of migration modes on indicated time points post T_{MBP} cell transfer. Data from at least 3 different experiments per time point are shown.

We furthermore observed that the intraluminal migratory phenotype of DiI⁺ monocytes and T_{MBP} cells clearly differed. The T cells showed much more independent looping and migrated preferentially against the direction of the blood flow (Bartholomäus et al., 2009), whereas the DiI⁺ monocytes migrated much straighter and preferentially in the direction of blood flow. To quantify this observation, we compared mean speed, duration, displacement, straightness, and directionality of monocytes and T cells. In order to quantify the directionality, the angle between each displacement step which a tracked cell takes along its trajectory and the direction vector of the blood flow was calculated by an algorithm from the trackdescriptor R package. The blood flow direction was manually extracted from the intravital TPLSM imaging (Figure 11). The median of all angles of a given trajectory was used.

By using this approach, we observed that the monocytes moved significantly slower and straighter on the vascular endothelium with a significantly increased displacement length than T_{MBP} cells (Figure 12). Additionally, T_{MBP} cells migrated with an average median angle in relation to the blood flow of 89.24° as compared to 46.11° for DiI⁺ monocytes, indicating that intravascular movement of T_{MBP} cells is independent of the blood flow.

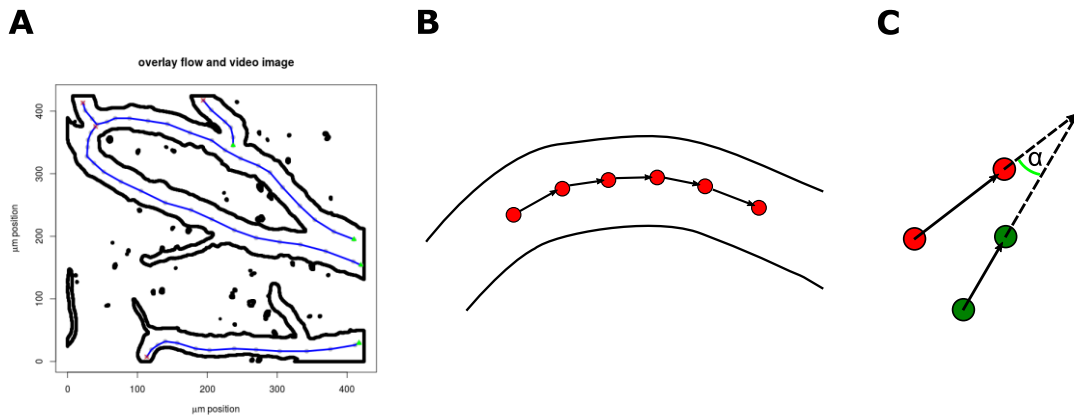


Figure 11 The median angle in relation to the blood flow as a new parameter to quantify intraluminal cell migration. Methodological approach to calculate the median migration angle of a migrating cell in relation to the blood flow direction. **A** Exemplary blood flow track projection (blue line) on top of blood vessel contours. **B** Displacement steps of the blood flow vector. **C** Calculation of the angle between cell displacement vector (green dots) and the nearest blood flow displacement vector (red dots)

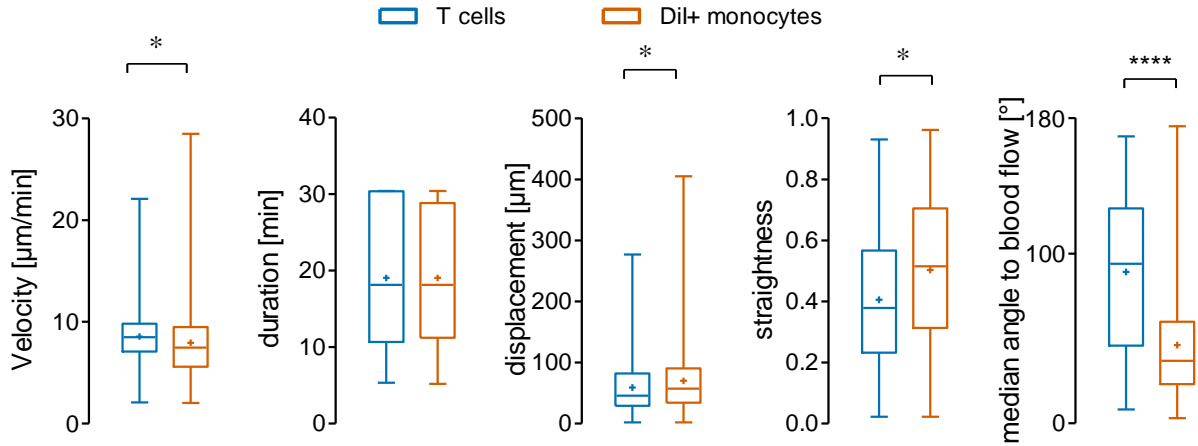


Figure 12 T_{MBP} cells and DiI⁺ monocytes exhibit different intraluminal migratory phenotypes. Motility parameters of T_{MBP} cells and DiI⁺ monocytes derived from intravital TPLSM 2 d.p.t. Boxplots with min-max whiskers and median are depicted. Mean is shown as +. Data from at least 5 experiments shown. *P<0.05, **P<0.01, ***P<0.001, two-sided t-test.

3.4 Computational analysis of cell migration patterns

Quantification of migratory phenotypes of DiI⁺ monocytes showed that these cells changed their migratory behaviour during the course of EAE based on the classification of the migration modes into the four mentioned categories (Figure 10 A, B). This analysis methodology had some intrinsic pitfalls. Indeed, the migration modes of DiI⁺ monocytes as recorded by intravital TPLSM were even more heterogeneous and complex than the applied classification could account for. Additionally, such kind of manual classification is very observer-biased.

For overcoming this problem, we reasoned that the migratory pattern of a single cell over time is encoded by the combination of several motility parameters. Based on this assumption, we went for developing an automated, unbiased classification of migratory patterns that addressed these two weak points and fulfilled following criteria: 1) classification of migratory modes according to patterns that are inherent (encoded) in the data. 2) elimination of observer bias.

Methodologically, we employed unsupervised machine learning, i.e., hierarchical clustering. This approach is often used for classification problems where features of unknown (unlabelled) data are used to detect “hidden” (common) structures in the data (Press W 2007).

As input for the clustering algorithm, several migratory parameters of immune cells over time (mean speed, track length, track duration, track displacement, straightness, and median angle to blood flow) were used. These parameters were derived from software-based 4D (x-y-z-t) cell tracking of the acquired intravital TPLSM-imaging data. The number of analysed cells and the

clinical phase when they were recorded by intravital TPLSM recording are summarized in Table 1.

Table 1 Summary of cell numbers and clinical phase for each cell type used for building database for clustering.

Cell type	Clinical phase	Counts
T _{MBP} cells	d2	747
	d3	232
DiI ⁺ monocytes	d1	82
	d2	2053
	d3	572
	naive	135

Six clusters generated by the applied algorithm were able to satisfactorily describe the motility of the diverse immune cell populations. The representative cell track for each of the six clusters was visualized for inspection and validation purposes (Figure 13 A, B)

- Cluster 1: The migration pattern of the representative cell of this cluster was characterized by short track duration in combination with large displacement, high straightness, and low median angle to blood flow. Taken together this indicated that this cluster represents cells that exhibit migratory phenotypes resembling leukocyte rolling and cells that transiently adhere to the vessel endothelium.
- Cluster 2: The migration pattern of the representative cell was straight. The cell migrated for intermediate duration with high straightness, large displacement, and a low median angle to the blood flow. This indicates that members of this cluster do not interact with the vessel endothelium very tightly and migrate straight in the direction of the blood flow.
- Cluster 3: The migration pattern of the representative cell of this cluster resembled the pattern of cluster 2 but migrated for a longer time, with lower straightness, and a higher median angle to the blood flow.
- Cluster 4: The representative cell showed a migration pattern resembling the looping phenotype previously observed in intraluminal T cell migration. Its motility parameters showed that the cells migrated for a long time on the endothelium with low straightness, small displacement, and a median angle to the blood flow of about 90°. Taken together this indicates that this cluster represents cells that show a classical intraluminal crawling migration pattern.

- Cluster 5: This cluster was characterized by intermediate track duration, intermediate median angle to blood flow, intermediate straightness together with small displacement in combination with small track length. This, together with the migration pattern of the representative track indicates that this cluster includes cells migrating for short periods independent of the blood flow direction.
- Cluster 6: Representative parameter fingerprints of cluster 5 showed that this class migration pattern was characterized by short track duration and small displacement in conjunction with small track length but, with a large median angle to blood flow and high straightness. This leads to the conclusion, that this cluster represents cells that migrate straight against the direction of the blood flow.

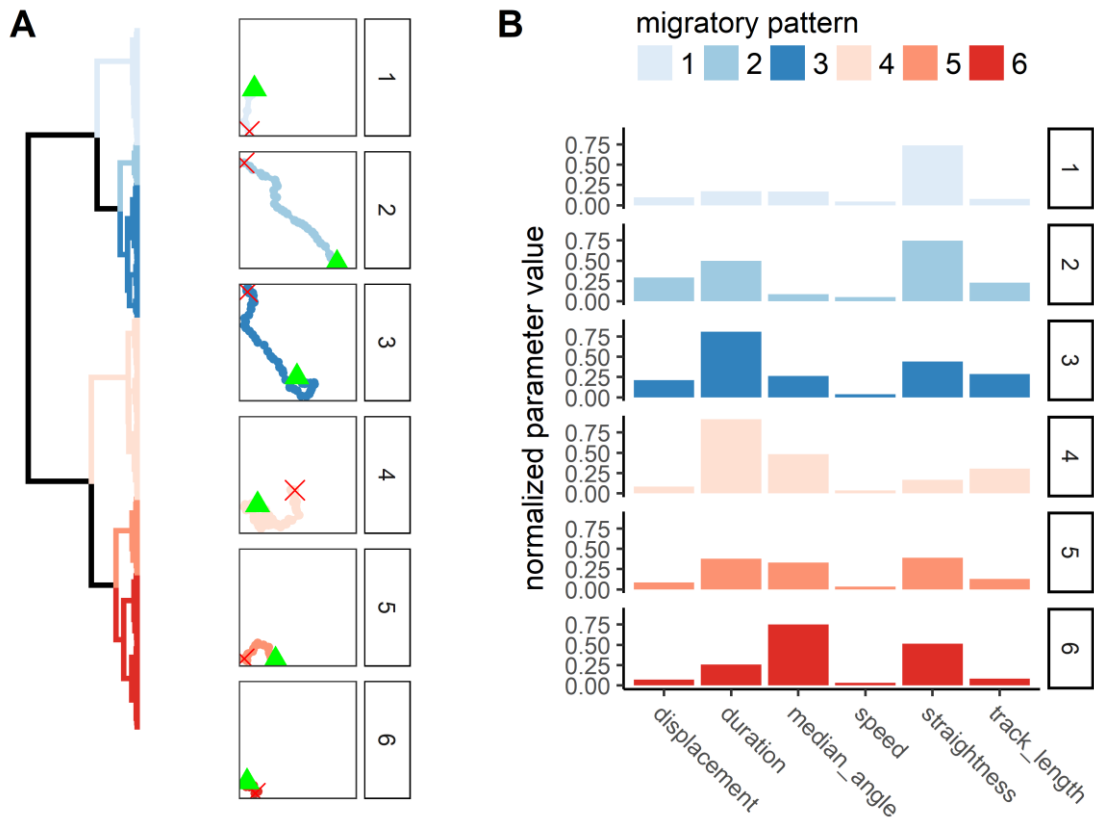


Figure 13 Clustering-based classification of migratory patterns of cells. Classification of migratory patterns into six classes using hierarchical clustering of 4739 tracked cells. Data input consisted of normalized motility parameters displacement length, track duration, median angle to blood flow, speed, straightness, and track length. **A** Dendrogram built during the clustering algorithm (left) and representative member of each cluster coded with distinct colours (right). **B** Corresponding fingerprint consisting of the normalized migratory parameter values shown as histograms.

3.5 Automated migratory pattern classification of DiI⁺ monocytes during atEAE

To validate the previously established method of automated, clustering-based analysis of migratory patterns, we analysed the frequency of migratory classes of DiI⁺ monocytes at different time points during EAE. We observed that with EAE progression the number of cells belonging to clusters 3, 4, and 5 were increasing (Figure 14 A and B). Based on the initial analysis of the automated classification, all these clusters were associated with patterns that were suggestive of stronger adhesion to the vessel endothelium. Notably, a drastic reduction in cells belonging to cluster 1, representing slow rolling and transiently adhering cells, was observed with EAE progression. Interestingly, cell numbers in cluster 6 remained constant. This cluster only represented a minor percentage of all clusters but was unaffected by the increasing inflammation during EAE (Figure 14 B). Additionally, we compared the distribution of migratory patterns for DiI⁺ monocytes and T_{MBP} cells from intravital TPLSM 2 d.p.t., the time point where both cell types are present in the leptomeningeal vessel, therefore migrating in the same milieu. The distribution of migratory phenotypes observed in DiI⁺ monocytes was different than the one observed in T_{MBP} cells (Figure 14 C). The DiI⁺ monocytes showed higher frequencies of clusters 1, 2, and 3 which all represent rather straight migration patterns that are suggestive of weak to intermediate adhesion to the vascular endothelium. In contrast, T cells showed higher numbers of migration patterns that are indicative of tight adhesion and intraluminal crawling, i.e., cluster 4 and cluster 6. Taken together, we applied the previously established automated classification to analyse the migratory behaviour of DiI⁺ monocytes during EAE. The results from this analysis were in line with our observation that DiI⁺ monocytes adopted more confined migratory patterns during progressing EAE (Figure 9). Furthermore, the observed differences in migratory patterns between the monocytes and T cells were correctly reproduced by this unsupervised classification method, ultimately validating it.

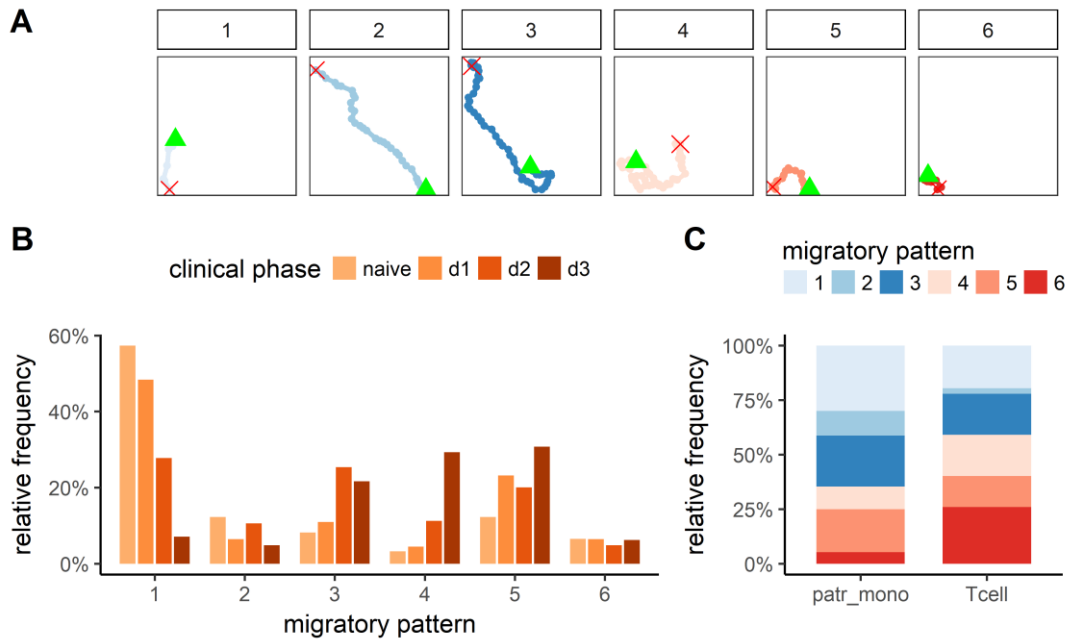


Figure 14 Automated migratory pattern classification of DiI⁺ monocytes and T_{MBP} cells. Data derived from intravital TPLSM of spinal cord leptomeningeal vessels. **A** Overview of representative members of the migratory classes derived from automated migratory pattern classification. **B** Relative frequency of migratory patterns of DiI⁺ monocytes (in %) occurring in naïve animals and at the indicated days after transfer of T_{MBP} cells. **C** Frequency of migratory patterns of DiI⁺ monocytes and T_{MBP} cells on day 2 p.t.

3.6 Identifying molecular cues shaping migratory patterns of immune cells during atEAE

Computer-assisted, automated classification of migratory patterns proved to be a powerful tool to analyse the intravascular motility of immune cells in great detail. By this means we could accurately classify and quantify migratory patterns of DiI^+ monocytes and T_{MBP} cells. Next, we used this tool to investigate the role played by molecular cues in shaping the migratory phenotypes of DiI^+ monocytes and T_{MBP} arriving in the leptomeningeal vessels during preclinical EAE. Methodologically we chose to block the integrins VLA-4 and LFA-1 by using monoclonal antibodies and to globally inhibit chemokines by using the $\text{G}_{\alpha\text{i}}$ inhibitor PTX. These targets were chosen because they are supposed to play a key role in intravascular immune cell adhesion and transmigration (Figure 15).

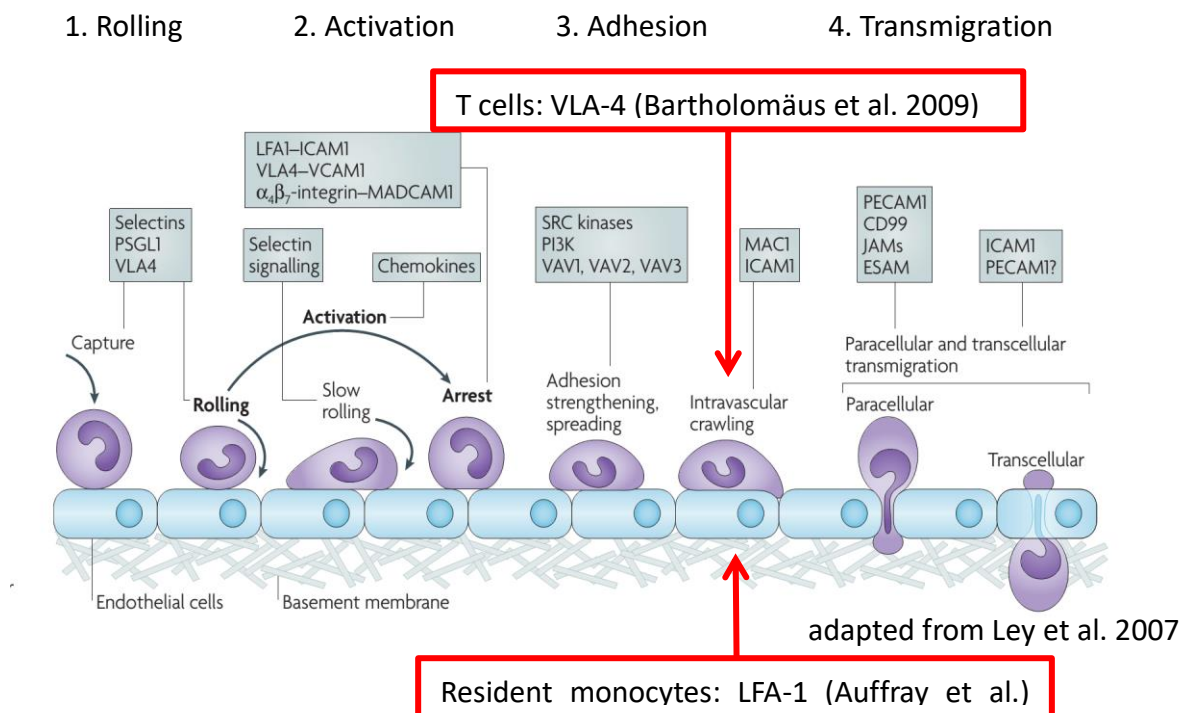


Figure 15 Leukocyte adhesion cascade. Steps leukocytes undergo during leukocyte adhesion cascade, consisting of 1) Rolling on vascular endothelium. 2) Activation of integrins by chemokine signalling. 3) Strengthening of adhesion and 4) subsequent intravascular crawling. Red arrow indicating points and molecules for possible targeting.

3.6.1 Interfering with VLA-4 signalling changes migratory pattern signature in DiI^+ monocytes but not T_{MBP} cells

In order to investigate the contribution of VLA-4 in shaping the intravascular migration pattern of DiI^+ monocytes and T_{MBP} cells during preclinical EAE, we interfered with VLA-4 signalling *in vivo*. Therefore, a monoclonal blocking antibody against VLA-4 (Issekutz, 1991; Issekutz

and Wykretowicz, 1991) was injected during spinal cord intravital imaging on day 2 p.t. At this time point, endogenous DiI⁺ monocytes, as well as transferred T_{MBP} cells can both be analysed simultaneously. Of note, as shown in Figure 27 C, at this time point both T_{MBP} cells and DiI⁺ monocytes expressed high amounts of VLA-4.

Blocking VLA-4 signalling lead to a rapid and significant decrease of DiI⁺ monocytes, as well as T_{MBP} cells, that were attached to the endothelial vessel wall (Figure 16 A). DiI⁺ monocytes and T_{MBP} cells showed no significant difference in the detachment response at 30-60 min after aVLA-4 injection (Figure 16 B). This detachment was not complete as we still could observe some intraluminal migrating DiI⁺ monocytes as well as T_{MBP} cells. Quantifying the absolute numbers of monocytes and T_{MBP} cells belonging to the six described migratory phenotypes, we saw that 60 min after aVLA-4 treatment in all migratory patterns both immune cell populations were reduced with the only exceptions being monocytes belonging to migratory classes 4, which stayed constant, and migratory pattern 6, which even increased after the treatment (Table 2). We then analysed the migratory pattern profile observed in DiI⁺ monocytes and T_{MBP} cells before VLA-4 blocking and after the treatment. In contrast to T_{MBP} cells, which showed no significant changes in their migratory pattern profile upon VLA-4-blocking, monocytes shifted their pattern profile towards the motility classes 4-6, patterns associated with the classical scanning locomotive behaviour (Figure 16 C) Here migratory pattern 4 was significantly increased and the classes 5 and 6 showed a strong tendency to be increased (Figure 16 C, Table 3).

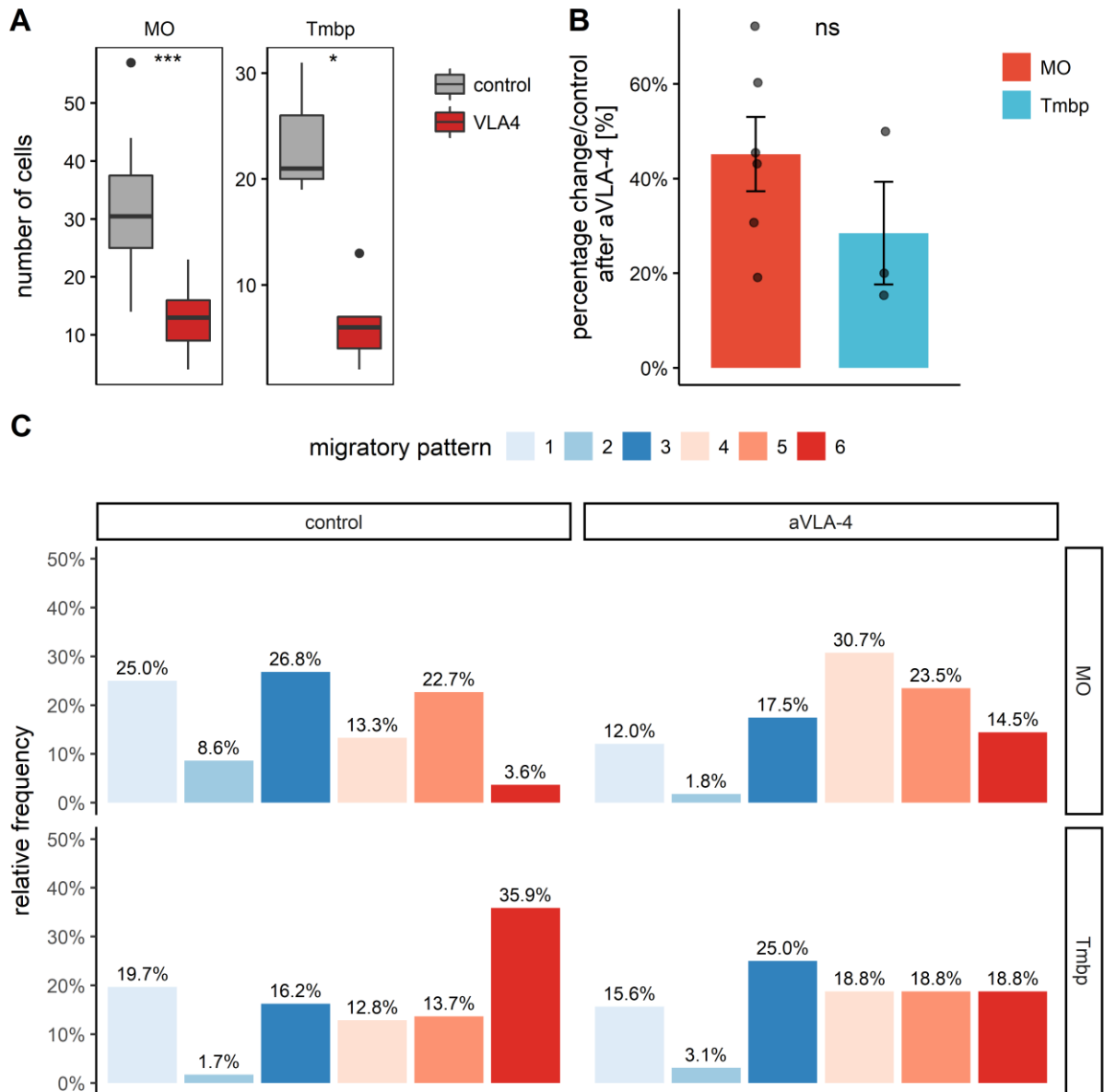


Figure 16 Blocking VLA-4 interferes partially with intraluminal DiI⁺ monocyte migration during preclinical EAE. Blocking of VLA-4 by injection of monoclonal antibody against its $\alpha 4$ -subunit during intravital imaging. Data derived from 4D (x-y-z-t) image data 30 min after treatment and analysed with automated migratory pattern classification. **A** Total number of cells migrating intraluminal before and after aVLA-4 treatment for monocytes and T_{MBP} cells. 10-90 percentile boxplots with median are depicted. **B** Percentages of intraluminal migrating DiI⁺ monocytes (MO) and T_{MBP} cells (Tmbp) 30 min after treatment are depicted. Values were calculated in relation to the starting condition (time point 0). Bars represent the mean \pm sem. **C** Migratory cluster distribution of monocytes (MO) and T_{MBP} cells (Tmbp) before and after aVLA-4 treatment. The percentage of each migratory pattern among all cells observed in each condition based on absolute cell numbers shown in Table 2 is depicted. Statistical significance was determined by Wilcoxon-Mann-Whitney test. Data from 3 independent experiments is shown.

Table 2 Absolute cell number of monocytes (MO) and T_{MBP} cells belonging to each of the migratory patterns before (control) and after aVLA-4 treatment

Cumulative number of cells from at least 3 independent experiments.

	1	2	3	4	5	6
<i>MO:control</i>	96	33	103	51	87	14
<i>MO:aVLA-4</i>	20	3	29	51	39	24
<i>TMBP:control</i>	23	2	19	15	16	42
<i>TMBP:aVLA-44</i>	5	1	8	6	6	6

Table 3 Relative frequency with 95% confidence intervals of each migratory pattern for monocytes (MO) and T_{MBP} cells before (control) and after aVLA-4 treatment

Multinomial confidence intervals were computed according to the method of Sison and Glaz.

	1	2	3	4	5	6
<i>MO:control</i>	25% [20-30]	9% [4-14]	27% [22-32]	13% [8-19]	23% [18-28]	4% [0-9]
<i>MO:aVLA-4</i>	12% [5-20]	2% [0-10]	17% [10-26]	31% [23-39]	23% [16-32]	14% [7-23]
<i>TMBP:control</i>	20% [11-29]	2% [0-11]	16% [8-26]	13% [4-22]	14% [5-23]	36% [27-45]
<i>TMBP :aVLA-4</i>	16% [0-33]	3% [0-20]	25% [9-42]	19% [3-36]	19% [3-36]	19% [3-36]

3.6.2 Interfering with LFA-1-signaling does not interfere with intraluminal migration of DiI⁺ monocytes

Next, we investigated how blocking LFA-1-signalling interfered with intraluminal migration of DiI⁺ monocytes during preclinical EAE. To elucidate this, we injected an anti-LFA-1-specific monoclonal blocking antibody during intravital TPLSM on day 2 p.t. The migratory behaviour of DiI⁺ monocytes and T_{MBP} cells was recorded before and after injection of LFA-1 blocking antibody and analysed using our computational motility phenotyping pipeline. Starting with 30 min after aLFA-1 injection we observed increasing numbers of both DiI⁺ monocytes and T_{MBP} cells attaching to the vasculature of the spinal cord leptomeninges. Although this increase compared to the control situation did not reach statistical significance, the data shows a clear trend (Figure 17 A, Table 4). This observed increase of intraluminal attached cells was not different between monocytes and T_{MBP} cells (Figure 17 B). Furthermore, we analysed if/how blocking LFA-1 affected the number of intravascular monocytes and T_{MBP} cells belonging to single clusters. We observed an increase in absolute numbers of both cell types in all the migratory patterns except the migratory pattern 2, which was decreased after blocking LFA-1 (Table 4). Next, we analysed the overall migratory pattern profile of monocytes and T_{MBP} cells before and after LFA-1 treatment. For both immune cell populations, we detected a shift towards the migratory phenotypes 4, 5, and 6. Here pattern 5 was most notably increased in

relative frequency of the migratory profile of monocytes and T_{MBP} cells, although this increase did not reach significance levels, a strong tendency was observed (Figure 17 C, Table 5). Interestingly, we detected a significant reduction of migratory pattern 2 in the profile of monocytes but not in T_{MBP} cells (Figure 17, Table 5)

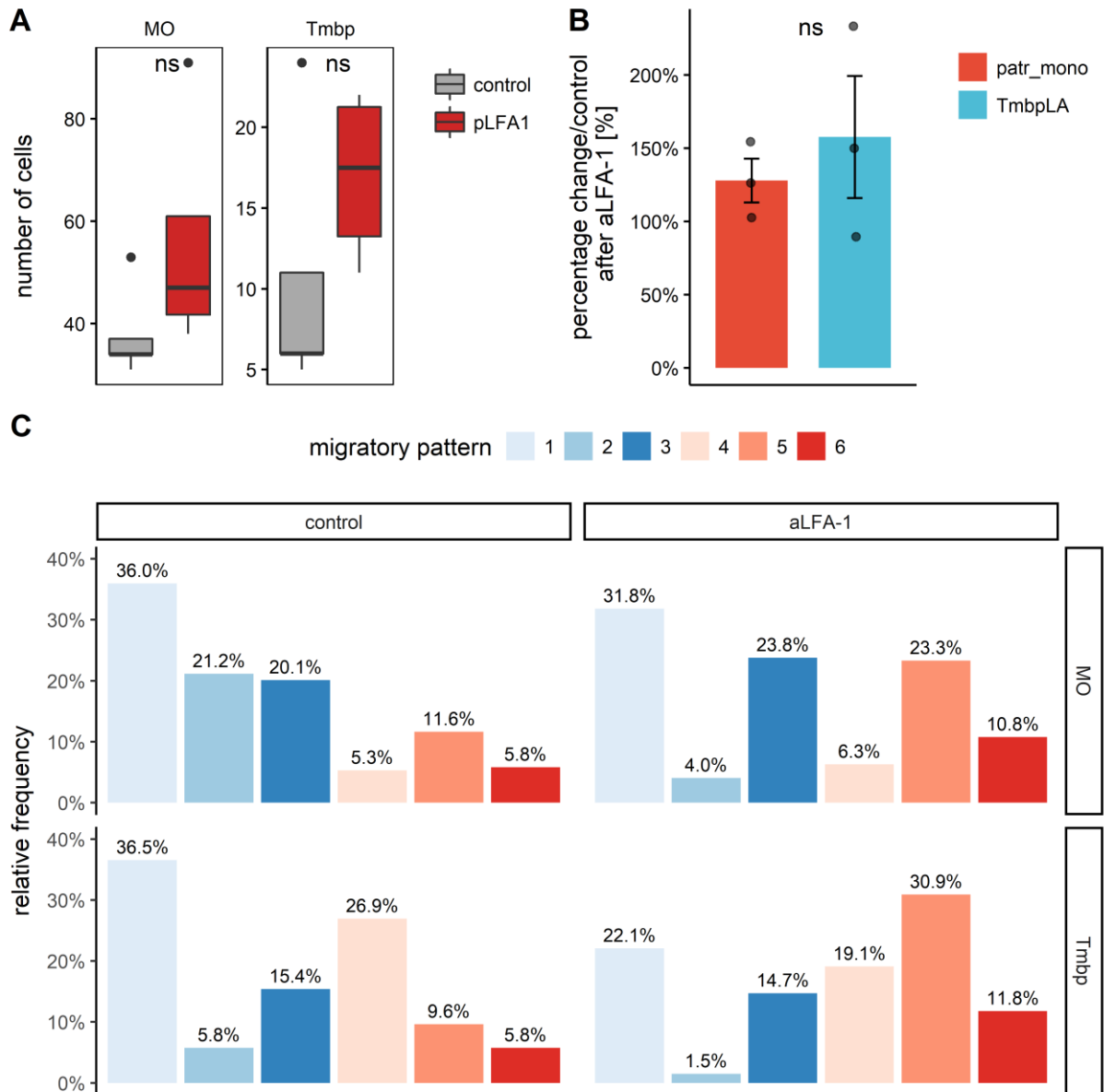


Figure 17 Blocking LFA-1 interferes partially with intraluminal DiI^+ monocyte during preclinical EAE.

Blocking of LFA-1 by injection of monoclonal antibody against its αL -subunit during intravital imaging. Data derived from 4D (x-y-z-t) image data 30 min after treatment and analysed with automated migratory pattern classification. **A** Total number of cells migrating intraluminal before and after anti-LFA-1 (aLFA-1) treatment for DiI^+ monocytes (MO) and T_{MBP} cells (Tmbp). 10-90 percentile boxplots with median are depicted. **B** Percentages of intraluminal migrating monocytes and T_{MBP} cells 30 min after treatment are depicted. Values were calculated in relation to the starting condition (time point 0). Bars represent the mean \pm sem. **C** Migratory cluster distribution of monocytes and T_{MBP} cells before and after aLFA-1 treatment. The percentage of each migratory pattern among all cells observed in each condition based on absolute cell numbers shown in Table 4. Absolute cell number of monocytes (MO) and T_{MBP} cells before (control) and after aLFA-1 treatment is

depicted. Statistical significance was determined by Wilcoxon-Mann-Whitney test. Data from 3 independent experiments is shown.

Table 4 Absolute cell number of monocytes (MO) and T_{MBP} cells before (control) and after aLFA-1 treatment

Cumulative number of cells from at least 3 independent experiments.

	1	2	3	4	5	6
<i>MO:control</i>	68	40	38	10	22	11
<i>MO:aLFA-1</i>	71	9	53	14	52	24
<i>T_{MBP}:control</i>	19	3	8	14	5	3
<i>T_{MBP}:aLFA-1</i>	15	1	10	13	21	8

Table 5 Relative frequency with 95% confidence intervals of each migratory pattern for monocytes (MO) and T_{MBP} cells before (control) and after aLFA-1 treatment

Multinomial confidence intervals were computed according to the method of Sison and Glaz.

	1	2	3	4	5	6
<i>MO:control</i>	36% [29-44]	21% [14-29]	20% [13-28]	5% [0-13]	12% [5-19]	6% [0-13]
<i>MO:aLFA-1</i>	32% [25-39]	4% [0-11]	24% [17-31]	6% [0-13]	23% [17-30]	11% [4-18]
<i>T_{MBP}:control</i>	37% [25-52]	6% [0-21]	15% [4-31]	27% [15-42]	10% [0-25]	6% [0-21]
<i>T_{MBP}:aLFA-1</i>	22% [12-35]	1% [0-15]	15% [4-28]	19% [9-32]	31% [21-44]	12% [1-25]

3.6.3 Global Gai inhibition interferes with initial steps of intravascular migration of DiI⁺ monocytes

In order to elucidate how chemokine signalling contributed to intraluminal locomotion of DiI⁺ monocytes and T_{MBP} cells *in vivo*, pertussis toxin (PTX) was injected during intravital TPLSM on d2 p.t. This bacterial exotoxin irreversibly inhibits Gai-mediated signalling pathways of G-protein-coupled protein, including chemokine receptors. Migratory behaviour was recorded before and after injection of PTX and analysed using our computational migratory pattern phenotyping. Quantification of monocytes and T_{MBP} cells that were migrating on the luminal side of leptomeningeal vessels showed reduced numbers of both immune cell populations at 2 h after treatment, although this change did not reach significant levels (Figure 18 A). T_{MBP} cells showed a tendency to be detached more by PTX treatment than DiI⁺ monocytes (Figure 18 B). Similar to the VLA-4-blocking experiments, not all cells were detached from the vessel walls. We analysed the migratory phenotypes of these remaining cells and found that all motility patterns except for pattern 4, which stayed constant, were reduced in terms of absolute number 2h after PTX treatment (Table 6). This was true for the monocytes and T_{MBP} cells. Notably, for

DiI⁺ monocytes, the cells belonging to motility pattern 1 were most affected and reduced by the G α i inhibition, whereas all observed motility patterns were reduced in similar magnitude in T_{MBP} cells (Table 6). The resulting migratory pattern profile of monocytes after PTX injection was shifted towards clusters 4 and 5 with a significant increase in cluster 4 compared to the profile in the control situation. This increase in the relative frequency of this motility pattern was due to the unresponsiveness to the PTX treatment of cells exhibiting this migratory phenotype and not an absolute increase (Figure 18, Table 7). Compared to the control pattern profile we observed a significant reduction of monocytes classified as motility pattern 1 after PTX (Figure 18, Table 6, and Table 7). The motility pattern profile of the remaining T_{MBP} cells was significantly changed compared to the control profile. The increase of relative frequency of T_{MBP} cells belonging to pattern 4 could indicate that cells exhibiting this migratory pattern are not responsive to chemokine signalling inhibition (Figure 18, Table 6, and Table 7).

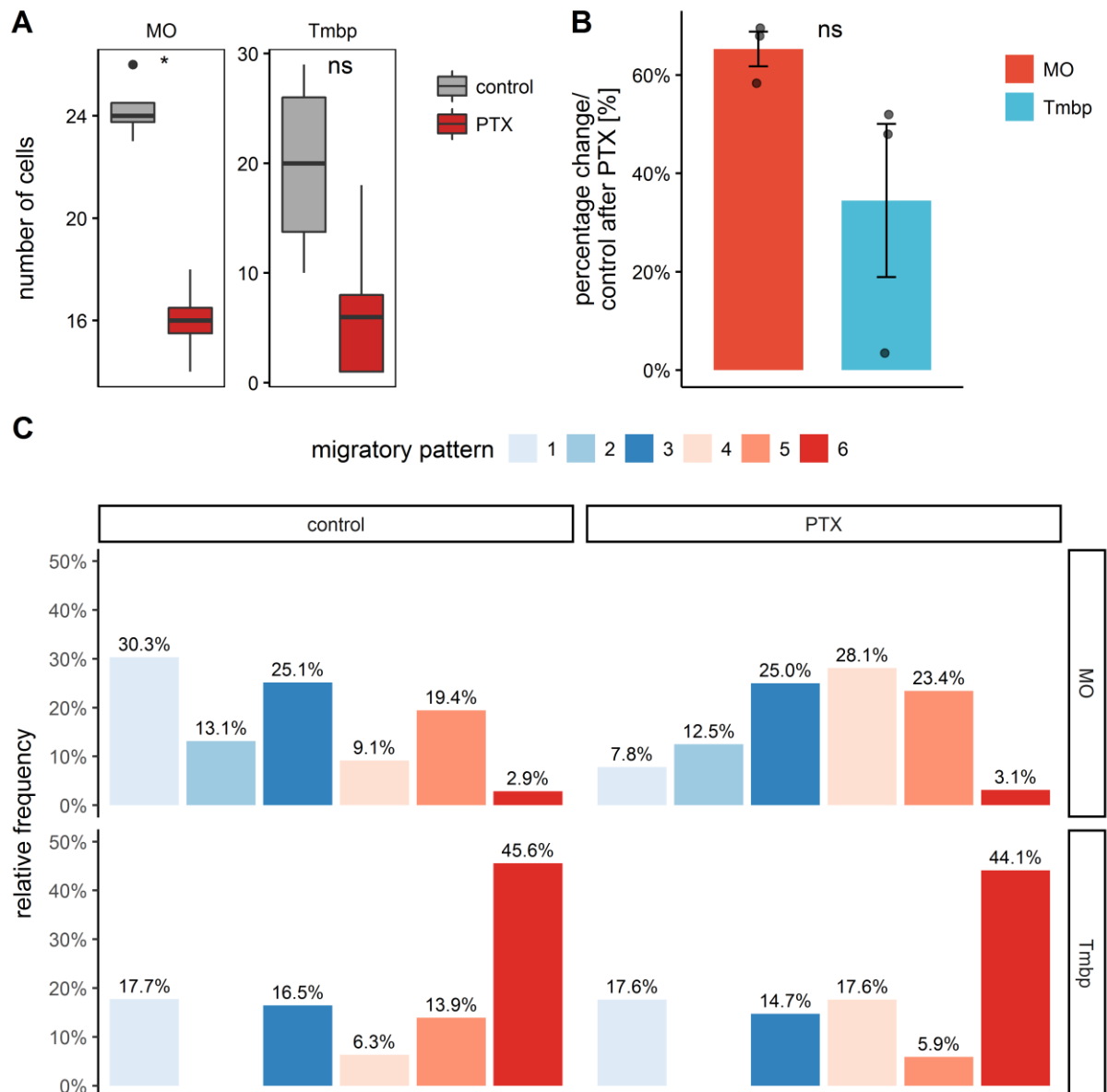


Figure 18 Global blocking of $G\alpha_i$ -signalling interferes partially with intraluminal DiI^+ monocyte during preclinical EAE.

Figure 18 Global blocking of $G\alpha_i$ -signalling interferes partially with intraluminal DiI^+ monocyte during preclinical EAE. Blocking global $G\alpha_i$ -signalling by injection of pertussis toxin (PTX) during intravital imaging. Data derived from 4D (x-y-z-t) image data before and 120 min after PTX treatment and analysed with automated migratory pattern classification. **A** Total number of cells migrating intraluminal before and after PTX treatment for DiI^+ monocytes (MO) and T_{MBP} cells (Tmbp). 10-90 percentile boxplots with median are depicted. **B** Percentages of intraluminal migrating monocytes and T_{MBP} cells 120 min after treatment are depicted. Values were calculated in relation to the starting condition (time point 0). Bars represent the mean \pm sem. **C** Migratory cluster distribution of monocytes and T_{MBP} cells before and after PTX treatment. The percentage of each migratory pattern among all cells observed in each condition based on absolute cell numbers shown in Table 6Table 4Table 4 Absolute cell number of monocytes (MO) and T_{MBP} cells before (control) and after aLFA-1 treatment is depicted. Statistical significance was determined by Wilcoxon-Mann-Whitney test. Data from 3 independent experiments is shown.

Table 6 Absolute cell number of monocytes (MO) and T_{MBP} cells before (control) and after PTX treatment

Cumulative number of cells from at least 3 independent experiments.

	1	2	3	4	5	6
<i>MO:control</i>	53	23	44	16	34	5
<i>MO:PTX</i>	5	8	16	18	15	2
<i>TMBP:control</i>	14	0	13	5	11	36
<i>TMBP:PTX</i>	6	0	5	6	2	15

Table 7 Relative frequency with 95% confidence intervals of each migratory pattern for monocytes (MO) and T_{MBP} cells before (control) and after PTX treatment

Multinomial confidence intervals were computed according to the method of Sison and Glaz.

	1	2	3	4	5	6
<i>MO:control</i>	30% [23-38]	13% [6-21]	25% [18-33]	9% [2-17]	19% [12-27]	3% [0-10]
<i>MO:PTX</i>	8% [0-21]	12% [2-26]	25% [14-38]	28% [17-42]	23% [12-37]	3% [0-17]
<i>TMBP:control</i>	18% [8-30]	0% [0-12]	16% [6-28]	6% [0-18]	14% [4-26]	46% [35-57]
<i>TMBP:PTX</i>	18% [3-36]	0% [0-18]	15% [0-33]	18% [3-36]	6% [0-24]	44% [29-62]

3.7 Cell-extrinsic factors shaping immune cell migratory patterns

3.7.1 Vessel diameter correlates with leukocyte migratory phenotypes

We have shown that monocytes and encephalitogenic T cells exhibit distinct motility patterns during intravascular migration in the spinal cord leptomeninges that are differentially responsive to chemokine and integrin interference (Figure 14 C). We next wanted to investigate if cell-extrinsic factors can play a role in shaping these different migratory phenotypes. *In vitro* not just molecular cues but also shear forces play a role in leukocyte migration (Valignat et al., 2013, 2014). In our system, immune cells migrate in leptomeningeal vessels of different calibre which could lead to changes in the hemodynamic shear stress. Therefore, we investigated if differences in vessel size could be involved in shaping migratory pattern profiles of monocytes and T cells. To address this question, we first developed a system to extract vessel diameter from intravital TPLS microscopy data. For this, we reconstructed the vascular tree from the imaging data in the statistical software programming language R and used the trackdescriptor and GriBMSO packages to derive the diameter of the whole vessel system (Figure 19 A). We validated the method by manual diameter measurement in ImageJ. The results showed that the automated measurement of the vascular tree gave similar results to the manual measurement

(Figure 19 A, B), with the advantage that by this approach we could derive the diameter over the whole vessel system, whereas manual measurement gives only localized diameters.

This system allowed us to derive for each tracked immune cell the diameter of the blood vessel the cell is located in at each time point along its track. We averaged for each cell the vessel diameter over all positions of its trajectory and plotted the average diameter for each migratory pattern for monocytes and T_{MBP} cells (Figure 20 A). The diameters of the analysed vessels were in the range between 25 and 50 μm in diameter (Figure 20 B). Despite these limited changes in calibre, we found a significant difference in the distribution of migratory patterns of monocytes according to the vessel diameter. There was a gradual increase in average diameter from pattern 1 to migratory pattern 6 i.e., from less adhesive to more adhesive pattern of migration (Figure 20 A). T_{MBP} cells did not show a significant difference in average diameter the single migratory patterns were preferentially observed in (Figure 20 A).

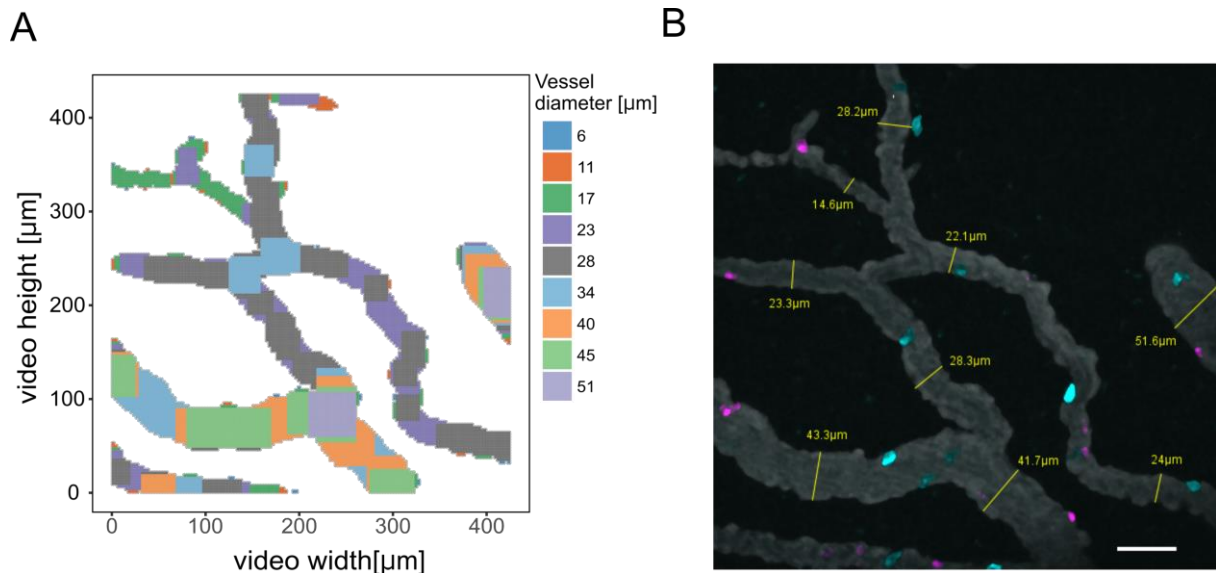


Figure 19 Comparison of automated vs manual vessel diameter measurement. Measurements based on reconstructed 4D (x-y-z-t) intravital TPLSM imaging data. **A** Automated reconstruction of the vascular tree from intravital TPLSM video with colours indicating vessel diameter. **B** Original intravital TPLSM video snapshot with manual measurements at indicated sites. Scale bar represents 50 μm .

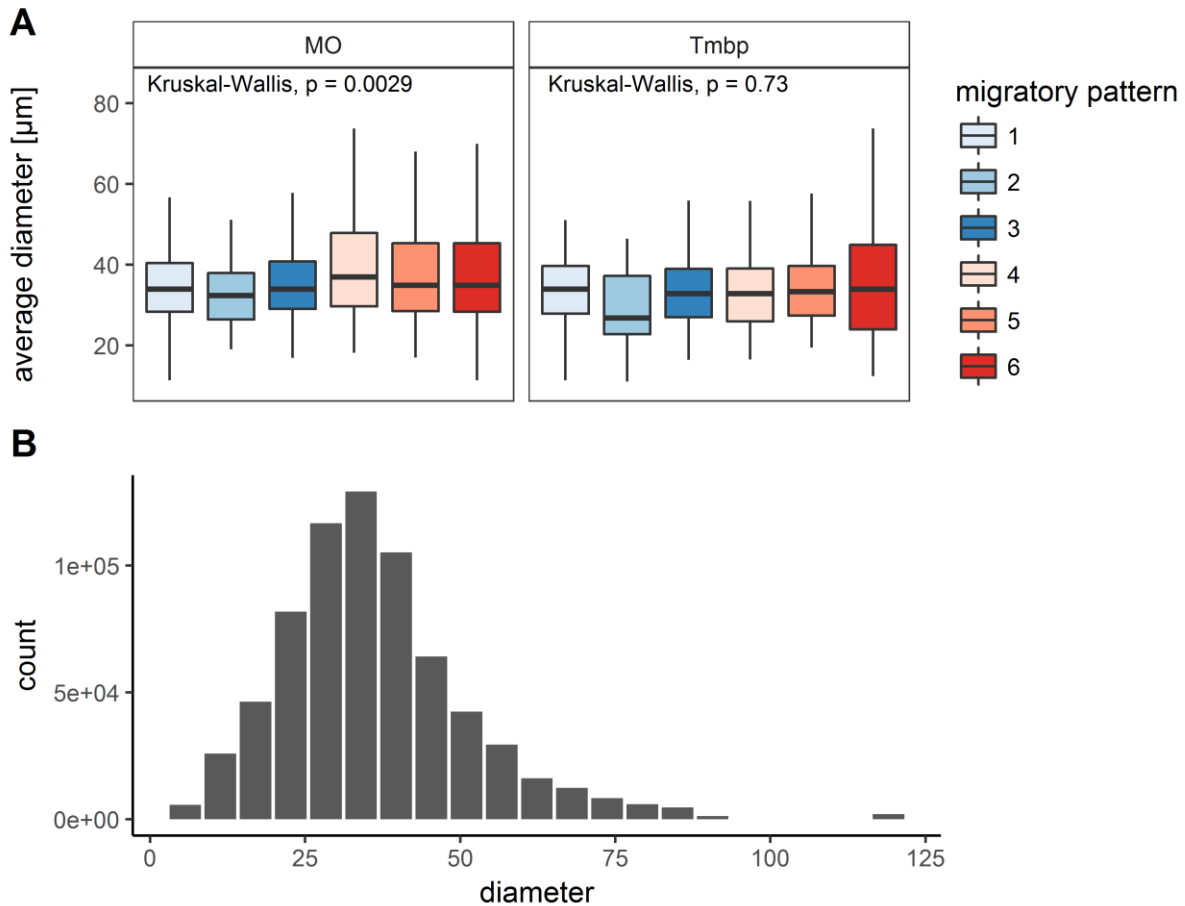


Figure 20 Blood vessel diameter correlates with monocyte migratory patterns. Analysis of blood vessel diameter as a cell-extrinsic factor that could shape immune cell intravascular migration. **A** Distribution of average vessel diameter migrating DiI^+ monocytes (MO) and T_{MBP} cells (Tmbp) were observed for each migratory pattern. **B** Overall distribution of vessel diameters derived from automated image analysis of all analysed intravital TPLSM videos.

3.7.2 Vessel junctions do not affect migratory patterns

Vascular trees in the leptomeninges of the spinal cord are highly branched (Figure 19 B) and at the junctions of blood vessels, the hemodynamic flow becomes turbulent (Liesch et al., 2012). We, therefore, asked if turbulences at these blood vessel junctions could influence leukocyte migratory phenotypes. To address this question, we developed an algorithm to detect blood vessel junction points in the intravital microscopy data (Figure 19) and analysed cell migration at these regions of interest. First, we assessed whether blood vessel junctions are a preferred location for either monocytes or T_{MBP} cells. We counted how often a tracked cell was located in- or outside of junction areas over the whole track observation period and normalized these counts for the total junction or non-junction areas of the respective video. No significant difference in cell observations inside or outside of vessel junction areas was seen for monocytes and T_{MBP} cells (Figure 21 A). Secondly, we assessed if different molecular cues guide immune

cell motility inside or outside the junction areas. Therefore, we subjected the imaging data from the integrin- and chemokine blocking experiments (chapters 3.6.1, 3.6.2, and 3.6.3) to the same analysis. No significant difference in the localization at junction or non-junction regions was seen for monocytes and T_{MBP} cells before and after interference with VLA-4, LFA-1, or chemokines (Figure 21 B, C, and D). Finally, we investigated if the presence of junctions influences the distribution of T_{MBP} cell or monocyte migratory patterns. We, therefore, analysed if one of the six described migratory phenotypes was preferentially observed in junction or non-junction areas. Migratory patterns of monocytes were not preferentially detected in either of the regions of interest, apart from pattern 6, which was not observed in junction areas (median of observation per non-junction area = 0,0030; median observations per junction area 0). Although we saw no significant difference in cells observed per region of interest, it is worth noting, that patterns 3, 4, and 5 had higher median observed monocytes in junction areas (Figure 22 A). T_{MBP} cells migratory patterns 1 and 5 showed significantly more observed cells in non-junction areas, whereas the remaining migratory phenotypes had similar cell observations in junction and non-junction areas (Figure 22 A).

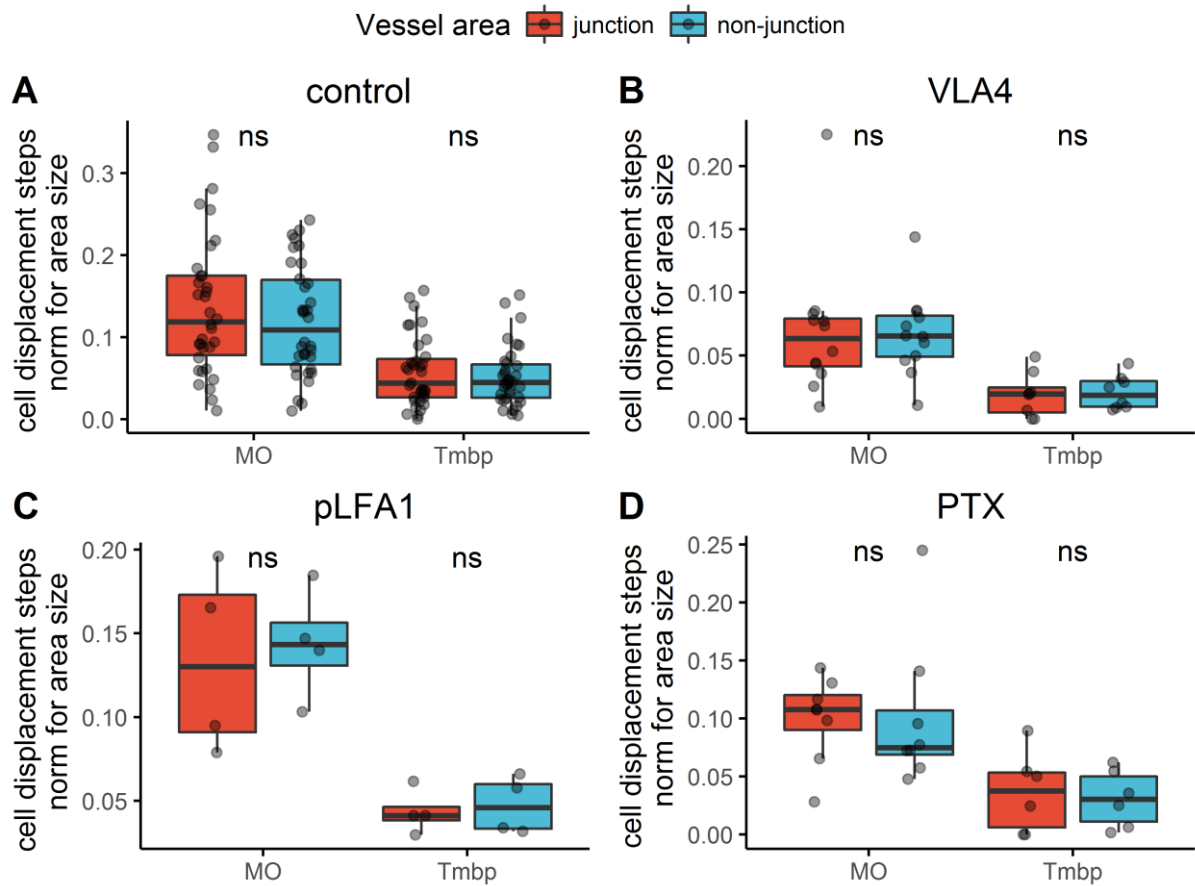


Figure 21 Intravascular migrating immune cells are not preferentially observed at vessel branch junctions. **A** Quantification of the number of displacement steps of immune cells along their tracks inside or outside of blood vessel-junction areas. Numbers were normalized for total junction or non-junction area of the respective time-lapse video. **D** Same quantification as **A** but after treatment with aVLA, aLFA, or PTX. Time points of analysis after treatments were 30 min, 30 min 120 min, respectively (ns = not significant, Wilcoxon-Mann-Whitney-test). Data from at least 3 independent experiments are depicted.

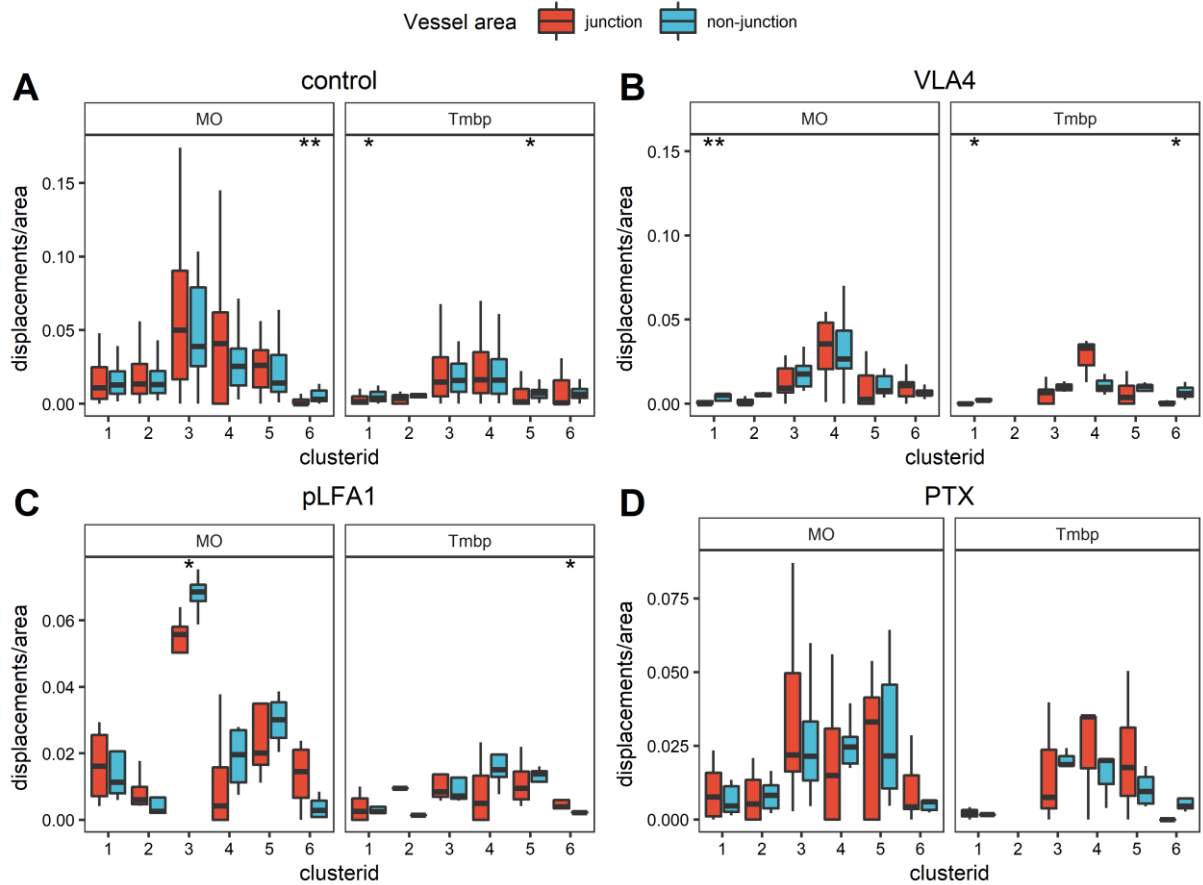


Figure 22 Analysis of monocyte and T_{MBP} motility pattern distribution at vessel branch junctions. Preferential location of migratory patterns 1-6 of homeostatic monocytes (MO) and T_{MBP} cells during preclinical EAE in leptomeningeal blood vessels was analysed. Data derived from 4D (x-y-z-t) intravital TPLSM imaging. **A** Quantification of the number of displacement steps of immune cell migratory patterns 1-6 for monocytes and T_{MBP} cells along their tracks inside or outside of blood vessel-junction areas. Numbers were normalized for total junction or non-junction area of the respective time-lapse video. **B-D** Same quantification as **A** but after treatment with aVLA, aLFA, or PTX. Time points of analysis after treatments were 30 min, 30 min 120 min, respectively (ns = not significant, Wilcoxon-Mann-Whitney-test). Data from at least 3 independent experiments are depicted.

3.8 Molecular cues shaping migratory phenotypes

3.8.1 DiI⁺ monocytes do not change their expression profile during the course of atEAE

The newly developed computational analysis revealed that DiI⁺ monocyte motility patterns in the vasculature of the leptomeninges change during the course of atEAE. These changes could be due to cell-intrinsic expression profile changes. To address this question, we daily FACS-sorted DiI⁺ and DiI⁻ monocytes from the blood starting on d0 until d5 post T_{MBP} cell transfer. We analysed the mRNA expression of the population-defining chemokine receptors CX₃CR1 and CCR2 and the integrins VLA-4 and LFA-1 by RT-qPCR. DiI⁺ as well DiI⁻ monocytes did not significantly regulate the expression of their signature chemokine receptors CX₃CR1 and CCR2, respectively throughout atEAE (Figure 23 A). When the integrin expression was

analysed, it became apparent that the DiI^+ monocytes showed a generally higher expression level of integrins compared to DiI^- monocytes. VLA-4 expression was higher than LFA-1 in both monocyte subpopulations. Over the time course of atEAE no significant changes in integrin expression levels could be detected (Figure 23 B). These results indicated that there is no change of VLA-4 and LFA-1 expression levels in DiI^+ and DiI^- monocytes during atEAE. However, this did not exclude that posttranslational regulation could affect the surface expression of these integrins and therefore cause the change of motility patterns of the monocytes. To address this, we isolated DiI^+ and DiI^- monocytes from blood each day during atEAE and surface-stained them for VLA-4, LFA-1, and additionally Mac-1. Flow cytometry analysis of the surface expression of these integrins corroborated the qRT-PCR data: DiI^+ monocytes had higher surface levels of VLA-4, LFA-1, and Mac-1 than DiI^- monocytes although throughout atEAE surface expression of these integrins did not change in both monocyte populations (Figure 24).

To get a global quantification of the genes expressed in blood-derived monocytes during atEAE, we then performed microarray transcriptome analysis of DiI^+ and DiI^- monocytes FACS-sorted from blood during atEAE, starting from day 0 p.t. until day 4. Clustering analysis of this transcriptome data clearly separated the two monocyte subpopulations, as is shown in the principal component analysis plot. Almost 50% of the variance in the data was explained by the cell population phenotype, clearly distinguishing DiI^+ from DiI^- monocytes. Samples from the different days post EAE induction did not separate in the PCA analysis, indicating that there are only few transcriptional changes over the course of the disease (Figure 25 A). This was also seen when differentially expressed genes between DiI^+ and DiI^- monocytes were plotted in a heat map: the two monocytic cell populations differed from each other but samples from each day did not show differentially expressed genes (Figure 25 B). Taken together, using RT-qPCR, flow cytometry, and microarray transcriptome analysis, we did not find cell-intrinsic regulations that could explain the change in migratory patterns that we observed in DiI^+ monocytes by intravital TPLSM.

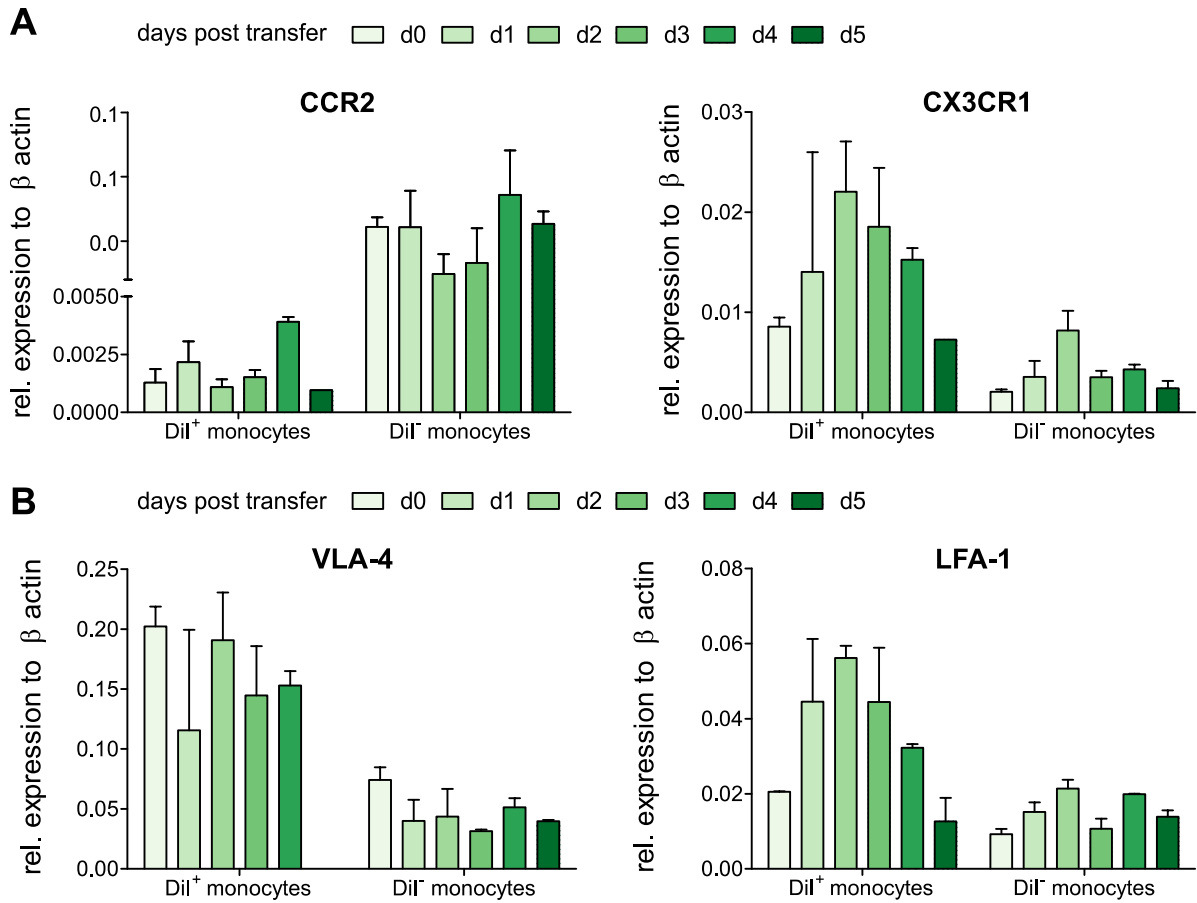


Figure 23 Dil⁺ and Dil⁻ monocytes do not change their expression of chemokine receptors and integrins. Monocyte subpopulations were FACS-sorted from blood according to their labelling by DiI liposomes during the course of atEAE. RT-qPCR analysis of **A** population defining chemokine receptors CX₃CR1 and CCR2 and **B** integrins VLA-4 and LFA-1. Mean values \pm SEM are plotted. Data from 3 independent experiments.

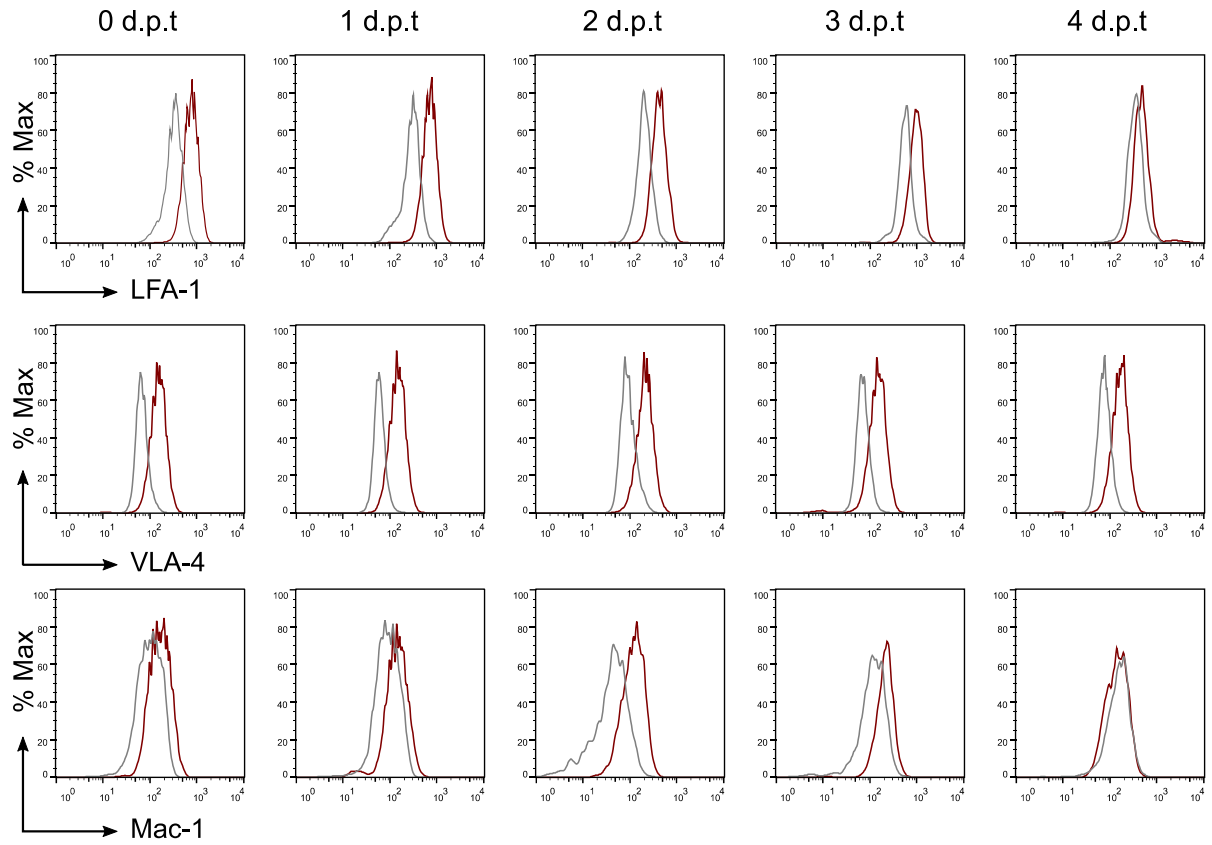


Figure 24 DiI^+ and DiI^- monocytes do not change their surface expression of integrins. Monocytes subpopulations were isolated from blood according to their labelling by DiI liposomes during the course of atEAE. Grey histograms represent DiI^- monocytes, red histograms represent DiI^+ monocytes. Flow cytometry of monocyte subpopulations surface-stained for VLA-4, LFA-1, and Mac-1. Representative histogram plots from 3 independent experiments are depicted.

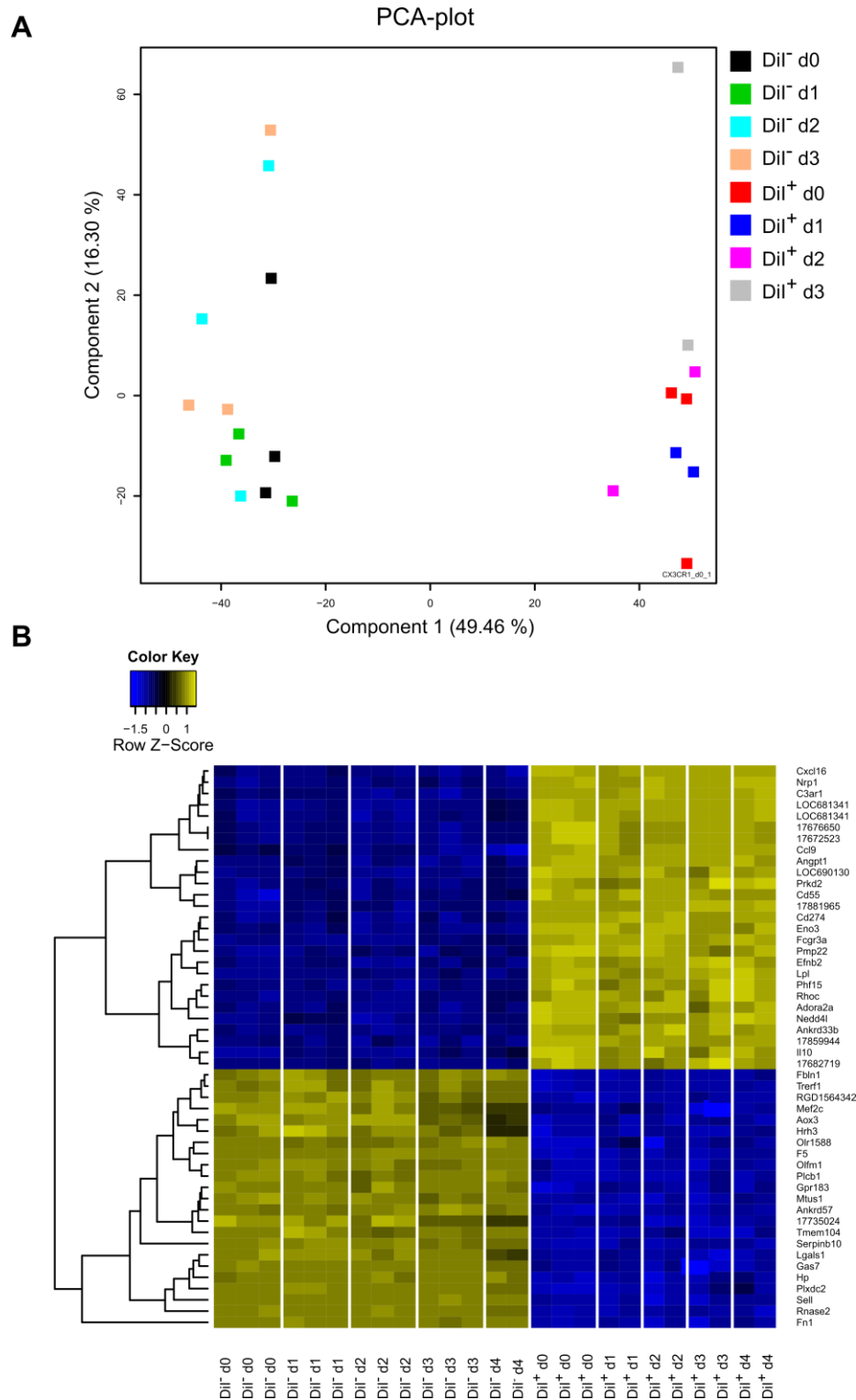


Figure 25 DiI^+ and DiI^- monocytes show distinct transcriptomes but in each monocyte subpopulation, transcriptional profiles do not change drastically during the course of atEAE. Microarray transcriptome analysis of DiI^+ and DiI^- monocytes sorted from blood during atEAE. **A** Principal component analysis plot of the data. **B** Heat map of top 50 differentially expressed genes between both subpopulations for each indicated day post EAE induction. Colour scale is the z-score of normalized expression values.

3.9 Impact of endothelial cell expression pattern on DiI⁺ motility patterns

In literature, it is described that during EAE endothelial cells of spinal cord micro vessels upregulate the expression of several chemokines and adhesion molecules required for recruiting lymphocytes, their adhesion, and transmigration (Elhofy et al., 2002; Fife et al., 2001; Narumi et al., 2002). Therefore, the change in the motility patterns of DiI⁺ monocytes could be due to a change in the expression profile of spinal cord micro vessel endothelial cells during EAE.

3.9.1 Spinal cord leptomeningeal endothelial cells change their expression profile during preclinical EAE

To assess whether the changes in monocyte motility patterns were due to EAE induced differential expression profiles in endothelial cells, we isolated blood vessel endothelial cells from spinal cord leptomeninges of naïve animals and from animals during preclinical EAE (3 d.p.t). Genome-wide expression profiles were obtained from FACS-sorted endothelial cells by RNA-Seq and compared. In the principal component analysis of the RNA-Seq data, the samples from naïve animals separated clearly from samples isolated from EAE animals. About 77% of the variance in the dataset was explained by the autoimmune inflammatory component (Figure 26 B). Out of 18768 expressed genes in these endothelial cells, we identified 1229 significantly differentially expressed genes (Figure 26 C, adjusted p-value < 0.05, fold change > 2). Further in-depth analysis showed that among the significant genes the adhesion molecules *Vcam1* and *Icam1* as well as E-selectin (*Sele*) were upregulated in preclinical EAE. We observed significant upregulation of *Cxcl9* and *Cxcl11*, ligands for the chemokine receptor *Cxcr3*, and thus, chemoattractants for activated T cells. *Cx3cl1* and *Ccl2*, chemoattractants for the monocyte subpopulation-defining chemokine receptors CX₃CR1 and CCR2 were not significantly regulated. Conversely, we observed a significant downregulation of the tight-junction molecules *claudin-5* and *Occludin* in endothelial cells from preclinical EAE (Figure 26 D). The results from the RNA-Seq indicated that during preclinical EAE endothelial cells upregulate adhesion molecules and inflammatory chemokines (Figure 26 D). But due to the limited amount of mRNA that could be extracted from sorted endothelial cells only 2 out of 4 biological replicates could be analysed. Therefore, RT-qPCR was performed on samples that were isolated exactly as for RNA sequencing to validate the results from the RNA-Seq. Similar to the RNA sequencing results *Vcam1* was significantly upregulated in EAE samples but not *Icam1* which showed high variance in expression in naïve endothelial cells. Similarly, the chemokines *Cxcl11* and *Cxcl9* were upregulated and the tight junction genes *claudin-5*(*cldn5*) and *Occludin* (*Ocln*) were downregulated in preclinical EAE (Figure 26 E).

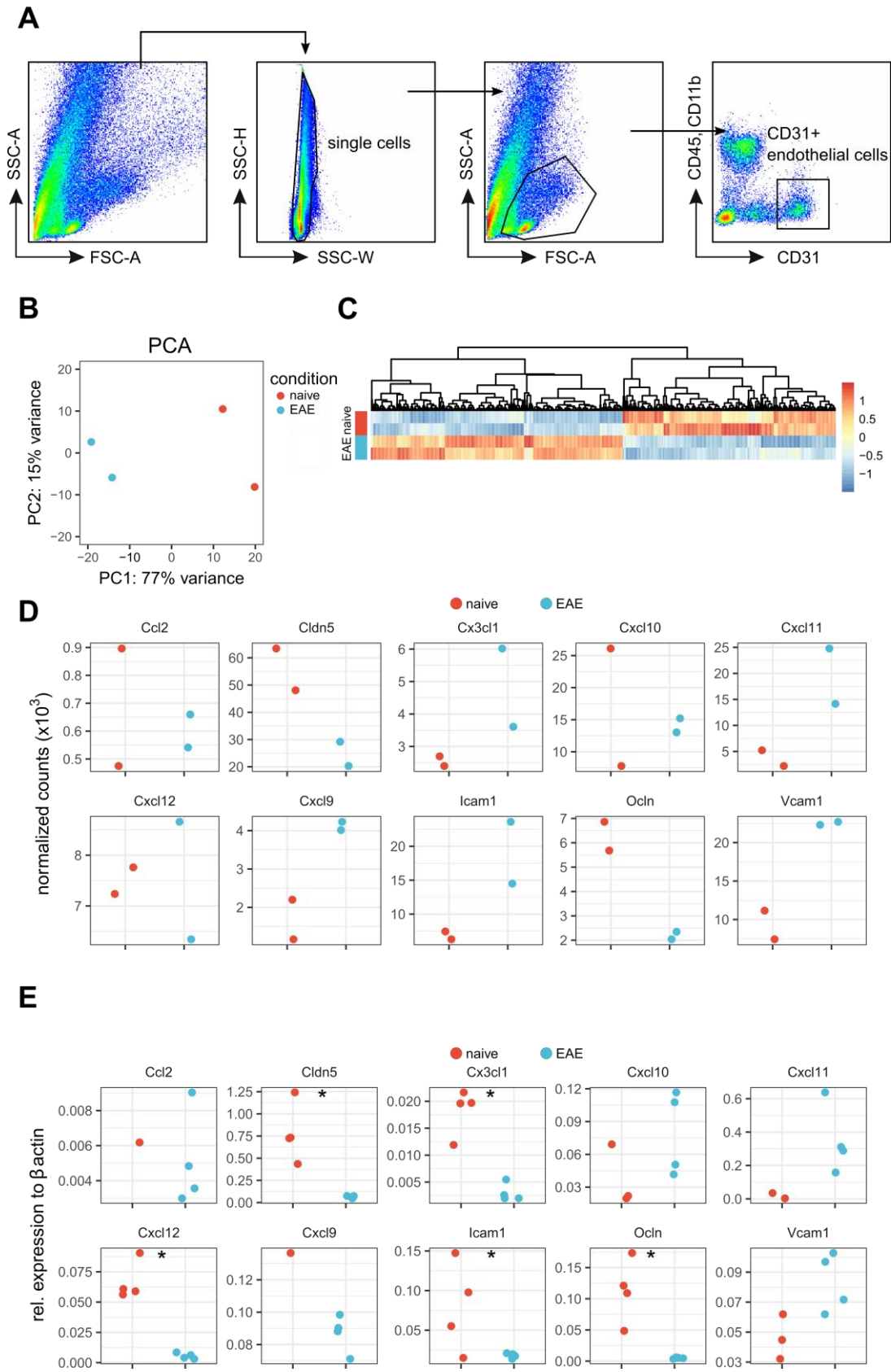


Figure 26 Leptomeningeal endothelial cells change their gene expression profiles during preclinical EAE and upregulate adhesion molecules and chemokines. RNA-Seq transcriptome analysis of FACS-sorted endothelial cells (EC) isolated from spinal cord leptomeninges of naïve animals and animals at preclinical EAE

stage. **A** Gating strategy for FACS-sorting of ECs. **B** Principal component analysis (PCA) of transcriptomes of leptomeningeal ECs (n = 2 biological replicates per group, each pooled from 4 individual animals). **C** Heat map of significantly up- and downregulated genes in meningeal ECs from preclinical EAE animals compared to naïve ECs. Colour scale is z-scores of rlog-transformed normalized counts ($p < 0.05$, fold-change > 2 , Wald-test). **D** normalized expression values of selected genes. **E** validation of selected targets from **D** with RT-qPCR (n = 4 biological replicates per group, * $p < 0.05$, t-test).

3.10 Comparison of expression profiles between blood monocytes and encephalitogenic T cells

Our analysis of motility patterns of monocytes and encephalitogenic T cells showed that these cells displayed very distinct motility pattern profiles during intravascular locomotion in the spinal cord leptomeninges (Figure 14 C). Therefore, we next asked which molecular cues govern these different migratory patterns. As monocytes and MBP-specific T cells are migrating in the same milieu, we hypothesized that cell-intrinsic factors shape the migratory patterns of these immune cells. Therefore, T_{MBP} cells, DiI^+ homeostatic monocytes, and DiI^- inflammatory monocytes were flow cytometry-purified from blood 2.5 days post transfer of T_{MBP} cells for mRNA extraction, and RNA sequencing was performed on these samples. This time point was chosen because distinct migratory patterns between DiI^+ monocytes and encephalitogenic T cells were observed by intravital TPLSM (Figure 14 C) in this phase of preclinical EAE. This opens the possibility to correlate RNA-Seq data with the TPLSM data. As expected, principal component analysis of the NGS data showed that T_{MBP} cells clustered separately from the monocyte population. But also, homeostatic and inflammatory monocytes were clearly separated from each other (Figure 27 A). Differential gene expression analysis identified 3403 out of 18977 expressed genes as differentially expressed across all three immune cell populations (Figure 27 B). Further in-depth analysis of the expression of adhesion molecules involved in intravascular migration revealed that VLA-4 (*Itga4*) and LFA-1 (*Itgal*) were higher expressed in homeostatic monocytes compared to T_{MBP} cells. We next investigated the expression of the adhesion molecules *Alcam* and *Ninjurin-1* (*Ninjl*), which are also involved in leukocyte adhesion to the BBB endothelium during autoimmune CNS-inflammation (Cayrol et al., 2008; Ifergan et al., 2011; Lécuyer et al., 2017). *Alcam* was not differentially expressed between monocytes and T_{MBP} cells and *Ninjurin-1* was higher expressed in homeostatic monocytes (Figure 27 C). We found no difference in expression of L-selectin which was expressed only very lowly in homeostatic monocytes and T_{MBP} cells. Results from RNA sequencing of endothelial cells showed that during autoimmune CNS-inflammation these cells upregulate *Cxcl11* and *Cxcl9*, thus we looked at the expression of the cognate receptor of these

Figure 27 Transcriptome analysis of monocytes and T_{MBP} cells. RNA-Seq transcriptome analysis of FACS-sorted homeostatic DiI⁺ monocytes (MH), inflammatory DiI⁺ monocytes (MI) and T_{MBP} cells isolated from blood at preclinical EAE stage (2,5 days p.t.). **A** Principal component analysis (PCA) of transcriptomes of homeostatic monocytes, inflammatory monocytes, and T_{MBP} cells (n = 3 biological replicates per group, each pooled from 4 individual animals, p < 0.05 fold-change > 2, Wald-test). **B** Heat map of top 50 regulated genes across all analysed

immune cell populations. Colour scale is rlog-transformed normalized counts. **C** normalized expression values of selected genes. **D** quantification of inferred ligand-receptor pair interaction between homeostatic monocytes, inflammatory monocytes, TMBP cells, and leptomeningeal endothelial cells.

4. Discussion

4.1 Establishing the system

Multiple Sclerosis is thought to be initiated by auto-reactive T cells, although several lines of evidence suggest that cells of the myeloid lineage play an important role in the pathology, too. Mononuclear phagocytes, such as macrophages and microglia, are indeed the dominant immune cells in MS lesions. They can interact with cells of the adaptive immune system but can also directly cause tissue damage. Myeloid phagocytes are the main perpetrators of myelin damage and removal, forming demyelinating lesions, the hallmark of MS (Henderson et al., 2009; Lassmann et al., 1998), but also contribute to axonal damage (Trapp et al., 1998).

Evidence of the importance of myeloid cells in the formation of CNS infiltrates and in the consequent development of clinical symptoms comes also from animal studies on EAE. In a Lewis rat EAE model depletion of peripheral monocytes abrogated clinical EAE (Huitinga et al., 1990, 1995; Tran et al., 1998). Moreover, genetic or Ab-mediated strategies for interfering with the CCR2/CCL2 axis, which play an essential role in determining the Ly6C^{hi} monocytic cell's trafficking to the CNS, resulted in delayed or abrogated EAE.

Although recruitment of myeloid cells seems to be crucial for EAE development, the detailed migratory steps prior to overcoming the BBB and molecular cues involved in them are not yet completely understood. Therefore, in the present work, we studied the migration of monocytes at the BBB in real-time *in vivo* in the Lewis rat adoptive transfer EAE model. We chose this model based on our long-standing experience and on the fact that the effector T cells can be tracked, allowing therefore the unique possibility to track together T cells and CD43^{high} and CD43^{low} monocytes. By using this approach, we could show that: (1) both subpopulations closely followed the infiltration kinetics of the transferred T cells into the CNS. (2) Moreover, we observed an increase of both monocyte subsets in the blood circulation before the disease onset (Figure 4). This result was in line with findings from King et al. which showed in a mouse EAE model that Ly6C^{high} and Ly6C^{low} monocytes increased in the blood circulation before EAE onset (King et al., 2009). Our results showed that in the Lewis rat atEAE model monocytes are recruited to the spinal cord leptomeninges before disease onset and this recruitment is closely followed by the transferred T cells.

In order to study the underlying mechanisms of the monocyte migration at BBB, we established a system to visualize the CD43^{high} monocytes for intravital TPLSM. Injecting fluorescently labelled liposomes intravenously specifically labelled this monocyte subpopulation. Using flow

cytometry and qPCR analysis on FACS sorted DiI⁺ we confirmed that the liposome-uptaking monocytes were of the CX₃CR1^{high} homeostatic monocyte subpopulation (Figure 6, Figure 7). A birth-dating study of mouse blood monocytes using a similar approach showed that 24h after injecting stained liposomes all of the labelled monocytes were of the Ly6C^{low} phenotype (Sunderkötter et al., 2004).

A study by Auffray and colleagues showed by intravital confocal microscopy in mice that homeostatic Ly6C^{low} CX₃CR1^{high} monocytes crawled inside the lumen of blood vessels of the ear dermis, the cremaster, and mesenteric blood vessels in steady-state condition (Auffray et al., 2007). These monocytes showed extensive scanning of the blood vessel endothelium and were therefore also termed patrolling monocytes. When we performed intravital TPLSM in naïve Lewis rats 24 hours after i.v. injection of DiI-liposomes, we could observe DiI⁺ cells in the leptomeningeal blood vessels of the spinal cord. These cells migrated intraluminally on the blood vessel endothelium (Figure 5, Figure 8 A). As we excluded unspecific labelling by the DiI-liposome labelling (Figure 6) we concluded that these cells belonged to the CD43^{high} homeostatic monocyte subpopulation. Inside the leptomeningeal blood vessels, they migrated very straight in the direction of the blood flow. This migratory behaviour was in contrast to the observations from Auffray et al. which described that patrolling monocytes crawled in looping patterns inside the blood vessels (Auffray et al., 2009). This could be due to differences between monocytes of rats and mice. As far as to our knowledge, the motility of homeostatic monocytes in blood vessels has not been studied by intravital microscopy in Lewis rats, therefore we can only speculate about differences between intraluminal migration of mouse and rat monocytes. Another explanation could be attributed to technical aspects. Auffray and colleagues used conventional confocal microscopy for intravital imaging studies which produces more photo toxicity compared to two-photon microscopy, which we used in the present work. Therefore, this could have resulted in minimal photoactivation of the blood vessel endothelium leading to increased adhesion and change in motility patterns.

4.2 Migratory behaviour of monocytes in spinal cord leptomeninges during adoptive transfer EAE

With the established system, we studied the migratory behaviour of homeostatic monocytes during EAE. We performed intravital TPLSM from day 0 until the peak of disease on day 5 post T cell transfer. We made the following observations:

- (1) We detected an increase of intraluminal migrating homeostatic monocytes until 3 days p.t.

This was the time point when the animals showed first signs of clinical symptoms (Figure

- 8). Thereafter homeostatic monocyte numbers decreased again. Notably, we rarely detected labelled homeostatic monocytes extravascular in the subarachnoid space (not shown).
- (2) With EAE progression the motility behaviour of the homeostatic monocytes changed: (Figure 9).
- (3) The motility parameters and migratory modes of the monocytes were distinct from the ones of the adoptively transferred autoreactive T cells (Figure 12). This observation will be discussed in a later paragraph.

The observed increase of homeostatic monocytes in the leptomeningeal blood vessels was in line with the kinetic data obtained by flow cytometry (Figure 4). The increase of homeostatic monocytes observed in the leptomeningeal vessels during intravital TPLSM (Figure 8) was accompanied by changes in their motility parameters: they migrated with lower mean speed inside the vessels, the time they spent migrating on the vessel endothelium increased, and the straightness of their movement decreased (Figure 10). This recruitment and changed motility behaviour of the monocytes coincided with the appearance of the autoreactive T cells in the leptomeningeal vessels and therefore it could be due to T-cell mediated activation of the blood vessel endothelium. This interpretation is in accordance with the vessel maintenance function of homeostatic monocytes described in the literature. Carlin and colleagues showed by intravital microscopy that $\text{Ly6C}^{\text{low}} \text{CX}_3\text{CR1}^{\text{high}}$ monocytes scavenged micro particles from the luminal side of blood vessels in steady-state. Perturbation of the steady-state by TLR7-dependent signalling leads to Ly6C^{low} monocyte retention in the kidney microvasculature and changes in their motility pattern characterized by decreased crawling velocities, increased track length, and track duration. In this model of TLR7-mediated inflammation, severe focal necrosis of endothelial cells was detected at sites where monocytes and neutrophils were retained. Ly6C^{low} monocytes adjacent to damaged endothelial cells could be observed phagocytosing cellular debris (Carlin et al., 2013). This report and previous observations that homeostatic monocytes crawl on blood vessel endothelia (Auffray et al., 2009; Hanna et al., 2011) and that they do not contribute to the pool of inflammatory monocytes that extravasate at sites of inflammation and give rise to macrophages and dendritic cells support their function as vascular “housekeepers”. Our observation that we rarely detected extravasated homeostatic monocytes by intravital TPLSM is in line with these previous reports and supports the hypothesis that homeostatic monocytes are also recruited to leptomeningeal vessels to maintain the CNS endothelium. An alternative interpretation could be, that the homeostatic monocytes are preparing the extravasation of autoaggressive T cells or inflammatory monocytes. A strategy to investigate this hypothesis could be to deplete the homeostatic monocytes and investigate the extravasation

and infiltration of the autoimmune T cells and inflammatory monocytes in combination with transcriptome analysis of leptomeningeal endothelial cells.

In our model, we could study the intravascular locomotive behaviour of homeostatic monocytes and autoreactive T cells simultaneously. Two days after T cell transfer, a time point where both cells can be observed migrating in the lumen of leptomeningeal blood vessels, we noted that both cell types exhibited profoundly different types of motility modes. The transferred MBP-specific T cells were crawling in looping patterns preferentially against the direction of the blood flow, whereas the homeostatic monocytes showed very heterogeneous migratory patterns, although at this time point the majority was migrating very straight in the direction of the blood flow (Figure 11, Figure 12). As both cell populations migrated in the same environment, this discrepancy was most likely due to different cell-type-specific and cell-intrinsic mechanisms of cell migration. *In vitro* studies using migration assays under flow conditions, have shown that T cells orient against the direction of the flow and migrate against the flow (Valignat et al., 2013). These studies supported earlier *in vivo* data which showed that T cells reactive against MBP preferentially migrated against the direction of the blood flow (Bartholomäus et al., 2009). In contrast, neutrophils did not show this orientation against the direction of the flow both *in vitro* and *in vivo* (Phillipson et al., 2006; Schenkel et al., 2004; Sumagin et al., 2010). Also, studies describing intravascular locomotion of homeostatic monocytes did not report any directional bias (Auffray et al., 2009; Carlin et al., 2011). These observations lead to the assumption that lymphocytes and myeloid cells respond differently to shear stress and that hemodynamic parameters are likely to be a factor shaping intravascular migration.

4.3 Automated characterization and classification of cell motility reveals heterogeneity in immune cell populations

Studying homeostatic monocytes in the leptomeningeal blood vessels of the spinal cord during atEAE it became evident that these cells were not homogeneous in their migratory behaviour. Various migratory patterns emerged, which indicated an additional level of complexity.

To account for this increased complexity, we employed unsupervised machine learning to classify and analyse immune cell motility patterns. Using this approach immune cells were classified into six motility patterns (Figure 13). With this approach we could not just reproduce the main results obtained by the manual analyses of the migratory behaviour of monocyte and T cells (Figure 14) but more importantly 1) we eliminated observer bias and 2) we were able to detect more patterns than the ones that were manually assigned to the cells. Therefore, the

heterogeneity of monocyte motility patterns could be better described. For example, the manually assigned firm adhesion phenotype (Figure 10 A and B) was further subdivided by the automated classification into the motility patterns 5 and 6 which differed mainly by their migration angle in relation to the blood flow and their track straightness, which was quite straight against the direction of blood flow in pattern 6 (Figure 13 A and B). This different motility behaviour suggested a potentially biological relevant difference in the quality of adhesion to the blood vessel endothelium between these two motility patterns which was not detected by manual classification. Moreover, motility pattern 6 represented only a minor fraction of migratory patterns in homeostatic monocytes and therefore could possibly escape as an emerging pattern in manual classification. Although being only an underrepresented motility pattern of homeostatic monocytes, pattern 6 is notable in the regard that it is the only motility pattern that is not modified by the ongoing inflammation induced by atEAE. In contrast, all other patterns either increase or decrease with ongoing inflammation (Figure 14 B). Taken together, the automated unsupervised classification methodology used in the present work was able to reliably detect and classify immune cell motility patterns in an unbiased manner. These patterns represent potentially biologically meaningful locomotion phenotypes and not artificial classes imposed by the hierarchical clustering algorithm. Furthermore, this methodological approach enabled us to quantitatively analyse immune cell migration on the single-cell level and avoided averaging motility parameters (i.e., speed, displacement etc.) on the population level, which limits the degree of heterogeneity that can be revealed in the data, and which is usually a drawback of the statistical analysis at the level of cell populations. This was best exemplified by the results from our VLA-4-blocking experiments. Injection of VLA-4-blocking antibody led to a significant detachment of homeostatic monocytes and T_{MBP} cells. Single-cell-level analysis of the remaining cells revealed a shift of homeostatic monocyte migratory pattern profile towards the more independently crawling motility phenotypes 4-6. This shift was mainly driven by the resistance of patterns 4 and 6 to VLA-4-blocking. Such a shift was not apparent in T_{MBP} cells, here all patterns were similarly affected by the treatment (Figure 16 C). Analysing the same data with conventional population-level analysis of the single migratory parameters did not show a difference in the response to VLA-4-blocking between homeostatic monocytes and T_{MBP} cells. Rather, changes of the parameters after treatment followed the same trend in homeostatic monocytes and T_{MBP} cells (Figure 28 A and B).

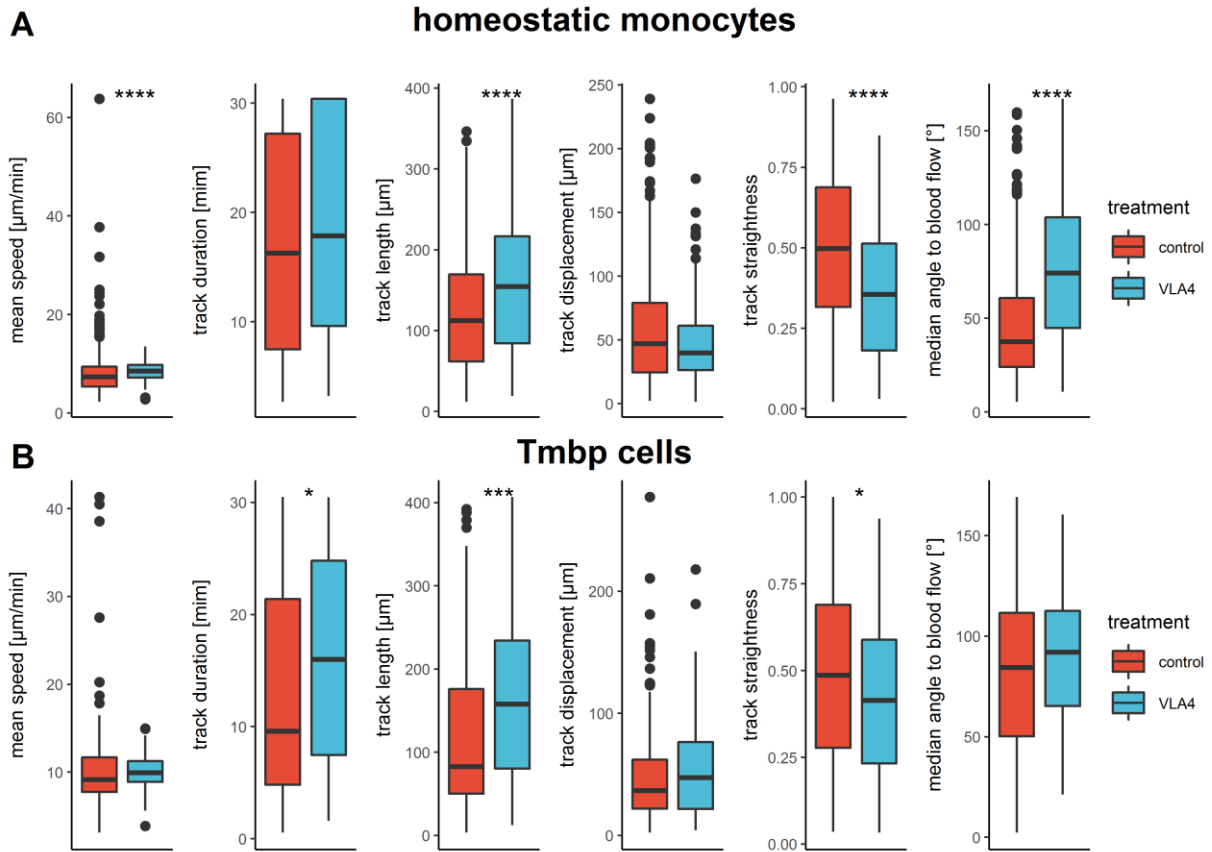


Figure 28 Migratory parameters of homeostatic monocytes and T_{MBP} cells before and after anti-VLA-4 treatment. Motility parameters derived from intravital TPLSM 2 days post T_{MBP} cell transfer.

4.4 Molecular cues shaping motility patterns

Applying automated characterization and parameter-free classification revealed heterogeneity in the migration modes of homeostatic monocytes and encephalitogenic T cells in leptomeningeal blood vessels. We investigated which molecular cues shaped the distinct motility patterns by blocking the integrins VLA-4 and LFA-1 by intravenous injection of blocking antibodies and by inhibiting global G_{ai}-signalling by injection of Pertussis toxin during intravital TPLSM.

Interfering with VLA-4 signalling led to significant detachment of T_{MBP} cells as well as homeostatic monocytes from leptomeningeal endothelium. Even though the magnitude of the detachment was not significantly different between monocytes and T_{MBP} cells (Figure 16 A and B), in-depth automated classification analysis on the single-cell level revealed that monocytes and T cells differed in their response to blocking VLA-4. The remaining T_{MBP} cells showed a similar reduction across all motility patterns (Figure 16 C, Table 2, and Table 3) indicating the T_{MBP} cell motility patterns are VLA-4-independent in the way that $\alpha 4$ -integrins are necessary to mediate T cell adhesion to the endothelium, but they are not involved in shaping their motility

patterns. In contrast, the remaining monocytes showed a general shift from the straight in direction of blood flow migrating motility patterns 1-3 to the more independent migrating patterns 4-6. Of note here are patterns 4 and 6 which were not removed from the endothelium by blocking VLA-4. These data indicate that motility patterns 1-3 in homeostatic monocytes are dependent on VLA-4, whereas the motility patterns 4-6 are rather VLA-4-independent (Figure 16 C, Table 2 and Table 3).

When we blocked LFA-1 we noticed an increase of monocytes as well T_{MBP} cells attached to leptomeningeal vessel endothelium. Furthermore, absolute numbers of motility patterns increased after the treatment in both cell populations, except pattern 2, which was decreased in monocytes (Figure 17 A-C, Table 4, and Table 5). This leads to the conclusion that motility pattern 2 is αL -integrin-dependent. Blocking LFA-1 leads to an influx of newly arriving monocytes and T_{MBP} cells which makes it difficult to assess the role of LFA-1 in shaping motility patterns because the state of these newcomers is unknown and no reference motility patterns from before treatment were recorded.

These data furthermore showed that our analysis methodology is able to reveal heterogeneity in the motility behaviour of cell populations that standard population-level analysis cannot detect. Our T cell data are in line with data from Bartholomäus et al. that showed that blocking LFA-1 in Lewis rat atEAE had no clear effect on intravascular encephalitogenic T cell crawling. Using flow cytometry, the authors of this study observed an increased number of these T cells recovered from spinal cord meninges after LFA-1 blocking compared to isotype control (Bartholomäus et al., 2009). The same study showed that blocking VLA-4 abrogated intravascular T cell crawling in leptomeningeal vessels which is in accordance with the results presented in this work. *In vivo*, VLA-4-mediated capture and rolling are mainly seen in venules in the CNS (Kerfoot and Kubes, 2002; Vajkoczy et al., 2001). Several lines of evidence show that VLA-4-mediated intravascular migration of T cells is one of the most critical factors for the development of EAE. Functional interference with VLA-4-mediated adhesion by blocking antibodies prevented the accumulation of infiltrating leukocytes in the CNS and the development of EAE (Baron, 1993; Engelhardt et al., 1998; Yednock et al., 1992). Due to this critical involvement of VLA-4 in EAE development, the molecule came into focus as a target for treatment in MS. The humanized monoclonal antibody against $\alpha 4$ -integrin Natalizumab is used to treat relapse-remitting multiple sclerosis (RRMS) and shows beneficial effects (Engelhardt and Kappos, 2008; Johnson, 2007).

It is described that intravascular crawling of patrolling homeostatic monocytes in mice is LFA-1 dependent (Auffray et al., 2007; Carlin et al., 2013), therefore it was surprising that blocking VLA-4 led to such a substantial detachment of homeostatic monocytes from the endothelium of leptomeningeal blood vessels and that homeostatic monocytes were not detached from blood vessel endothelium by blocking $\alpha\text{L}\beta 2$ -integrin. All these previous studies were carried out on mouse models, therefore one possible explanation could be that integrin-usage of homeostatic monocytes could be substantially different between rats and mice. VLA-4 is described in the literature to be also involved in monocyte capture and rolling (Chan et al., 2001; Huo et al., 2000; Kerfoot and Kubes, 2002). This can lead to the assumption that the motility patterns 1-3 are in fact rolling cells instead of cells that show a form of intravascular crawling, and the observed effect of blocking VLA-4 is therefore the blocking of monocyte capture and rolling. Rolling leukocytes only transiently adhere to the vascular endothelium and rolling velocities are in the range of several $\mu\text{m s}^{-1}$, therefore it is very difficult to observe these events with TPLSM (Kawakami, 2016). In contrast, monocyte motility patterns of 1-3 have much lower average velocities of $11.1 \pm 0.49 \mu\text{m min}^{-1}$, $16.3 \pm 1.86 \mu\text{m min}^{-1}$ and $7.38 \pm 0.163 \mu\text{m min}^{-1}$ and observation times of $5.85 \pm 0.182 \text{ min}$, $16.0 \pm 0.53 \text{ min}$ and $26.3 \pm 0.282 \text{ min}$, respectively. These parameters clearly exclude these motility patterns from being classified as conventional rolling. After blocking LFA-1, we saw the tendency to an overall increase in the numbers of monocytes attached to the endothelium (Figure 17 A and B). In-depth analysis on the single-cell level revealed that motility pattern 2 was in fact LFA-1-dependent and removed by blocking LFA-1 (Figure 17 C, Table 4). These findings again indicate that homeostatic monocytes, that we observed by TPLSM, in the rat are a heterogeneous population and that monocytes exhibiting motility pattern 2 could be the closest counterparts to the patrolling monocytes described by Auffray et al. It furthermore exemplifies that automated classification analysis on the single-cell level is a useful tool to detect cell population heterogeneity in terms of cell motility behaviour. Another possible explanation is that endothelial cells differ in the cell adhesion ligands they express from endothelial cells of peripheral veins and venules where most of the data from published studies are from (i.e. dermis of the ear, mesentery, liver, [Auffray et al., 2007; Carlin et al., 2013]). Indeed, we have preliminary RNA-sequencing data that show that endothelial cells from the spinal cord leptomeninges have a different transcriptional profile from peripheral endothelial cells derived from the cremaster muscle. This difference was observed in naïve ECs as well as in ECs during atEAE.

In addition to the role of integrins, we also investigated if and how chemokine signalling contributed to shaping immune cell motility patterns. After infusion of pertussis toxin, which

globally inhibits $G_{\alpha i}$ -signalling and therefore also chemokine signalling, during intravital TPLSM, the results were similar to the VLA-4-blocking experiments. Monocytes and T_{MBP} cells were significantly but not completely detached from the blood vessel endothelium. The detachment was not as profound as with blocking VLA-4 and the response to PTX was not significantly different between monocytes and T cells, although T cells were by trend more affected (Figure 18 A-B). The automated classification analysis of the remaining monocytes showed a shift in their migratory pattern profile towards the independent crawling patterns 4-6. Again, motility pattern 4 stood out as it was not affected by PTX and showed no reduction after the treatment. In contrast to the results from the VLA-4-blocking experiments, T_{MBP} cells responded in the same way as monocytes to inhibition of chemokine signalling (Figure 18, Table 6, and Table 7). These results imply that the motility patterns 1-3 of monocytes and encephalitogenic T cells are chemokine signalling-dependent. As this phenotype very much recapitulated the observations from VLA-4-blocking experiments, it is to be assumed that VLA-4 is activated through $G_{\alpha i}$ -signalling in cells exhibiting motility patterns 1-3. This chemokine-mediated activation of integrins seems to be much less necessary for the motility patterns 4-6, especially pattern 4, which is completely independent of it. This indicates that this type of motility closely resembles the patrolling of homeostatic monocytes described in the literature, which has been shown to be independent of the chemokine receptor CX₃CR1 and $G_{\alpha i}$ in general under steady-state conditions (Carlin et al., 2013).

4.5 Change of monocyte motility patterns is due to transcriptional changes of leptomeningeal blood vessel endothelial cells

We observed that with the progression of autoimmune inflammation homeostatic monocytes changed their motility phenotypes (Figure 10 B). It has been shown that GM-CSF can elicit an inflammatory transcription program in classical inflammatory monocytes, licensing them to cause tissue damage during EAE (Croxford et al., 2015). This raised the question if the observed changes are *mediated* by cell-intrinsic expression profile reprogramming or rather facilitated by cell-extrinsic molecular cues. Transcriptome analysis of monocytes isolated from the blood daily over the time course of EAE did not reveal substantial changes in the transcriptional profile of monocytes (Figure 25 A-B). These results were confirmed by RT-qPCR of a selected subset of genes, including adhesion molecules and chemokine receptors, and on the protein level by flow cytometry (Figure 23 A-B, Figure 24). Next, we focused on inflammation-induced changes in leptomeningeal endothelial cells and performed RNA-sequencing on these cells isolated in naïve conditions and at the preclinical phase of atEAE when most of the T cells are still localized inside the vessels. Global transcriptome analysis revealed that endothelial cells

significantly changed their transcriptional profile as indicated by the clear segregation of the two isolated populations in PC1 (Figure 26 A-B). Most notably, they upregulated adhesion molecules (*Icam-1*, *Vcam-1*) and chemokines (*Cxcl9-11*, *Cx3cl1*), and downregulated tight-junction molecules (*Occludin*, *claudin-5*) at the preclinical phase of atEAE (Figure 26 B-D). This data indicates that ECs become more “sticky” with progressing inflammation and that the higher availability of cell adhesion ligands likely facilitates the change of monocyte motility patterns. Interestingly, among the upregulated genes we found chemokines that are associated with T cells (*Cxcl9* and *Cxcl11*) and with homeostatic monocytes (*Cx3cl1*) but not inflammatory monocyte chemokine (*Ccl2*). Although the number of samples for RNA-sequencing was only 2, we could verify the results by RT-qPCR for most of the genes (Figure 26). Interestingly, we had opposite results for *Cx3cl1* and *Cxcl9* which were downregulated in the RT-qPCR samples. It should be noted that both these genes were very lowly expressed. These discrepancies could be explained by differences in amplification and quantification methods of these protocols as well as by expression levels of the genes. A benchmark study to compare RNA-sequencing with RT-qPCR revealed that about 85% of genes showed a high correlation between these methods. But the study also revealed a small but specific set of genes that showed inconsistent results. These genes were typically shorter, had fewer exons, and showed low expression (Everaert et al., 2017). To finally address this point, in the future we have to sequence the second batch of ECs.

4.6 Cell extrinsic factor shaping motility patterns

Cell migration is an essential component of the immune response: to perform their complex functions efficiently immune cells are guided towards target locations by external cues such as soluble chemoattractants (chemotaxis), surface-bound molecules (haptotaxis), or mechanical stimuli. In the present work we observed that whereas intravascular crawling T_{MBP} cells preferentially migrated against the direction of the blood flow as previously reported (Bartholomäus et al.), monocytes mainly followed blood flow direction. Similar results were also reported *in vitro* by using flow chamber assays (Valignat et al., 2013, 2014). Thus, we asked if not just molecular cues but also mechanical cues such as shear force play a role in shaping the motility patterns of monocytes and/or T cells. In our system, immune cells migrate in leptomeningeal post-capillary venules with high shear stress ($>6\text{dyn/cm}^2$, [Ley and Gaehtgens, 1991]). It is well established that there is a negative correlation between shear stress and vessel diameter (Secomb, 2016) and therefore investigated if differences in vessel size could be involved in shaping migratory pattern profiles of monocytes and T cells. Thus, we established a system to automatically derive vessel diameters from the recorded intravital

microscopy videos and correlated each cell track to the blood vessel diameter it was located in during its observation. We found that the distinct T_{MBP} cell motility patterns were equally distributed across all diameters and therefore seem to be independent of this vascular feature (Figure 20 A). This was not the case for homeostatic monocytes: indeed, migratory patterns 1-3 showed a preference towards blood vessels with smaller diameters (Figure 20 A). This could be explained by the observation that monocytes are in general less adhesive and less interacting with the vascular wall and therefore they will attach more loosely to vessels with a lower diameter and higher shear stress. Apart from the diameter, other architectural features of blood vessels influence the hemodynamic parameters. From literature it is known that at blood vessel bifurcations, mainly in the arterial vascular tree, the laminar blood flow becomes turbulent (Ku, 1997). Therefore, we investigated the distribution of motility patterns at sites of blood vessel junctions and non-junction regions to elucidate if these vessel features influence motility phenotypes. We developed an algorithm to automatically detect junction points in the microscopy data and assessed whether these regions are preferential locations for either monocytes or T cells. As it turned out, neither monocytes nor T cells showed any preference for junction or non-junction areas. The data suggested that location was distributed randomly between these regions of interest. We additionally used the recorded videos of the integrin- and chemokine-blocking experiments as input for the analysis pipeline to evaluate if these molecules are involved in the distribution of the cells to these regions of interest. Blocking any of these molecules did not change the seemingly random distribution of monocytes and T cells (Figure 21 A-D). From this, we conclude that areas of vessel junctions play no role in shaping motility phenotypes. There are two possible explanations. (1) There are no or minimal perturbations of laminar flow at the investigated vessel junction. For this argues that disturbances in the laminar flow are mainly described in the arterial vessel tree, especially at the carotid artery bifurcation (Ku, 1997). A possible approach to explore this would be to use intravenously injected blood tracer beads in combination with high-speed intravital laser scanning microscopy. Modern resonant scanners in multiphoton microscopes are able to achieve scanning rates from 30 frames per second to up to 420 frames per second in small area scans. With this acquisition rate, it would be possible to follow fluorescent beads passively swimming in the blood flow and resolve perturbations in laminar flow. (2) Perturbations of laminar flow are not relevant for shaping the intravascular motility behaviour of immune cells in the spinal cord leptomeninges. Additional experiments are needed to investigate this possibility. In order to provide controlled experimental conditions, an artificial *in vitro* bifurcation system would be needed.

4.7 Monocytes display different motility pattern profiles than encephalitogenic T cell

Our model of atEAE in combination with the possibility to fluorescently label homeostatic monocytes and encephalitogenic T cells allowed us to study both cell types simultaneously *in vivo* by intravital TPLSM. Automated motility pattern classification analysis on the single-cell level of the recorded time-lapse imaging data revealed that intravascular migrating homeostatic monocytes and T_{MBP} cells displayed different motility pattern profiles in leptomeningeal blood vessels. Monocyte motility profiles were shifted towards straight in the direction of the blood patterns 1-3, whereas T cells displayed profiles shifted towards independent crawling patterns 4-6 (Figure 12 A and C). These cells were migrating in the same milieu; therefore, it was interesting that motility patterns differed to such a high extent. We asked what factors could facilitate the different motility pattern profiles. We addressed this question by global transcriptome analysis of monocytes and T_{MBP} cells. Among the 3377 significantly expressed genes we found several cell adhesion-associated genes. Surprisingly, monocytes expressed more Itga4, Itgal, Itgb2, Alcam, and Ninjurin than T_{MBP} cells (Figure 27 C), although their motility pattern profile suggests that their interaction with blood vessel endothelium is weaker than that of T cells. Thus, we hypothesized that the observed differences in motility phenotypes could be due to the utilization of further cell adhesion receptors by T cells and monocytes. We conducted a sub-analysis focused on receptor-ligand pairs associated with cell migration and – adhesion. For this, we assembled a list of cell adhesion receptors located on the external surface and which are associated with adhesion and cell migration. From this list, we quantified the number of receptor interactions with their cognate ligands, which showed up in our endothelial cell RNA-sequencing dataset, which were upregulated either in monocytes or T_{MBP} cells. We found that ligand-receptor interactions in T cells significantly exceeded the ones of monocytes (Figure 27 D). This implies that T_{MBP} cells utilize a broader repertoire of molecules interacting with vascular endothelial cells than monocytes which could explain the differences in their motility profile patterns. Although these results are inferential, they provide a basis for the rational design of future experiments.

5. Summary

In summary, we have established a system to specifically label the homeostatic monocyte subset in Lewis rats for intravital TPLSM. With this system, we could study and characterize the recruitment and motility of these cells in the adoptive transfer Lewis rat EAE model. We have shown that in this model homeostatic monocytes are recruited to the leptomeninges of the spinal cord during the preclinical phase of EAE. A further advantage of the model is that the adoptively transferred MBP-reactive T cells express fluorescent reporter proteins, therefore enabling us to study the motility of T cells and homeostatic monocytes in parallel. Using a novel machine learning-based analysis of immune cell motility, we observed that homeostatic monocytes exhibited heterogeneous motility phenotypes inside of leptomeningeal vessels and that these motility modes are distinct to T_{MBP} cell motility phenotypes. Furthermore, this analysis platform enabled us to investigate the effect of hemodynamic parameters on intravascular immune cell migration. By interfering with integrin- and chemokine signalling we could show that the observed immune cell migratory phenotypes responded differently to these interfering strategies. Notably, homeostatic monocytes showed greater heterogeneity in their response to these interferences than T_{MBP} cells, indicating a possible heterogeneous monocyte subpopulation. Our analysis approach could be useful to link immune cell subpopulations, identified by state-of-the-art single-cell sequencing techniques, with immune cell behaviour *in situ*.

Bibliography

Ahuja, V., Miller, S.E., and Howell, D.N. (1995). Identification of two subpopulations of rat monocytes expressing disparate molecular forms and quantities of CD43. *Cell. Immunol.* *163*, 59–69.

Allen, A.C., Kelly, S., Basdeo, S.A., Kinsella, K., Mulready, K.J., Mills, K.H., Tubridy, N., Walsh, C., Brady, J.J., Hutchinson, M., et al. (2012). A pilot study of the immunological effects of high-dose vitamin D in healthy volunteers. *Mult. Scler. J.* *18*, 1797–1800.

Ascherio, A., Munger, K.L., and Simon, K.C. (2010). Vitamin D and multiple sclerosis. *Lancet Neurol.* *9*, 599–612.

Auffray, C., Fogg, D., Garfa, M., Elain, G., Join-Lambert, O., Kayal, S., Sarnacki, S., Cumano, A., Lauvau, G., and Geissmann, F. (2007). Monitoring of blood vessels and tissues by a population of monocytes with patrolling behaviour. *Science* *317*, 666–670.

Auffray, C., Sieweke, M.H., and Geissmann, F. (2009). Blood monocytes: development, heterogeneity, and relationship with dendritic cells. *Annu. Rev. Immunol.* *27*, 669–692.

Bar-Or, A., Nuttall, R.K., Duddy, M., Alter, A., Kim, H.J., Ifergan, I., Pennington, C.J., Bourgoin, P., Edwards, D.R., and Yong, V.W. (2003). Analyses of all matrix metalloproteinase members in leukocytes emphasize monocytes as major inflammatory mediators in multiple sclerosis. *Brain* *126*, 2738–2749.

Baron, J.L. (1993). Surface expression of alpha 4 integrin by CD4 T cells is required for their entry into brain parenchyma. *J. Exp. Med.* *177*, 57–68.

Bartholomäus, I., Kawakami, N., Odoardi, F., Schläger, C., Miljkovic, D., Ellwart, J.W., Klinkert, W.E.F., Flügel-Koch, C., Issekutz, T.B., Wekerle, H., et al. (2009). Effector T cell interactions with meningeal vascular structures in nascent autoimmune CNS lesions. *Nature* *462*, 94–98.

Beecham, A.H., Patsopoulos, N.A., Xifara, D.K., Davis, M.F., Kempainen, A., Cotsapas, C., Shah, T.S., Spencer, C., Booth, D., Goris, A., et al. (2013). Analysis of immune-related loci identifies 48 new susceptibility variants for multiple sclerosis. *Nat. Genet.* *45*, 1353–1360.

Beltman, J.B., Marée, A.F.M., and de Boer, R.J. (2009). Analysing immune cell migration. *Nat. Rev. Immunol.* *9*, 789–798.

Ben-Nun, A., Wekerle, H., and Cohen, I.R. (1981). The rapid isolation of clonable antigen-

specific T lymphocyte lines capable of mediating autoimmune encephalomyelitis. *Eur. J. Immunol.* *11*, 195–199.

Berlin, C., Bargatze, R.F., Campbell, J.J., von Andrian, U.H., Szabo, M.C., Hasslen, S.R., Nelson, R.D., Berg, E.L., Erlandsen, S.L., and Butcher, E.C. (1995). $\alpha 4$ integrins mediate lymphocyte attachment and rolling under physiologic flow. *Cell* *80*, 413–422.

Brocke, S., Piercy, C., Steinman, L., Weissman, I.L., and Veromaa, T. (1999). Antibodies to CD44 and integrin $\alpha 4$, but not L-selectin, prevent central nervous system inflammation and experimental encephalomyelitis by blocking secondary leukocyte recruitment. *Proc. Natl. Acad. Sci. U. S. A.* *96*, 6896–6901.

Bullard, D.C., Hu, X., Schoeb, T.R., Collins, R.G., Beaudet, A.L., and Barnum, S.R. (2007). Intercellular Adhesion Molecule-1 Expression Is Required on Multiple Cell Types for the Development of Experimental Autoimmune Encephalomyelitis. *J. Immunol.* *178*, 851–857.

Carlin, L.M., Evans, R., Milewicz, H., Fernandes, L., Matthews, D.R., Perani, M., Levitt, J., Keppler, M.D., Monypenny, J., Coolen, T., et al. (2011). A Targeted siRNA Screen Identifies Regulators of Cdc42 Activity at the Natural Killer Cell Immunological Synapse. *Sci. Signal.* *4*, ra81.

Carlin, L.M., Stamatiades, E.G., Auffray, C., Hanna, R.N., Glover, L., Vizcay-Barrena, G., Hedrick, C.C., Cook, H.T., Diebold, S., and Geissmann, F. (2013). Nr4a1-dependent Ly6C(low) monocytes monitor endothelial cells and orchestrate their disposal. *Cell* *153*, 362–375.

Carman, C. V., and Springer, T.A. (2004). A trans migratory cup in leukocyte diapedesis both through individual vascular endothelial cells and between them. *J. Cell Biol.* *167*, 377–388.

Cayrol, R., Wosik, K., Berard, J.L., Dodelet-Devillers, A., Ifergan, I., Kebir, H., Haqqani, A.S., Kreymborg, K., Krug, S., Moudjian, R., et al. (2008). Activated leukocyte cell adhesion molecule promotes leukocyte trafficking into the central nervous system. *Nat. Immunol.* *9*, 137–145.

Chan, J.R., Hyduk, S.J., and Cybulsky, M.I. (2001). Chemoattractants Induce a Rapid and Transient Upregulation of Monocyte $\alpha 4$ Integrin Affinity for Vascular Cell Adhesion Molecule 1 Which Mediates Arrest. *J. Exp. Med.* *193*, 1149–1158.

Codarri, L., Gyölvézi, G., Tosevski, V., Hesske, L., Fontana, A., Magnenat, L., Suter, T., and Becher, B. (2011). ROR γ t drives production of the cytokine GM-CSF in helper T cells, which

is essential for the effector phase of autoimmune neuroinflammation. *Nat. Immunol.* 12, 560–567.

Compston, A., and Coles, A. (2008). Multiple sclerosis. *Lancet* 372, 1502–1517.

Croxford, A.L., Lanzinger, M., Hartmann, F.J., Schreiner, B., Mair, F., Pelczar, P., Clausen, B.E., Jung, S., Greter, M., and Becher, B. (2015). The Cytokine GM-CSF Drives the Inflammatory Signature of CCR2⁺ Monocytes and Licenses Autoimmunity. *Immunity* 43, 502–514.

Denk, W., and Svoboda, K. (1997). Photon upmanship: why multiphoton imaging is more than a gimmick. *Neuron* 18, 351–357.

Denk, W., Strickler, J.H., and Webb, W.W. (1990). Two-photon laser scanning fluorescence microscopy. *Science* 248, 73–76.

Doring, A., Wild, M., Vestweber, D., Deutsch, U., and Engelhardt, B. (2007). E- and P-Selectin Are Not Required for the Development of Experimental Autoimmune Encephalomyelitis in C57BL/6 and SJL Mice. *J. Immunol.* 179, 8470–8479.

Elhofy, A., Kennedy, K.J., Fife, B.T., and Karpus, W.J. (2002). Regulation of experimental autoimmune encephalomyelitis by chemokines and chemokine receptors. *Immunol. Res.* 25, 167–175.

Engelhardt, B., and Kappos, L. (2008). Natalizumab: targeting alpha4-integrins in multiple sclerosis. *Neurodegener. Dis.* 5, 16–22.

Engelhardt, B., and Ransohoff, R.M. (2005). The ins and outs of T-lymphocyte trafficking to the CNS: anatomical sites and molecular mechanisms. *Trends Immunol.* 26, 485–495.

Engelhardt, B., and Ransohoff, R.M. (2012). Capture, crawl, cross: the T cell code to breach the blood-brain barriers. *Trends Immunol.* 33, 579–589.

Engelhardt, B., Laschinger, M., Schulz, M., Samulowitz, U., Vestweber, D., and Hoch, G. (1998). The development of experimental autoimmune encephalomyelitis in the mouse requires alpha4-integrin but not alpha4beta7-integrin. *J. Clin. Invest.* 102, 2096–2105.

Everaert, C., Luybaert, M., Maag, J.L. V, Cheng, Q.X., Dinger, M.E., Hellemans, J., and Mestdagh, P. (2017). Benchmarking of RNA-sequencing analysis workflows using whole-transcriptome RT-qPCR expression data. *Sci. Rep.* 7, 1559.

Eylar, E.H., Kniskern, P.J., and Jackson, J.J. (1974). [31] Myelin Basic Proteins. *Methods Enzymol.* 32.

Farh, K.K.-H., Marson, A., Zhu, J., Kleinewietfeld, M., Housley, W.J., Beik, S., Shores, N., Whitton, H., Ryan, R.J.H., Shishkin, A.A., et al. (2014). Genetic and epigenetic fine mapping of causal autoimmune disease variants. *Nature* 518, 337–343.

Fife, B.T., Huffnagle, G.B., Kuziel, W.A., and Karpus, W.J. (2000). CC chemokine receptor 2 is critical for induction of experimental autoimmune encephalomyelitis. *J. Exp. Med.* 192, 899–905.

Fife, B.T., Kennedy, K.J., Paniagua, M.C., Lukacs, N.W., Kunkel, S.L., Luster, a D., and Karpus, W.J. (2001). CXCL10 (IFN-gamma-inducible protein-10) control of encephalitogenic CD4⁺ T cell accumulation in the central nervous system during experimental autoimmune encephalomyelitis. *J. Immunol.* 166, 7617–7624.

Fischer, M.T., Sharma, R., Lim, J.L., Haider, L., Frischer, J.M., Drexhage, J., Mahad, D., Bradl, M., van Horssen, J., and Lassmann, H. (2012). NADPH oxidase expression in active multiple sclerosis lesions in relation to oxidative tissue damage and mitochondrial injury. *Brain* 135, 886–899.

Flügel, A., Willem, M., Berkowicz, T., and Wekerle, H. (1999). Gene transfer into CD4⁺ T lymphocytes: green fluorescent protein-engineered, encephalitogenic T cells illuminate brain autoimmune responses. *Nat. Med.* 5, 843–847.

Flügel, A., Berkowicz, T., Ritter, T., Labeur, M., Jenne, D.E., Li, Z., Ellwart, J.W., Willem, M., Lassmann, H., and Wekerle, H. (2001). Migratory activity and functional changes of green fluorescent effector cells before and during experimental autoimmune encephalomyelitis. *Immunity* 14, 547–560.

Geissmann, F., Jung, S., and Littman, D.R. (2003). Blood monocytes consist of two principal subsets with distinct migratory properties. *Immunity* 19, 71–82.

Glabinski, a R., Bielecki, B., and Ransohoff, R.M. (2003). Chemokine upregulation follows cytokine expression in chronic relapsing experimental autoimmune encephalomyelitis. *Scand. J. Immunol.* 58, 81–88.

Haider, L., Fischer, M.T., Frischer, J.M., Bauer, J., Hoftberger, R., Botond, G., Esterbauer, H., Binder, C.J., Witztum, J.L., and Lassmann, H. (2011). Oxidative damage in multiple sclerosis lesions. *Brain* 134, 1914–1924.

Hanna, R.N., Carlin, L.M., Hubbeling, H.G., Nackiewicz, D., Green, A.M., Punt, J. a, Geissmann, F., and Hedrick, C.C. (2011). The transcription factor NR4A1 (Nur77) controls

- bone marrow differentiation and the survival of Ly6C⁺ monocytes. *Nat. Immunol.* *12*, 778–785.
- Harkiolaki, M., Holmes, S.L., Svendsen, P., Gregersen, J.W., Jensen, L.T., McMahon, R., Friese, M.A., van Boxel, G., Etzensperger, R., Tzartos, J.S., et al. (2009). T Cell-Mediated Autoimmune Disease Due to Low-Affinity Crossreactivity to Common Microbial Peptides. *Immunity* *30*, 348–357.
- Hauser, S.L., and Oksenberg, J.R. (2006). The neurobiology of multiple sclerosis: genes, inflammation, and neurodegeneration. *Neuron* *52*, 61–76.
- Helmchen, F., and Denk, W. (2005). Deep tissue two-photon microscopy. *Nat. Methods* *2*, 932–940.
- Hemmer, B., Kerschensteiner, M., and Korn, T. (2015). Role of the innate and adaptive immune responses in the course of multiple sclerosis. *Lancet. Neurol.* *14*, 406–419.
- Henderson, A.P.D., Barnett, M.H., Parratt, J.D.E., and Prineas, J.W. (2009). Multiple sclerosis: Distribution of inflammatory cells in newly forming lesions. *Ann. Neurol.* *66*, 739–753.
- Hojo, M., Maghni, K., Issekutz, T.B., and Martin, J.G. (1998). Involvement of alpha-4 integrins in allergic airway responses and mast cell degranulation in vivo. *Am. J. Respir. Crit. Care Med.* *158*, 1127–1133.
- Huang, D.R., Wang, J., Kivisakk, P., Rollins, B.J., and Ransohoff, R.M. (2001). Absence of monocyte chemoattractant protein 1 in mice leads to decreased local macrophage recruitment and antigen-specific T helper cell type 1 immune response in experimental autoimmune encephalomyelitis. *J. Exp. Med.* *193*, 713–726.
- Huitinga, I., van Rooijen, N., de Groot, C.J., Uitdehaag, B.M., and Dijkstra, C.D. (1990). Suppression of experimental allergic encephalomyelitis in Lewis rats after elimination of macrophages. *J. Exp. Med.* *172*, 1025–1033.
- Huitinga, I., Ruuls, S.R., Jung, S., Van Rooijen, N., Hartung, H.P., and Dijkstra, C.D. (1995). Macrophages in T cell line-mediated, demyelinating, and chronic relapsing experimental autoimmune encephalomyelitis in Lewis rats. *Clin. Exp. Immunol.* *100*, 344–351.
- Huo, Y., Hafezi-Moghadam, A., and Ley, K. (2000). Role of Vascular Cell Adhesion Molecule-1 and Fibronectin Connecting Segment-1 in Monocyte Rolling and Adhesion on Early Atherosclerotic Lesions. *Circ. Res.* *87*, 153–159.
- Ifergan, I., Kebir, H., Terouz, S., Alvarez, J.I., Lécuyer, M.-A., Gendron, S., Bourbonnière, L., Dunay, I.R., Bouthillier, A., Moumdjian, R., et al. (2011). Role of Ninjurin-1 in the migration

of myeloid cells to central nervous system inflammatory lesions. *Ann. Neurol.* 70, 751–763.

Issekutz, T.B. (1991). Inhibition of in vivo lymphocyte migration to inflammation and homing to lymphoid tissues by the TA-2 monoclonal antibody. A likely role for VLA-4 in vivo. *J. Immunol.* 147, 4178–4184.

Issekutz, T.B., and Wykretowicz, A. (1991). Effect of a new monoclonal antibody, TA-2, that inhibits lymphocyte adherence to cytokine stimulated endothelium in the rat. *J. Immunol.* 147, 109–116.

Izikson, L., Klein, R.S., Charo, I.F., Weiner, H.L., and Luster, a D. (2000). Resistance to experimental autoimmune encephalomyelitis in mice lacking the CC chemokine receptor (CCR)2. *J. Exp. Med.* 192, 1075–1080.

Johnson, K.P. (2007). Natalizumab (Tysabri) Treatment for Relapsing Multiple Sclerosis. *Neurologist* 13, 182–187.

Kawakami, N. (2016). In vivo imaging in autoimmune diseases in the central nervous system. *Allergol. Int.* 65, 235–242.

Kawakami, N., and Flügel, A. (2010). Knocking at the brain's door: intravital two-photon imaging of autoreactive T cell interactions with CNS structures. *Semin. Immunopathol.* 32, 275–287.

Kawakami, N., Lassmann, S., Li, Z., Odoardi, F., Ritter, T., Ziemssen, T., Klinkert, W.E.F., Ellwart, J.W., Bradl, M., Krivacic, K., et al. (2004). The activation status of neuroantigen-specific T cells in the target organ determines the clinical outcome of autoimmune encephalomyelitis. *J. Exp. Med.* 199, 185–197.

Kawakami, N., Nägerl, U.V., Odoardi, F., Bonhoeffer, T., Wekerle, H., and Flügel, A. (2005). Live imaging of effector cell trafficking and autoantigen recognition within the unfolding autoimmune encephalomyelitis lesion. *J. Exp. Med.* 201, 1805–1814.

Kerfoot, S.M., and Kubes, P. (2002). Overlapping roles of P-selectin and alpha 4 integrin to recruit leukocytes to the central nervous system in experimental autoimmune encephalomyelitis. *J. Immunol.* 169, 1000–1006.

King, I.L., Dickendesher, T.L., and Segal, B.M. (2009). Circulating Ly-6C⁺ myeloid precursors migrate to the CNS and play a pathogenic role during autoimmune demyelinating disease. *Blood* 113, 3190–3197.

Kobayashi, Y., Kawai, K., Honda, H., Tomida, S., Niimi, N., Tamatani, T., Miyasaka, M., and

- Yoshikai, Y. (1995). Antibodies against Leukocyte Function-Associated Antigen-1 and against Intercellular Adhesion Molecule-1 Together Suppress the Progression of Experimental Allergic Encephalomyelitis. *Cell. Immunol.* 164, 295–305.
- Korn, T., Mitsdoerffer, M., and Kuchroo, V.K. (2009). Immunological Basis for the Development of Tissue Inflammation and Organ-Specific Autoimmunity in Animal Models of Multiple Sclerosis. In *Results and Problems in Cell Differentiation*, pp. 43–74.
- Kouwenhoven, M., Teleshova, N., Özenci, V., Press, R., and Link, H. (2001). Monocytes in multiple sclerosis: phenotype and cytokine profile. *J. Neuroimmunol.* 112, 197–205.
- Ku, D.N. (1997). BLOOD FLOW IN ARTERIES. *Annu. Rev. Fluid Mech.* 29, 399–434.
- Laschinger, M., Vajkoczy, P., and Engelhardt, B. (2002). Encephalitogenic T_H1 cells use LFA-1 for transendothelial migration but not during capture and initial adhesion strengthening in healthy spinal cord microvessels *in vivo*. *Eur. J. Immunol.* 32, 3598–3606.
- Lassmann, H., Raine, C.S., Antel, J., and Prineas, J.W. (1998). Immunopathology of multiple sclerosis: report on an international meeting held at the Institute of Neurology of the University of Vienna. *J. Neuroimmunol.* 86, 213–217.
- Lécuyer, M.-A., Saint-Laurent, O., Bourbonnière, L., Larouche, S., Larochelle, C., Michel, L., Charabati, M., Abadier, M., Zandee, S., Haghayegh Jahromi, N., et al. (2017). Dual role of ALCAM in neuroinflammation and blood–brain barrier homeostasis. *Proc. Natl. Acad. Sci.* 114, E524–E533.
- Levin, L.I., Munger, K.L., O'Reilly, E.J., Falk, K.I., and Ascherio, A. (2010). Primary infection with the Epstein-Barr virus and risk of multiple sclerosis. *Ann. Neurol.* 67, 824–830.
- Ley, K., and Gaehtgens, P. (1991). Endothelial, not hemodynamic, differences are responsible for preferential leukocyte rolling in rat mesenteric venules. *Circ. Res.* 69, 1034–1041.
- Ley, K., Laudanna, C., Cybulsky, M.I., and Nourshargh, S. (2007). Getting to the site of inflammation: the leukocyte adhesion cascade updated. *Nat. Rev. Immunol.* 7, 678–689.
- Liepsch, D., Balasso, A., Berger, H., and Eckstein, H.-H. (2012). How local hemodynamics at the carotid bifurcation influence the development of carotid plaques. *Perspect. Med.* 1, 132–136.
- Love, M.I., Huber, W., and Anders, S. (2014). Moderated estimation of fold change and dispersion for RNA-seq data with DESeq2. *Genome Biol.* 15, 550.
- Lyck, R., Lécuyer, M.-A., Abadier, M., Wyss, C.B., Matti, C., Rosito, M., Enzmann, G., Zeis,

- T., Michel, L., García Martín, A.B., et al. (2016). ALCAM (CD166) is involved in extravasation of monocytes rather than T cells across the blood–brain barrier. *J. Cereb. Blood Flow Metab.* 0271678X1667863.
- Mempel, T.R., Henrickson, S.E., and von Andrian, U.H. (2004). T-cell priming by dendritic cells in lymph nodes occurs in three distinct phases. *Nature* 427, 154–159.
- Mildner, A., Mack, M., Schmidt, H., Brück, W., Djukic, M., Zabel, M.D., Hille, A., Priller, J., and Prinz, M. (2009). CCR2+Ly-6Chi monocytes are crucial for the effector phase of autoimmunity in the central nervous system. *Brain* 132, 2487–2500.
- Miller, S.D., and Karpus, W.J. (2007). Experimental Autoimmune Encephalomyelitis in the Mouse. In *Current Protocols in Immunology*, (Hoboken, NJ, USA: John Wiley & Sons, Inc.), p. Unit 15.1.
- Miller, M.J., Safrina, O., Parker, I., and Cahalan, M.D. (2004). Imaging the Single Cell Dynamics of CD4 + T Cell Activation by Dendritic Cells in Lymph Nodes. *J. Exp. Med.* 200, 847–856.
- Mrass, P., Kinjyo, I., Ng, L.G., Reiner, S.L., Puré, E., Weninger, W., Tsukita, S., Andrian, U.H. von, Ertl, H.C., Haydon, P.G., et al. (2008). CD44 mediates successful interstitial navigation by killer T cells and enables efficient antitumor immunity. *Immunity* 29, 971–985.
- Münz, C., Lünemann, J.D., Getts, M.T., and Miller, S.D. (2009). Antiviral immune responses: triggers of or triggered by autoimmunity? *Nat. Rev. Immunol.* 9, 246–258.
- Narumi, S., Kaburaki, T., Yoneyama, H., Iwamura, H., Kobayashi, Y., and Matsushima, K. (2002). Neutralization of IFN-inducible protein 10/CXCL10 exacerbates experimental autoimmune encephalomyelitis. *Eur. J. Immunol.* 32, 1784.
- Odoardi, F., Sie, C., Streyl, K., Ulaganathan, V.K., Schläger, C., Lodygin, D., Heckelsmiller, K., Nietfeld, W., Ellwart, J., Klinkert, W.E.F., et al. (2012). T cells become licensed in the lung to enter the central nervous system. *Nature* 488, 675–679.
- Olson, J.K., Croxford, J.L., Calenoff, M.A., Dal Canto, M.C., and Miller, S.D. (2001). A virus-induced molecular mimicry model of multiple sclerosis. *J. Clin. Invest.* 108, 311–318.
- Palframan, R.T., Jung, S., Cheng, G., Weninger, W., Luo, Y., Dorf, M., Littman, D.R., Rollins, B.J., Zweerink, H., Rot, A., et al. (2001). Inflammatory chemokine transport and presentation in HEV: a remote control mechanism for monocyte recruitment to lymph nodes in inflamed tissues. *J. Exp. Med.* 194, 1361–1373.

- Paterson, P.Y. (1960). TRANSFER OF ALLERGIC ENCEPHALOMYELITIS IN RATS BY MEANS OF LYMPH NODE CELLS. *J. Exp. Med.* *111*, 119–136.
- Patro, R., Duggal, G., Love, M.I., Irizarry, R.A., and Kingsford, C. (2017). Salmon provides fast and bias-aware quantification of transcript expression. *Nat. Methods* *14*, 417–419.
- Phillipson, M., Heit, B., Colarusso, P., Liu, L., Ballantyne, C.M., and Kubes, P. (2006). Intraluminal crawling of neutrophils to emigration sites: a molecularly distinct process from adhesion in the recruitment cascade. *J. Exp. Med.* *203*, 2569–2575.
- Potter, S.M. (1996). Vital imaging: two photons are better than one. *Curr. Biol.* *6*, 1595–1598.
- Qi, H., Cannons, J.L., Klauschen, F., Schwartzberg, P.L., and Germain, R.N. (2008). SAP-controlled T–B cell interactions underlie germinal centre formation. *Nature* *455*, 764–769.
- Raj, T., Rothamel, K., Mostafavi, S., Ye, C., Lee, M.N., Replogle, J.M., Feng, T., Lee, M., Asinowski, N., Frohlich, I., et al. (2014). Polarization of the effects of autoimmune and neurodegenerative risk alleles in leukocytes. *Science* *344*, 519–523.
- Ramagopalan, S. V., Dymment, D.A., and Ebers, G.C. (2008). Genetic epidemiology: the use of old and new tools for multiple sclerosis. *Trends Neurosci.* *31*, 645–652.
- Ramilowski, J.A., Goldberg, T., Harshbarger, J., Kloppman, E., Lizio, M., Satagopam, V.P., Itoh, M., Kawaji, H., Carninci, P., Rost, B., et al. (2015). A draft network of ligand–receptor-mediated multicellular signalling in human. *Nat. Commun.* *6*, 7866.
- Reboldi, A., Coisne, C., Baumjohann, D., Benvenuto, F., Bottinelli, D., Lira, S., Uccelli, A., Lanzavecchia, A., Engelhardt, B., and Sallusto, F. (2009). C-C chemokine receptor 6-regulated entry of TH-17 cells into the CNS through the choroid plexus is required for the initiation of EAE. *Nat. Immunol.* *10*, 514–523.
- Rubart, M. (2004). Two-Photon Microscopy of Cells and Tissue. *Circ. Res.* *95*, 1154–1166.
- Saederup, N., Cardona, A.E., Croft, K., Mizutani, M., Coteleur, A.C., Tsou, C.-L., Ransohoff, R.M., and Charo, I.F. (2010). Selective chemokine receptor usage by central nervous system myeloid cells in CCR2-red fluorescent protein knock-in mice. *PLoS One* *5*, e13693.
- Sawcer, S., Hellenthal, G., Pirinen, M., Spencer, C.C.A., Patsopoulos, N.A., Moutsianas, L., Dilthey, A., Su, Z., Freeman, C., Hunt, S.E., et al. (2011). Genetic risk and a primary role for cell-mediated immune mechanisms in multiple sclerosis. *Nature* *476*, 214–219.
- Schenkel, A.R., Mamdough, Z., and Muller, W.A. (2004). Locomotion of monocytes on endothelium is a critical step during extravasation. *Nat. Immunol.* *5*, 393–400.

- Schläger, C., Körner, H., Krueger, M., Vidoli, S., Haberl, M., Mielke, D., Brylla, E., Issekutz, T., Cabañas, C., Nelson, P.J., et al. (2016). Effector T-cell trafficking between the leptomeninges and the cerebrospinal fluid. *Nature* 530, 349–353.
- Secomb, T.W. (2016). Hemodynamics. *Compr. Physiol.* 6, 975–1003.
- Shechter, R., London, A., Varol, C., Raposo, C., Cusimano, M., Yovel, G., Rolls, A., Mack, M., Pluchino, S., Martino, G., et al. (2009). Infiltrating Blood-Derived Macrophages Are Vital Cells Playing an Anti-inflammatory Role in Recovery from Spinal Cord Injury in Mice. *PLoS Med.* 6, e1000113.
- Shechter, R., Miller, O., Yovel, G., Rosenzweig, N., London, A., Ruckh, J., Kim, K.-W., Klein, E., Kalchenko, V., Bendel, P., et al. (2013). Recruitment of beneficial M2 macrophages to injured spinal cord is orchestrated by remote brain choroid plexus. *Immunity* 38, 555–569.
- Simmons, S.B., Pierson, E.R., Lee, S.Y., and Goverman, J.M. (2013). Modeling the heterogeneity of multiple sclerosis in animals. *Trends Immunol.* 34, 410–422.
- Singbartl, K., Thatte, J., Smith, M.L., Wethmar, K., Day, K., and Ley, K. (2001). A CD2-green fluorescence protein-transgenic mouse reveals very late antigen-4-dependent CD8+ lymphocyte rolling in inflamed venules. *J. Immunol.* 166, 7520–7526.
- Soneson, C., Love, M.I., and Robinson, M.D. (2016). Differential analyses for RNA-seq: transcript-level estimates improve gene-level inferences. *F1000Research* 4, 1521.
- Spitzer, M.H., Gherardini, P.F., Fragiadakis, G.K., Bhattacharya, N., Yuan, R.T., Hotson, A.N., Finck, R., Carmi, Y., Zunder, E.R., Fantl, W.J., et al. (2015). IMMUNOLOGY. An interactive reference framework for modeling a dynamic immune system. *Science* 349, 1259425.
- Steiner, O., Coisne, C., Cecchelli, R., Boscacci, R., Deutsch, U., Engelhardt, B., and Lyck, R. (2010). Differential roles for endothelial ICAM-1, ICAM-2, and VCAM-1 in shear-resistant T cell arrest, polarization, and directed crawling on blood-brain barrier endothelium. *J. Immunol.* 185, 4846–4855.
- Strauss-Ayali, D., Conrad, S.M., and Mosser, D.M. (2007). Monocyte subpopulations and their differentiation patterns during infection. *J. Leukoc. Biol.* 82, 244–252.
- Sumagin, R., Prizant, H., Lomakina, E., Waugh, R.E., and Sarelius, I.H. (2010). LFA-1 and Mac-1 define characteristically different intraluminal crawling and emigration patterns for monocytes and neutrophils in situ. *J. Immunol.* 185, 7057–7066.
- Sunderkötter, C., Nikolic, T., Dillon, M.J., Van Rooijen, N., Stehling, M., Drevets, D. a, and

- Leenen, P.J.M. (2004). Subpopulations of mouse blood monocytes differ in maturation stage and inflammatory response. *J. Immunol.* *172*, 4410–4417.
- Tran, E.H., Hoekstra, K., van Rooijen, N., Dijkstra, C.D., and Owens, T. (1998). Immune invasion of the central nervous system parenchyma and experimental allergic encephalomyelitis, but not leukocyte extravasation from blood, are prevented in macrophage-depleted mice. *J. Immunol.* *161*, 3767–3775.
- Trapp, B.D., Peterson, J., Ransohoff, R.M., Rudick, R., Mörk, S., and Bö, L. (1998). Axonal Transection in the Lesions of Multiple Sclerosis. *N. Engl. J. Med.* *338*, 278–285.
- Uboldi, C., Döring, A., Alt, C., Estess, P., Siegelman, M., and Engelhardt, B. (2008). L-Selectin-deficient SJL and C57BL/6 mice are not resistant to experimental autoimmune encephalomyelitis. *Eur. J. Immunol.* *38*, 2156–2167.
- Vajkoczy, P., Laschinger, M., Engelhardt, B., Holzmann, B., and Butcher, E. (2001). Alpha4-integrin-VCAM-1 binding mediates G protein-independent capture of encephalitogenic T cell blasts to CNS white matter microvessels. *J. Clin. Invest.* *108*, 557–565.
- Valignat, M.-P., Theodoly, O., Gucciardi, A., Hogg, N., and Lellouch, A.C. (2013). T lymphocytes orient against the direction of fluid flow during LFA-1-mediated migration. *Biophys. J.* *104*, 322–331.
- Valignat, M.-P., Nègre, P., Cadra, S., Lellouch, A.C., Gallet, F., Hénon, S., and Theodoly, O. (2014). Lymphocytes can self-steer passively with wind vane uropods. *Nat. Commun.* *5*, 5213.
- Welsh, C.T., Rose, J.W., Hill, K.E., and Townsend, J.J. (1993). Augmentation of adoptively transferred experimental allergic encephalomyelitis by administration of a monoclonal antibody specific for LFA-1 alpha. *J. Neuroimmunol.* *43*, 161–167.
- Yednock, T.A., Cannon, C., Fritz, L.C., Sanchez-Madrid, F., Steinman, L., and Karin, N. (1992). Prevention of experimental autoimmune encephalomyelitis by antibodies against alpha 4 beta 1 integrin. *Nature* *356*, 63–66.
- Yrlid, U., Jenkins, C.D., and MacPherson, G.G. (2006). Relationships between distinct blood monocyte subsets and migrating intestinal lymph dendritic cells in vivo under steady-state conditions. *J. Immunol.* *176*, 4155–4162.
- Zipfel, W.R., Williams, R.M., and Webb, W.W. (2003). Nonlinear magic: multiphoton microscopy in the biosciences. *Nat. Biotechnol.* *21*, 1369–1377.

Lebenslauf

// Persönliche Daten

Name: **Haberl**
 Vorname: Michael, Maximilian

// Ausbildung:

2003 bis 2010 Biologiestudium an der TU Darmstadt
 Abschluss: Diplom
 Diplomarbeit im Institut für Stammzellforschung
 Helmholtz Zentrum München bei Prof. Dr. Magdalena Götz

1992 bis 2001 Käthe Kollwitz Gymnasium München
 Abschluss: Abitur

// Forschungs- Schwerpunkte:

Motilität von T- und myeloiden Zellen an der Blut-Hirn-Schranke. Der Schwerpunkt hierbei liegt in der Kombination von intravitaler Bildgebung und mathematischen Ansätzen, um entzündliche Prozesse im ZNS zu verstehen.

// Berufserfahrung:

März 2011
 bis heute Wissenschaftlicher Mitarbeiter/Doktorand
 Institut für Neuroimmunologie und Multiple-Sklerose-Forschung
 Gruppe: Dr. Francesca Odoardi,
 „Echtzeitdarstellung neuroimmunologischer Prozesse“
 Titel der Doktorarbeit: „Characterization of immune cell motility
 at CNS border during CNS autoimmunity“

November 2010
 bis Februar 2011 Wissenschaftlicher Gastaufenthalt Ruprecht-Karl-Universität
 Heidelberg, Center for Organismic Studies,
 Abteilung Neuroentwicklungsbiologie, Prof. Dr. G.E. Pollerberg

Juni 2010
 bis November 2010 Max von Pettenkofer-Institut, München
 Virologie AG Ehrhardt

// Publikationen

Winkler A, Wrzos C, **Haberl M**, Weil M-T, Gao M, Möbius W, Odoardi F, Thal DR, Chang M, Opdenakker G, Bennett JL, Nessler S, Stadelmann C. *Blood-brain barrier resealing in neuromyelitis optica occurs independently of astrocyte regeneration.*

J Clin Invest (2021), 131: 141694. doi: 10.1038/s41593-020-00757-6. PMID 33645550.

Lodygin D⁺, Hermann M⁺, Schweingruber N, Flügel-Koch C, Watanabe T, Schlosser C, Merlini A, Körner H, Chang H-F, Fischer HJ, Reichardt HM, Zagrebelsky M, Mollenhauer B, Frahm J, Stadelmann C, Kügler S, Fitzner D, **Haberl M**, Odoardi F* & Flügel A* (2019) β -Synuclein reactive T cells induce autoimmune CNS grey matter degeneration. **Nature 566(7745): 503-508.** DOI 10.1038/s41586-019-0964-2. *equal contribution, * co-senior authors

Flach A*, Litke T*, Strauss J*, **Haberl M**, Cordero Gómez C, Reindl M, Saiz A, Fehling HJ, Wienands J, Odoardi F, Lühder F[§], Flügel A[§] (2016) Autoantibody-boosted T-cell reactivation in the target organ triggers manifestation of autoimmune CNS disease. **Proc Natl Acad Sci USA 113(12): 3323-3328.** *[§]equal contribution

Schläger C*, Körner H*, Krueger M, Vidoli S, **Haberl M**, Mielke D, Brylla E, Issekutz T, Cabañas C, Nelson PJ, Ziemssen T, Rohde V, Bechmann I, Lodygin D, Odoardi F*, Flügel A* (2016) Effector T-cell trafficking between the leptomeninges and the cerebrospinal fluid. **Nature 530(7590): 349-353.** *equal contribution

Lodygin D, Odoardi F, Schläger C, Körner H, Kitz A, Nosov M, van den Brandt J, Reichardt HM, **Haberl M**, Flügel A (2013) A combination of fluorescent NFAT and H2B sensors uncovers dynamics of T cell activation in real time during CNS autoimmunity. **Nature Medicine 19(6): 784-790.**

// Konferenzen

Posterbeitrag, Chemotactic Cytokine Gordon Research Conference, Sunday River, Main, USA, 2-14 Juni 2018. Titel: „T cell and myeloid cell motility at the BBB: a combined intravital and mathematical approach to understand CNS inflammatory processes“.

Vortrag, International Workshop on Image-based Systems Biology, HKI-Center for Systems Biology of Infection, Jena, 29-30 September 2016. Titel: “T-cell and myeloid cell motility at the BBB: a mathematical approach to understand inflammatory processes”.